

JAERI - M
84-182

NEANDC(J)100/U

PROCEEDINGS OF THE NEANDC TOPICAL CONFERENCE ON
"MEASUREMENTS AND EVALUATIONS OF NUCLEAR DATA
AND DECAY HEAT FOR FISSION PRODUCTS"

October 1984

JAPANESE NUCLEAR DATA COMMITTEE

日 本 原 子 力 研 究 所
Japan Atomic Energy Research Institute

JAERI-Mレポートは、日本原子力研究所が不定期に公刊している研究報告書です。
入手の問い合わせは、日本原子力研究所技術情報部情報資料課（〒319-11茨城県那珂郡東海村）あて、お申しこしください。なお、このほかに財団法人原子力弘済会資料センター（〒319-11茨城県那珂郡東海村日本原子力研究所内）で複写による実費頒布をおこなっております。

JAERI-M reports are issued irregularly.

Inquiries about availability of the reports should be addressed to Information Section, Division of Technical Information, Japan Atomic Energy Research Institute, Tokai-mura, Naka-gun, Ibaraki-ken 319-11, Japan.

©Japan Atomic Energy Research Institute, 1984

編集兼発行 日本原子力研究所
印 刷 いばらき印刷㈱

Proceedings of the NEANDC Topical Conference on
"Measurements and Evaluations of Nuclear Data and
Decay Heat for Fission Products"

Japanese Nuclear Data Committee
Tokai Research Establishment, JAERI

(Received September 11, 1984)

The topical conference was held on March 14, 1984 in the middle of the 24th meeting of the Nuclear Energy Agency Nuclear Data Committee (NEANDC) from March 12 through 16, 1984 in Tokai Research Establishment of JAERI. The topical conference was organized jointly by JAERI and Japanese Nuclear Data Committee. About 60 researchers including the attendants of the NEANDC meeting participated in the conference.

The proceedings consist of 10 papers presented in the conference.

Keywords: Nuclear Data, NEANDC, Measurement, Evaluation,
Decay Heat, Fission Products, Proceedings

Organizing Committee and Editors

Sin-iti IGARASI (Member of the NEANDC, JAERI)
Masatsugu AKIYAMA (University of Tokyo)
Zyun-itiro MATUMOTO (JAERI)
Yutaka NAKAJIMA (JAERI)
Masayoshi KAWAI (NAIG)

「核分裂生成物の核データについての測定と評価」
に関する NEANDC トピカルコンファレンス報告

日本原子力研究所東海研究所シグマ研究委員会

(1984 年 9 月 11 日受理)

1984 年 3 月 12 日から 16 日の 5 日間日本原子力研究所東海研究所において開催された NEA 核データ委員会 (NEANDC) 第 24 回会合の中間の 1 日, 3 月 14 日の午後に表記の研究会が開催された。研究会は原研とシグマ研究委員会との共同で準備された。研究会には NEANDC 会合出席者を含めて約 60 名の研究者が参加した。

本報告書は研究会で発表された 10 編の論文をまとめたものである。

プログラム編集委員会

五十嵐信一	(NEANDC 委員, 原研)
秋山 雅胤	(東京大学)
松本純一郎	(原研)
中島 豊	(原研)
川合 将義	(NAIG)

CONTENTS

SESSION I (Chairman: J. L. Rowlands)

I-1	Fission Product and Actinide Data Status in ENDF/B -----	1
	T. R. England, P. G. Young, R. E. Schenter, F. M. Mann and C. W. Reich. (presented by P. G. Young)	
I-2	Evaluation of Fission Product Neutron Cross Sections for JENDL -----	23
	JNDC FP Neutron Cross Section Data Working Group. (presented by S. Iijima)	
I-3	Present Status and Future Programs of Evaluation of Decay Heat for Fission Products in Japan -----	31
	JNDC Decay Heat Evaluation Working Group. (presented by S. Iijima)	
I-4	Fission Product Nuclear Data Measurements and Evaluations at the Studsvik Science Research Laboratory -----	40
	G. Rudstam (presented by H. Condé)	

SESSION II (Chairman: K. H. Böckhoff)

II-1	Decay Heat Calculation with the C.E.A. Radioactivity Data Bank -----	42
	B. Duchemin, J. Blachot, B. Nimal, J. C. Nimal and J. P. Veillaut. (presented by E. Fort)	
II-2	Measurements of Global Fission Products Cross Sections in PWR Spectrum -----	47
	P. Gaucher and L. M. Deidier. (presented by E. Fort)	
II-3	Some Investigation on the Contribution of the Internal Conversion Process to the Decay Heat of a LMFBR -----	55
	N. K. Cohen (presented by E. Fort)	
II-4	A Model for Fission-Product Calculations -----	61
	A. B. Smith	
II-5	Fission Product Nuclear Data Measurements at the JAERI LINAC -----	75
	M. Mizumoto, Y. Nakajima, M. Ohkubo, M. Sugimoto, Y. Furuta and Y. Kawarasaki.	
II-6	Pygmy Resonance Appeared in keV-Neutron Capture Gamma-Ray Spectra of Nuclei N=82-126 -----	100
	M. Igashira, K. Udagawa, T. Natsume, H. Fukui, M. Shimizu, H. Komano, H. Kitazawa and N. Yamamuro.	

SESSION I

I-1 FISSION PRODUCT AND ACTINIDE DATA STATUS IN ENDF/B

T. R. England and P. G. Young
Theoretical Division, Los Alamos National Laboratory
Los Alamos, New Mexico 87545

R. E. Schenter and F. M. Mann
Hanford Engineering Development Laboratory
PO Box 1970, Richland, WA 99352

C. W. Reich
Idaho National Engineering Laboratory
TRA652, PO Box 1625, Idaho Falls, ID 83415

Presentation at the Twenty-fourth Meeting of
The Nuclear Energy Agency Nuclear Data Committee
Tokai-mura, Japan
March 12-16, 1984

I. INTRODUCTION

The U.S. Evaluated Nuclear Data Files (ENDF/B)¹ have been very successful in this country and internationally. The data are used directly in calculations or as a reference for comparison with new measurements and other international data bases. The data formats,² being particularly suited for computer processing codes, have been recommended by the IAEA³ as the preferred method of exchange for international data. Part of this success is due to a remarkably free exchange of data nationally and internationally. Primarily, of course, it is due to the many needs for such a comprehensive, evaluated data base.

The current version, ENDF/B-V was largely released in 1979 and 1980. Both ENDF/B-IV and -V were greatly expanded in the areas of fission products and actinides, and the cross section evaluations have been improved in each new version. ENDF/B-VI was originally scheduled for completion in late 1986. However, this schedule is now questionable, as is the extent of its content.

In this report, we direct our comments at the improvements we feel are needed for ENDF/B-VI, irrespective of the time scale or probability of implementation. Additionally, we limit our considerations to fission products and heavy nuclides (which we loosely call "actinides") and specifically to plans at Los Alamos National Laboratory (LANL), Hanford Engineering and Development Laboratory (HEDL), and Idaho National Engineering Laboratory (INEL). In our coverage we emphasize cross sections and yields for fission products and decay data for both fission products and actinides. We do not attempt complete coverage of planned evaluations of actinide cross sections nor other ENDF/B general and special purpose files (e.g., General Purpose, Activation, Standards, etc.), although some of the data we cite lies in those files. However, our summary of data content in the current ENDF/B-V files is complete for fission products and actinides.

Section II compares the content of Versions IV and V of ENDF/B and provides references for more complete descriptions of the fission product and actinide data files. The "Pandemonium" problem is described in Sec. III, and illustrations of discrepancies between experimental and calculated results that we attribute to this effect are given. Section IV summarizes the data expansion that is planned for ENDF/B-VI in the areas of fission-product yields and cross sections as well as decay data for fission products and actinides. Finally, our concluding remarks are given in Sec. V.

II. GENERAL CONTENT IN ENDF/B-IV AND -V.

ENDF/B-IV was the first version containing extensive decay data for fission products and their neutron cross sections. Previous versions contained no fission yields or decay data and only included ~ 55 fission products having cross sections. Actinide data were limited to cross sections of only a few important fuel nuclides even in ENDF/B-IV. There were many aggregate comparisons of the fission-product data with decay energies, spectra, and cross sections.⁴⁻⁶ References 7, 8, and 9 summarize the specific data content, and Refs. 10-15 describe some of the evaluation procedures and data sources.

Extensive aggregate tests of the ENDF/B-V fission-product decay data have been made,¹⁶⁻¹⁸ but similar tests of the actinide data are more limited. Some results are reported in Ref. 19 and in the compiled data testing report.¹⁷

A summary data report, similar to Ref. 7 for ENDF/B-IV, has been completed for ENDF/B-V.²⁰ It contains all major decay parameters, processed cross sections appropriate for fast and thermal neutron spectra, mass chain yields, and some augmentation of the ENDF/B-V data necessary for completeness. To date, there is no decay spectra summary similar to that in Ref. 9 for the ENDF/B-IV spectra. References 10-15 provide some additional information and are particularly suited for summaries of evaluation methods and procedures.

Tables I and II compare the general content in Versions -IV and -V. The dominant changes over Version IV are these:

- o Actinides were greatly expanded; all 60 are radioactive and have decay spectra, and 41 have partial or complete cross-section evaluations.
- o Most fission-product cross sections were reevaluated and several were added.¹⁸
- o Fission yield sets were greatly expanded. A set is characterized by the fissionable nuclide, incident neutron energy, and type of yield, i.e., independent or cumulative. Each set contains 1100 to 1200 yields. ENDF/B-IV contains independent yields for six nuclides at one or more energies and no uncertainties for a total of ten yield sets. ENDF/B-V contains both cumulative and independent yields for 11 fissionable nuclides for a total of 40 sets, and uncertainties are included. Thus, the data expanded by a factor of eight. In addition, models for yield distributions were improved.

- o Decay spectra were greatly expanded, and each nuclide having spectra now includes, if appropriate, electron capture or β^+ , β^- , α , γ , X-ray, proton, and discrete electrons. The formats were expanded to permit these and other spectra.

TABLE I

ENDF/B-IV vs ENDF/B-V GROSS COMPARISON OF DATA CONTENT IN FILES

=====FISSION PRODUCTS=====

<u>TYPE OF QUANTITY</u>	<u>ENDF/B-IV</u>	<u>ENDF/B-V</u>
<u>General Content</u>		
Total nuclides	824	877
Nuclides having cross sections	181	196
Stable nuclides	113	127
Unstable nuclides	711	750
Total isomeric states ($\geq 0.1s$)	123	154
First isomeric states ($\geq 0.1s$)	117	148
Average energies derived from exp	181	317
Delayed neutron precursors	57	105
Fission yield sets	10	20

FP Nuclides having detailed spectral data

Beta and/or gamma	180	264
Electron related	163(β -only)	233
Photon related	172(γ only)	247
Conversion electron	38	157
Positron or EC	0	12
X-ray	0	166
Discrete electron	0	166

=====ACTINIDES=====

Total actinides with decay spec (41 Have cross sections in ENDF/B-V)	0	60
---	---	----

TABLE II
COMPARISON OF FP YIELDS IN ENDF/B-IV AND ENDF/B-V^a
Characteristic Neutron Incident Energy

Target Nuclide	Thermal	Fast	High (14 MeV)	Spontaneous
²³² Th		4.5	5	
²³³ U	4.5	5	5	
²³⁵ U	4.5	4.5	4.5	
²³⁸ U		5		
²³⁸ U		4.5	4.5	
²³⁷ Np		5		
²³⁹ Pu	4.5	4.5	5	
²⁴⁰ Pu		5		
²⁴¹ Pu	4.5	5		
²⁴² Pu		5		
²⁵² Cf				5

^a10 sets of direct yields in ENDF/B-IV (~ 11 000 yields).

40 sets of direct and cumulative yields (by A and Z) in ENDF/B-V,
now including uncertainties (~ 44 000 yields plus uncertainties).

III. THE "PANDEMONDIUM" PROBLEM

The expansion of decay spectral data for ENDF/B-V apparently improved the shape of the aggregate spectra but worsened the magnitude. In particular, we found that the overall gamma energy decreased and the beta energy increased, making the comparisons with experiment worse than those with ENDF/B-IV. This problem is evident in Fig. 1, where the total gamma and beta decay energies calculated for a fission pulse using ENDF/B data are compared with experimental values at various cooling times. The effect is even more pronounced in Figs. 2-5, which compare the calculated and measured decay energies for individual spectral energy bins. (Note that the 1-100-s irradiation experimental results from Oak Ridge are in good agreement with the 5.56-h irradiation data from Los Alamos when both are reduced to a pulse equivalent.) This problem was first observed by the Japanese in formation of their files²¹ and most recently discussed in Ref. 22. The problem was anticipated in a paper by Hardy et al.²³ based on a fictitious nuclide they called Pandemonium. In general, it results from evaluations and/or experiments that are missing high-energy γ -transitions in the complex spectra of some high-Q nuclides. As can be seen in Fig. 6, most of the calculated aggregate decay energy now results from nuclides having experimentally based energies.

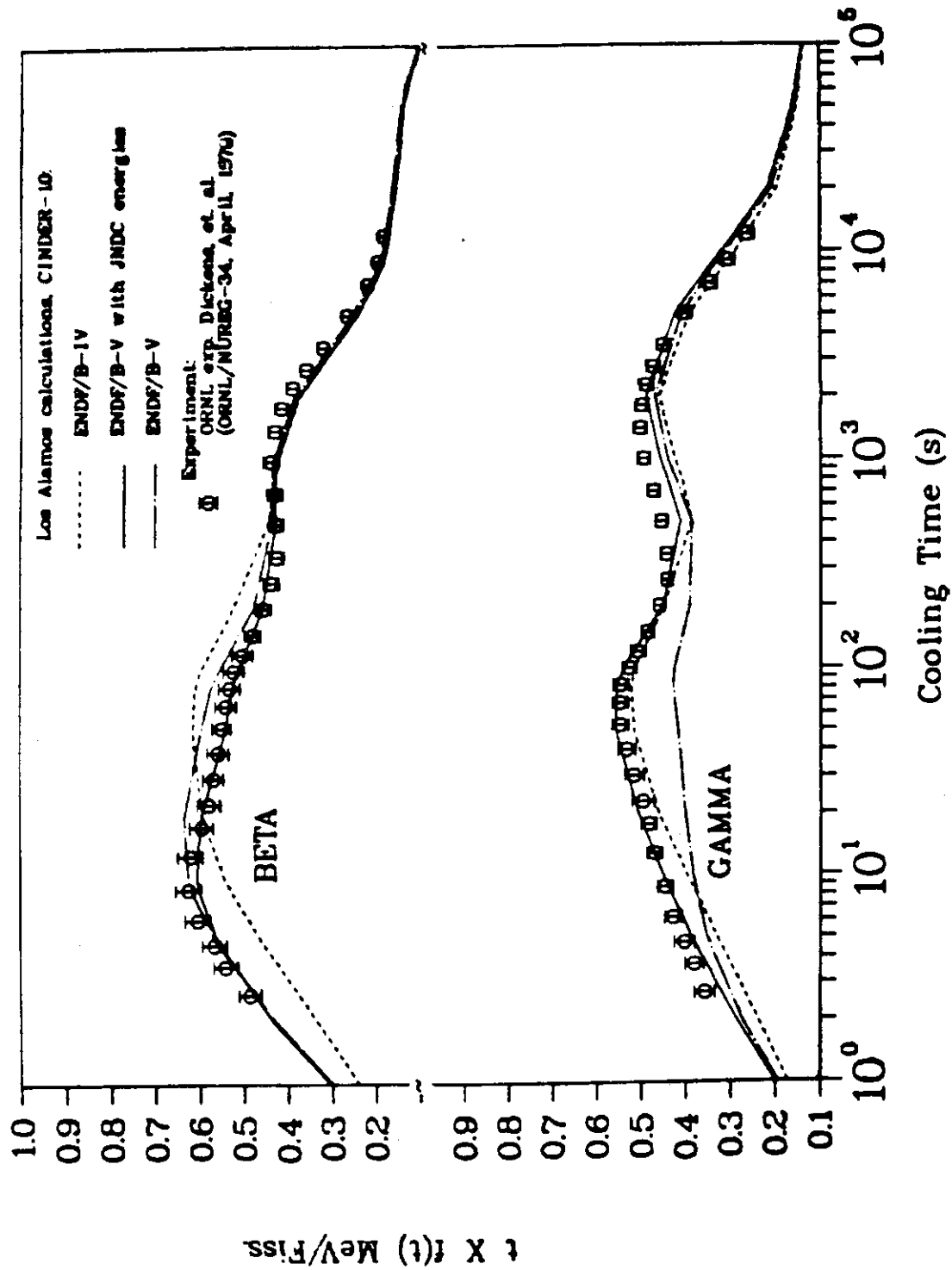
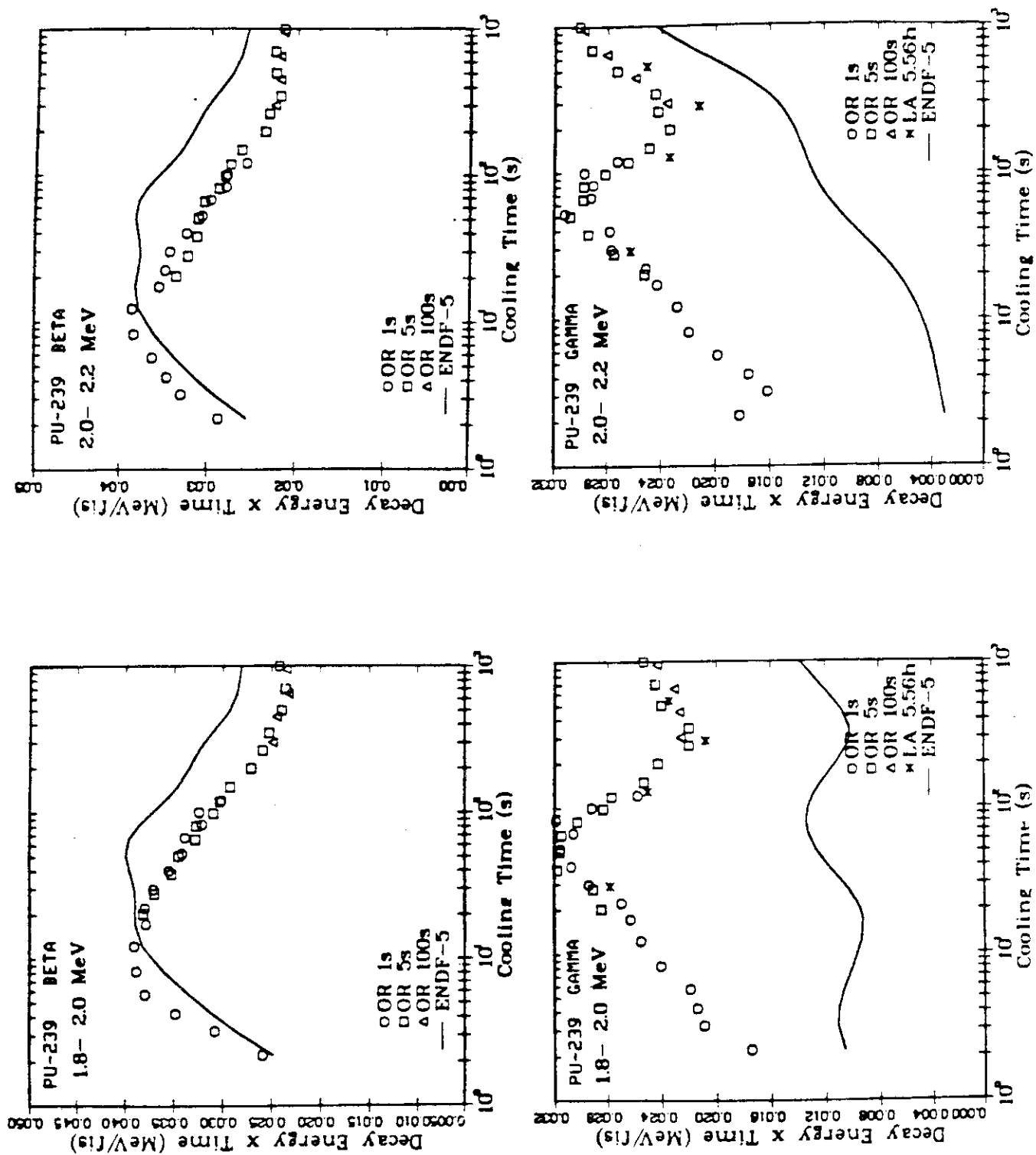


Fig. 1 ^{239}Pu thermal fission pulse comparisons.

Fig. 2 Group spectra comparisons for 1.8-2.0 MeV and 2.0-2.2 MeV for a ^{239}Pu fission pulse.

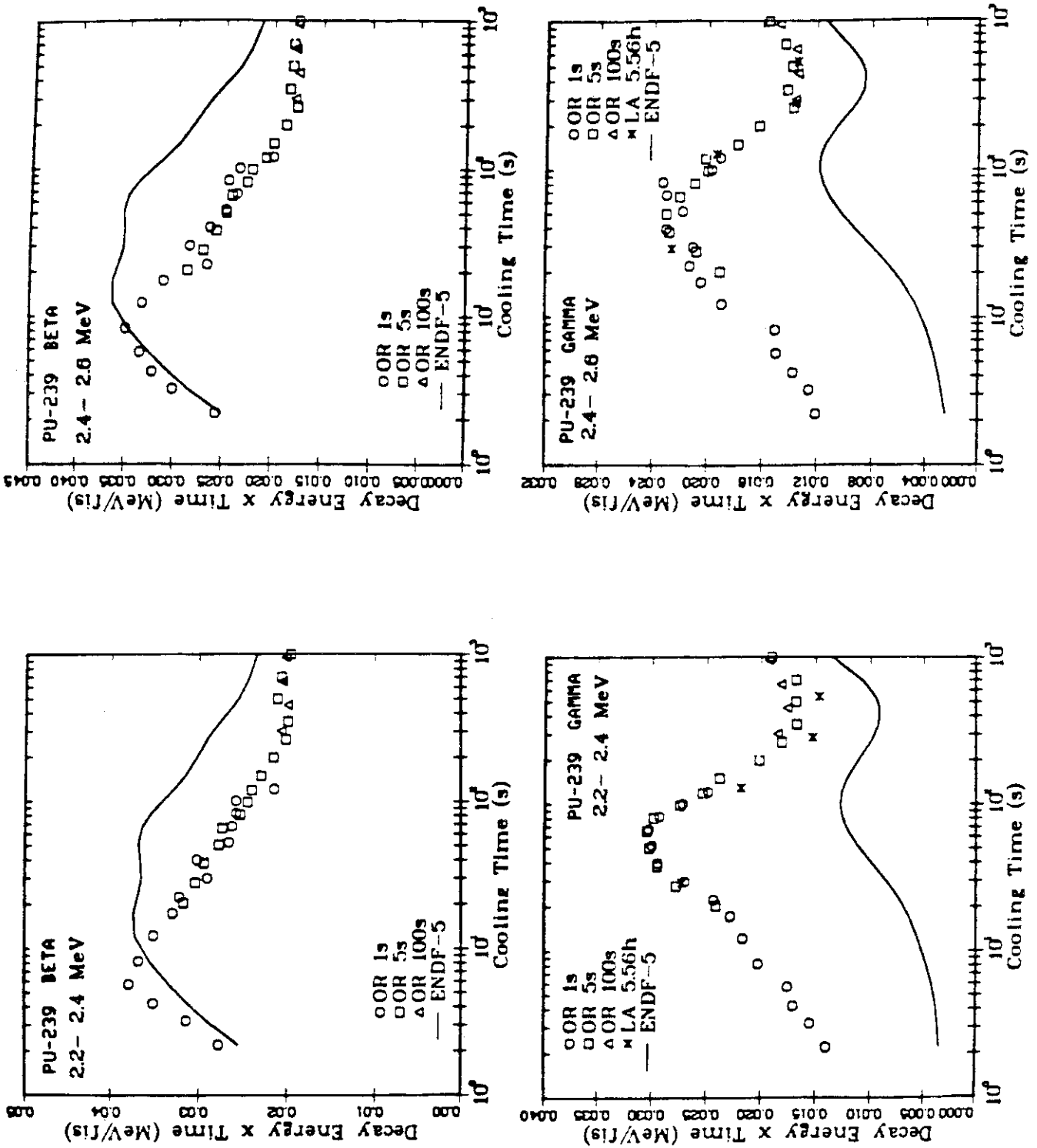


Fig. 3 Group spectra comparisons for 2.2-2.4 MeV and 2.4-2.6 MeV for a ^{239}Pu fission pulse.

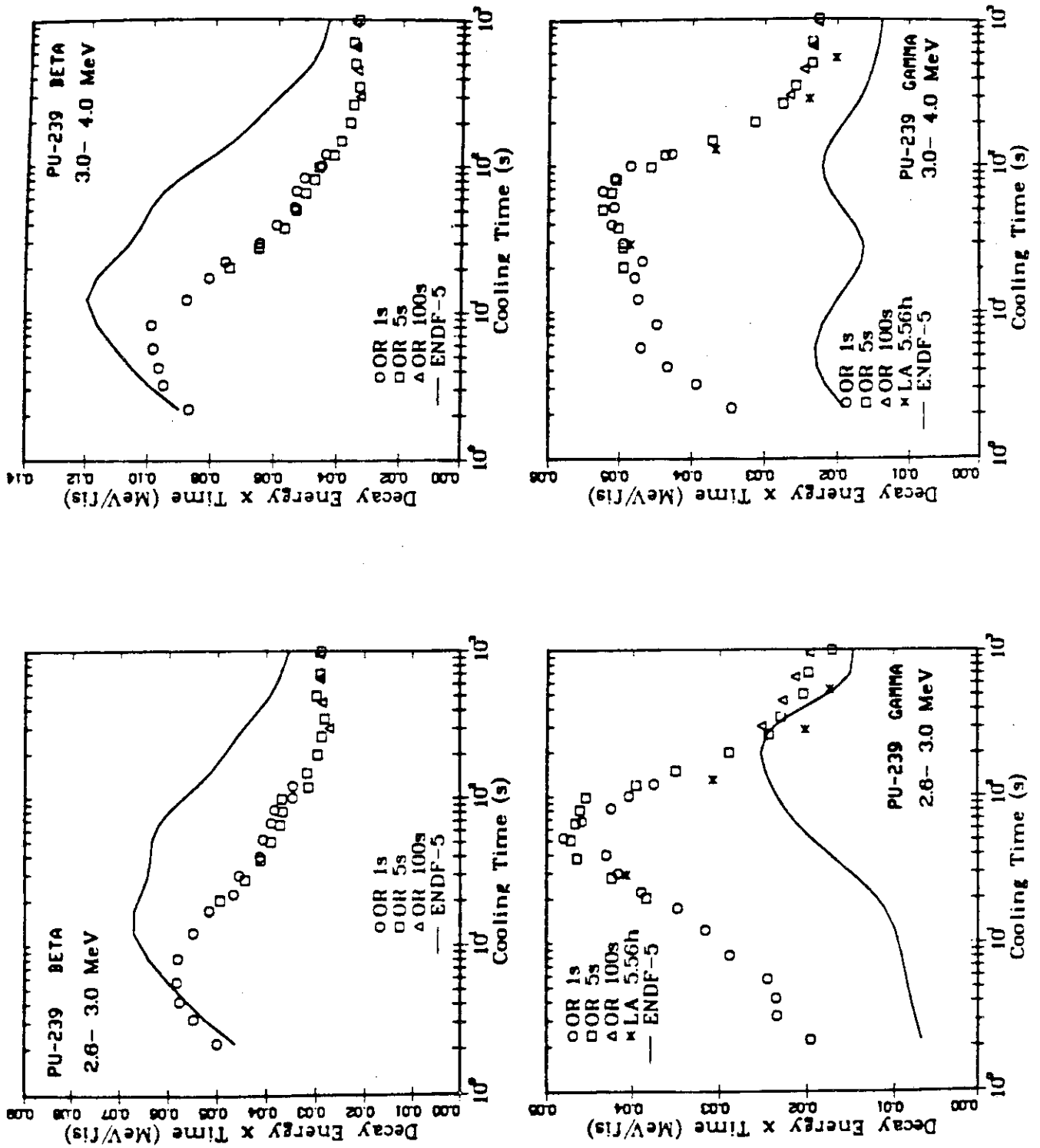


Fig. 4 Group spectra comparisons for 2.6-3.0 MeV and 3.0-4.0 MeV for a ^{239}Pu fission pulse.

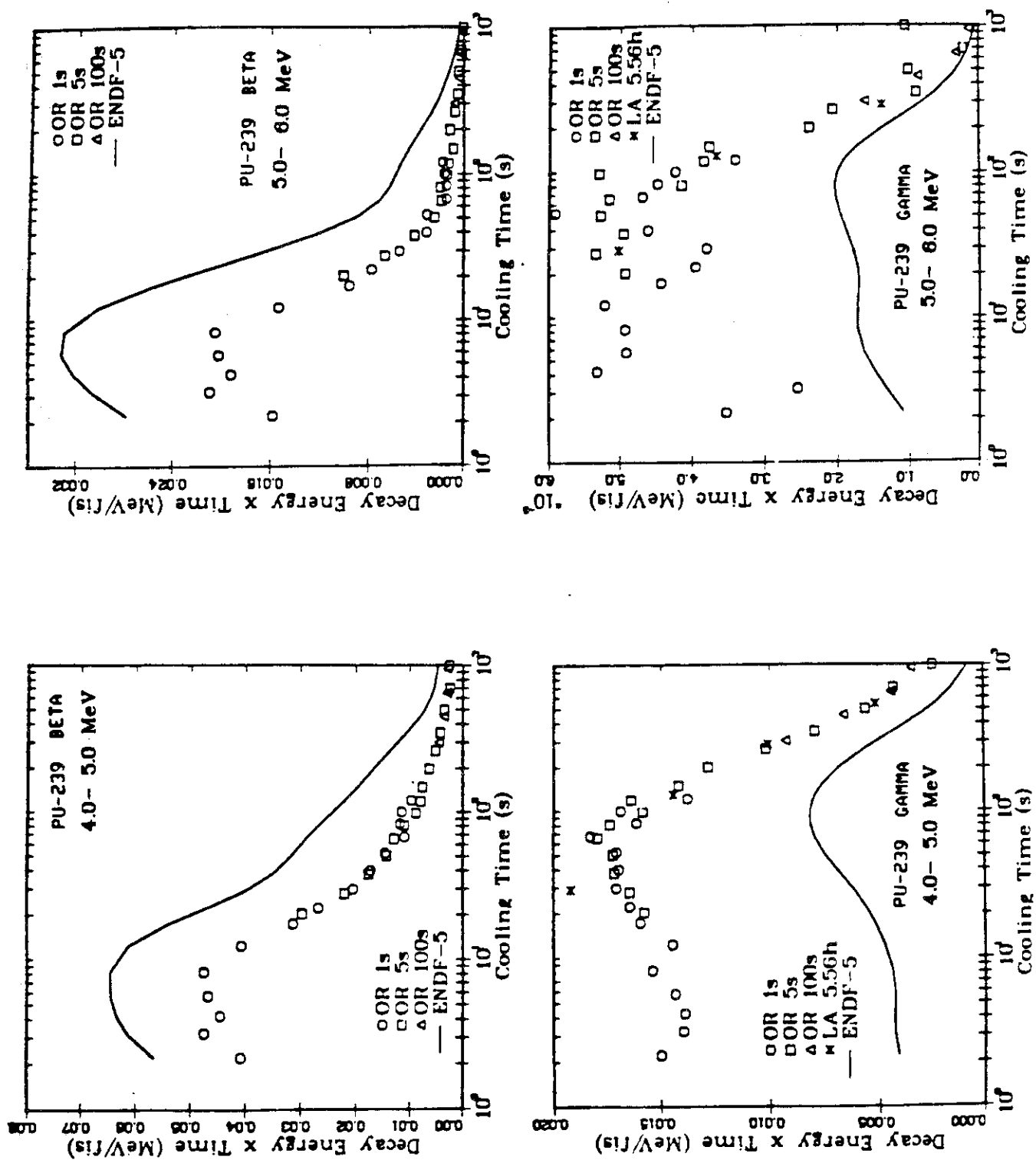


Fig. 5 Group spectra comparisons for 4.0-5.0 MeV and 5.0-6.0 MeV for a ^{239}Pu fission pulse.

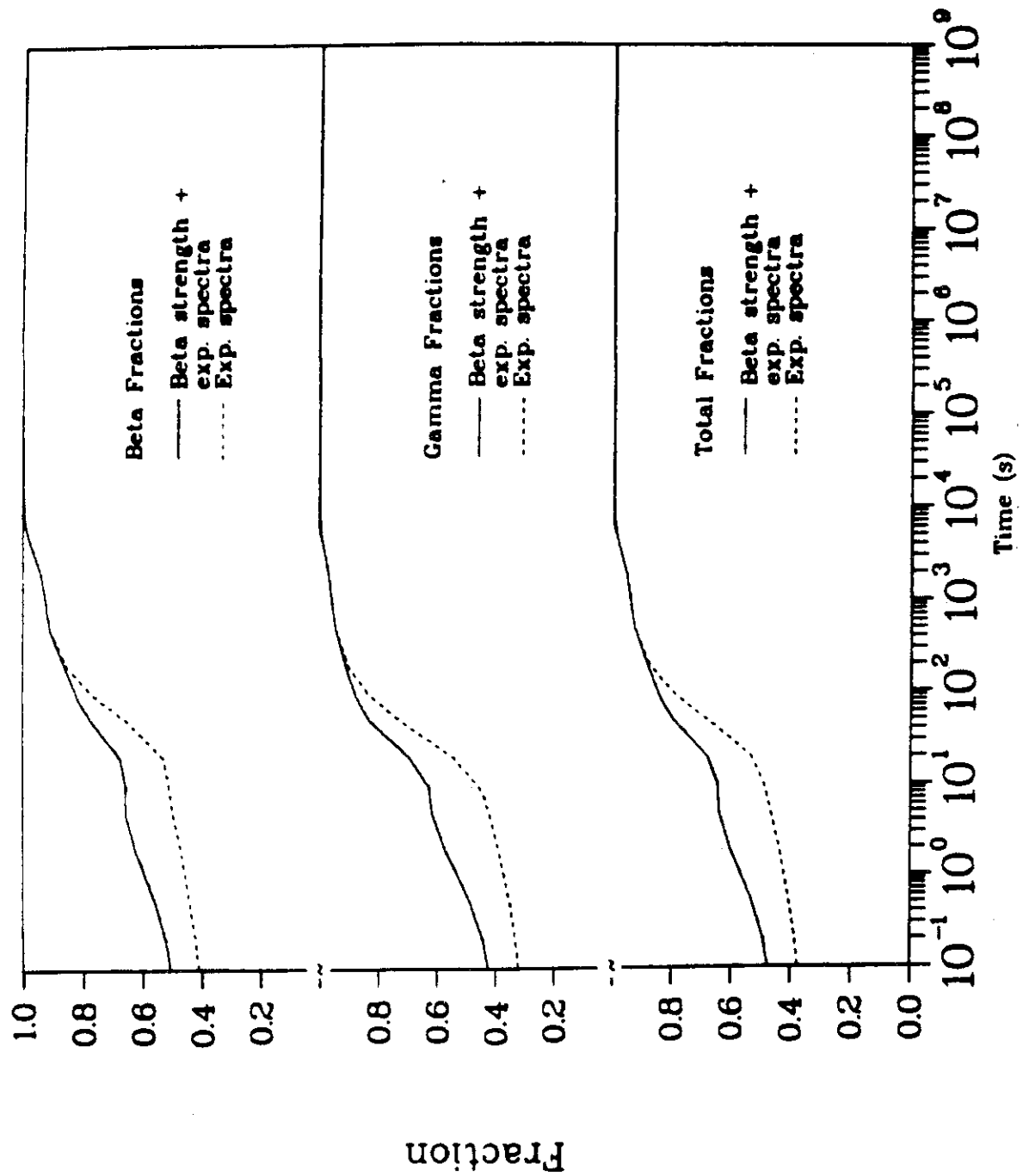


Fig. 6 ^{235}U thermal fission pulse: fractional energies from experimental data in ENDF/B-V.

The Japanese have used model calculations based on the Gross Theory of Takahashi and Yamada²⁴ to get average energies for such nuclides, with very good results. In ENDF/B the average energies are derived from spectra if present in the files. The procedure presents us with a major problem for the next version of ENDF/B. As noted in the next section, we expect to add more spectra for the nuclides. Clearly, we must also consider (in some cases) renormalizing the average energies derived from these spectra or supplementing the spectra using model calculations such as could be done with, e.g., the BETA code.²⁵

A list of nuclides that may be in the Pandemonium class, hence requiring a new examination, is given in Table III. Table IV provides a comparison of some average beta and gamma energies in ENDF/B-V with 1981 JNDC values.

IV. PLANNED EXPANSION OF DATA FOR ENDF/B-VI.

A. Yields

All current yield sets will be reevaluated and the number of sets will be increased from 40 to perhaps 100. Table V summarizes the evolution of these data and Table VI indicates the specific nuclides and energies scheduled to have yields. Most of the increase is clearly for spontaneous and 14.7-MeV fission. The data should be updated through 1985, the distribution model parameters reevaluated, and the basis for uncertainty estimates reexamined. Some preliminary results are given in Ref. 15. As noted by the working groups at the conference in which this yield paper was given, fission product yields are important to all applications of fission-product data.

B. Decay Data

Table VII summarizes the planned expansion.

The current 60 actinides in ENDF/B-V Mod "O" all have decay spectra. These will be updated including results from the IAEA Coordinated Research Program for Transactinium Nuclides. In addition, approximately 48 actinides with spectra will be added. The reevaluation includes half-lives and branching ratios.

For fission products, approximately 450 will have partial or complete spectra, compared with ~ 264 in ENDF/B-V. Some will also have average energies based on beta strength functions. The Pandemonium nuclides discussed in Sec. III will be reevaluated and/or have energies based on new measurements, including results from a program being started this year at INEL. In many cases we expect to use the BETA model code for average

TABLE III

NUCLIDES IN ENDF/B-V TO BE EXAMINED FOR PANDEMONDIUM EFFECT^a

Nuclide	Half-life(s)	Q (MeV)
33-As-80	1.650+01	6.000
33-As-82	2.100+01	7.200
33-As-82m	1.300+01	7.200
35-Br-87	5.570+01	6.840
35-Br-88	1.600+01	8.600
36-Kr-91	6.570+00	6.120
36-Kr-92	1.840+00	5.970
37-Rb-92	4.530+00	7.770
36-Kr-93	1.289+00	7.510
37-Rb-93	5.860+00	7.360
39-Y-96	6.000+00	6.500
39-Y-96m	1.000+01	7.000
38-Sr-97	4.000-01	7.400
39-Y-97	3.700+00	6.670
39-Y-97m	1.110+00	7.337
38-Sr-98	6.500-01	5.810
39-Y-98	2.000+00	7.300
39-Y-98m	6.500-01	7.300
41-Nb-98	2.860+00	4.585
39-Y-99	1.400+00	6.390
40-Zr-99	2.100+00	4.445
41-Nb-101	7.000+00	4.570
43-Tc-102	5.280+00	4.500
43-Tc-102m	2.610+02	5.000
43-Tc-104	1.092+03	5.400
44-Ru-107	2.520+02	3.150
45-Rh-108	1.680+01	4.500
45-Rh-108m	3.540+02	4.500
45-Rh-110	2.850+01	5.400
45-Rh-110m	3.000+00	5.400
49-In-120	3.080+00	5.400
49-In-120m	4.440+01	5.300
49-In-121	3.000+01	3.380
49-In-121m	2.256+02	3.700
51-Sb-134	1.070+01	8.490
51-Sb-134m	8.500-01	8.400
54-Xe-139	4.040+01	5.020
54-Xe-140	1.360+01	4.060
55-Cs-140	6.370+01	6.050
54-Xe-141	1.720+00	6.000
55-Cs-141	2.490+01	4.980
57-La-142	5.550+03	4.517
55-Cs-144	1.001+00	8.100
57-La-144	4.030+01	5.300
59-Pr-148	1.380+02	4.800
59-Pr-149	1.500+02	3.000
61-Pm-152	2.460+02	3.470
61-Pm-152m	4.500+02	3.470
61-Pm-154	1.080+02	4.000
61-Pm-154m	1.680+02	4.000

^aSee text. These nuclides have complex spectra and their average energies need to be examined.

TABLE IV
COMPARISON OF AVERAGE BETA- AND GAMMA-RAY ENERGIES^a
(ENDF/B-V vs 1981 JNDC Values)

Nuclide	E-Beta (MeV)			E-Gamma (MeV)		
	JNDC(E)	JNDC(G)	ENDF/B-V	JNDC(E)	JNDC(G)	ENDF/B-V
*34Se 85	1.70	1.63	2.18	2.24	2.39	1.39
*34Se 86	1.15	1.35	1.86	2.35	1.96	1.07
35Br 86	1.74	1.95	1.78	3.64	2.94	3.30
*34Se 87	2.49	2.08	2.54	1.96	2.64	1.71
*35Br 87	1.54	1.81	2.50	3.86	2.41	1.55
*34Se 88	2.38	2.40	2.39	1.72	1.72	1.47
*35Br 88	2.82	2.45	2.54	3.06	3.21	3.00
37Rb 88	2.09	1.19	2.06	0.64	2.49	0.66
*35Br 90	4.39	3.09	3.21	1.13	3.66	2.62
37Rb 90m	1.29	1.54	1.36	3.35	2.67	3.10
37Rb 90	1.89	1.57	2.20	2.16	2.76	1.08
*36Kr 91	1.99	2.08	1.94	1.73	1.62	1.73
37Rb 91	1.52	1.48	1.50	2.22	2.30	2.23
*36Kr 92	2.41	2.28	2.37	0.72	1.08	0.75
*37Rb 92	3.49	2.86	3.46	0.27	1.57	0.26
*36Kr 93	2.89	2.73	2.34	2.28	2.76	2.24
37Rb 93	2.72	2.15	2.61	1.39	2.68	1.32
*36Sr 95	2.27	1.59	2.11	1.03	2.44	1.40
*38Sr 96	1.98	1.98	1.88	0.91	0.96	1.13
*38Sr 97	2.54	2.60	2.62	1.49	1.50	1.49
*39Y 97m	2.40	2.68	2.42	1.81	1.47	1.82
*39Y 97	2.15	2.47	2.15	1.81	1.23	1.80
37Rb 98	3.81	3.71	4.15	1.25	2.92	4.68
*38Sr 98	2.53	2.14	2.53	0.17	1.05	0.18
*39Y 98m	2.68	2.99	2.98	3.11	2.60	0.61
*39Y 98	3.95	3.22	1.81	0.81	2.04	3.15
*39Y 99	2.48	2.38	2.61	0.49	1.15	0.61
*40Zr101	2.50	2.16	2.21	0.35	1.09	1.53
*43Tc104	1.68	1.24	1.58	1.84	2.68	1.94
*42Mo105	2.28	1.29	1.68	0.15	2.37	1.09
*43Tc108	3.29	2.25	2.47	0.80	2.99	1.88
*45Rh110m	1.35	2.24	2.37	2.21	0.78	0.06
*45Rh110	2.38	2.20	1.18	0.06	0.49	2.48
*50Sn131m	1.17	1.10	1.47	1.63	2.39	1.00
*49In132	2.24	3.16	3.63	4.78	2.90	5.00
51Sb132	1.20	1.20	1.38	2.57	2.73	2.60
*50Sn133	3.10	2.41	2.39	0.39	1.86	1.98
*51Sb134m	3.14	2.28	3.78	2.03	3.27	0.0
*51Sb134	3.84	2.78	2.80	0.00	2.26	2.04
52Te135	2.44	1.53	2.40	0.69	2.62	0.74
53I 136m	2.31	1.76	2.13	2.00	2.94	2.00
53I 136	2.05	1.76	1.97	2.47	2.94	2.38
53I 137	1.97	1.27	2.29	0.75	2.46	0.97
55Cs138m	0.40	0.28	0.39	0.53	0.73	0.54
55Cs138	1.25	1.09	1.20	2.33	2.68	2.36
*54Xe139	1.74	1.00	1.70	0.89	2.24	0.76
*55Cs140	1.75	1.43	1.65	2.22	2.79	2.30
*54Xe141	2.36	2.05	2.35	1.04	1.49	0.76
55Cs141	2.09	1.28	1.91	0.67	2.14	0.80
*54Xe142	1.85	1.76	1.86	1.19	0.98	1.12
55Cs142	2.62	2.45	2.50	3.81	1.79	1.17
*57La144	1.79	1.34	1.46	1.31	2.09	1.82
*57La146	2.46	2.18	2.05	0.72	1.35	1.73
*57La148	2.74	2.18	2.21	0.68	1.36	2.04
*59Pr150	2.31	2.02	1.84	0.26	1.08	1.43

^aThis comparison was supplied by T. Yoshida, April 1981. JNDC(G) refers to model calculations using the Gross Theory of Beta Decay. These values were adopted into the JNDC fission product library. JNDC(E) refers to experimentally based energies.

^bThese nuclides are scheduled to be reevaluated for ENDF/B-VI.

^cThese nuclide energies are not based on spectra or beta strength functions in ENDF/B-V.

TABLE V
SUMMARY OF ENDF YIELD EVALUATIONS^a

Quantity	ENDF/B-IV	ENDF/B-V	Prelim. ENDF/B-VI
Year	1974	1978	1983
Fissionable Nucs.	6	11	34
No. of Yield Sets	10	20	50
Isomer Ratio Est.	50/50	Yes	Yes
Pairing	No	Yes	Yes
Delayed Neutron	No	Yes	Yes
Charge Balance	No	Yes	Yes
Ternary Fission	No	Yes	Yes
Indep. Yields ^b	Yes	Yes	Yes
Cumulative Yields	No	Yes	Yes
Uncertainties	No	Yes	Yes
No. of References	956	1119	1274
No. of Yields	11000	44000	110000

^a ENDF/B yields through ENDF/B-V have been based on evaluations by B. F. Rider at G. E. and modified at Los Alamos to extend the chains. Current results for preliminary ENDF/B-VI were produced at Los Alamos using corrections and some additions to the 1981 G. E. Files.

Final results are planned to be updated through 1985 at Los Alamos, including changes in the distribution model.

^b Beginning with ENDF/B-V, delayed neutron branching fractions have been incorporated into evaluations. Independent yields apply before delayed neutron emission and cumulative yields apply after emission.

TABLE VI
ENDF/B FISSION-PRODUCT YIELD SETS^a

Nuclide	Thermal	Fast	14 MeV	Spon.	Nuclide	Thermal	Fast	14 MeV	Spon.
²²⁷ Th	6				²⁴² Pu		56		
²²⁹ Th	6				²⁴¹ Am	6	6	6	
²³² Th		456	56		^{242m} Am	6			
²³¹ Pa		6			²⁴³ Am		6		
²³² U		6			²⁴² Cm		6		
²³³ U	456	56	56		²⁴⁴ Cm				6
²³⁴ U		6	6		²⁴⁵ Cm	6			
²³⁵ U	456	456	456		²⁴⁸ Cm				6
²³⁶ U		56	6		²⁴⁹ Cf	6			
²³⁷ U		6			²⁵⁰ Cf				6
²³⁸ U		456	456	6	²⁵¹ Cf	6			
²³⁷ Np		56	6		²⁵² Cf				56
²³⁸ Np		6			²⁵³ Es				6
²³⁸ Pu		6			²⁵⁴ Es	6			
²³⁹ Pu	456	456	56		²⁵⁴ Fm				6
²⁴⁰ Pu		56	6		²⁵⁵ Fm	6			
²⁴¹ Pu	456	56			²⁵⁶ Fm				6

^a 4, 5, and 6 refer to ENDF/B versions IV, V, and proposed VI (using updated models and data).

TABLE VII
ENDF/B-VI PROJECTED DECAY DATA CONTENT^a

- ACTINIDES:**
- a) 108, ALL UNSTABLE AND HAVE LINE DATA (vs 60 IN ENDF/B-V, REV. "0")
 - b) ALL IMPORTANT ACTINIDES FOR REACTOR TECH. TO BE REEVALUATED. (e.g., RESULTS FROM IAEA COORDINATED RESEARCH PROGRAM ON TRANSACTINIUM NUCLIDE DECAY DATA TO BE INCORPORATED.)
- FISSION PRODUCTS:**
- a) APPROX. 450 WITH PARTIAL OR COMPLETE LINE DATA.
 - b) AV. BETA AND GAMMA ENERGIES FOR MANY IMPORTANT NUCLIDES TO BE BASED ON INEL DIRECT MEAS. (BEING STARTED 1984), OR RE-EVALUATED. MODEL CALCULATIONS WILL BE USED FOR AVERAGES WHERE LINE DATA ARE SUSPECT OR INCOMPLETE AND FOR ALL UNSTABLE NUCLIDES HAVING NO MEAS. SPECTRA (e.g., USING THE BETA CODE).
 - c) 110 NUCLIDES WILL HAVE DELAYED NEUTRON SPECTRA AND P_n VALUES (VS HAD NO DELAYED NEUTRON SPECTRA FOR INDIVIDUAL PRECURSORS)
 - d) SELECTED NUCLIDES WILL HAVE AVERAGE ENERGIES BASED ON BETA STRENGTH MEAS.

^a ENDF/B contains several other nuclide classifications such as dosimetry, standards, and activation. The activation files, for example, contain 77 unstable nuclides all having line data plus 47 stable nuclides. (To various extents, the other categories overlap parts of the actinide and fission product files.) All files will receive some review and updating.

energies, especially for those nuclides having no spectra or whose spectra we suspect are incomplete. Therefore, as with the fission yields and cross sections, we expect to use both experimental and model data for decay data.

This last comment also applies to delayed neutrons. There were no delayed neutron spectra for individual nuclides in ENDF/B-V. We expect to add evaluated measured spectra for > 30 precursors and model calculated spectra for another ~ 80. Currently there are time-of-flight and proton-recoil measurements (e.g., at INEL) in progress for low energy spectra. We expect to use these, and, where necessary, model calculations, to extend the evaluated measured spectra to lower and possibly higher energy ranges. These individual nuclide spectra are primarily useful only when the evaluated emission probabilities (P_n) and fission product yields are

of high quality. Pn evaluations were recently completed and unmeasured values estimated from systematics.²⁶

We also expect to use the fission yields, Pn values, and delayed neutron spectra of individual nuclides to calculate the conventional aggregate time-group spectra, and possibly the group and total delayed neutron yields; such aggregate data are also required in ENDF/B. A preliminary calculation of the group $\bar{\nu}_d$ and spectra has been published based on 105 precursors,²⁷ and the normalized spectra already appear to be superior to the evaluated aggregate group spectra in ENDF/B-V.

C. Fission Product and Actinide Cross Sections

While a detailed work plan is not yet available, it is likely that the cross section data for several primary fuel nuclides (including ^{235}U and ^{239}Pu) will be reevaluated for Version VI of ENDF/B. Supporting nuclear model calculations will be performed using, for example, the GNASH Hauser-Feshbach statistical-theory code²⁸ and the ECIS deformed optical model code.²⁹ The extent of the reevaluations depends upon the amount of new information that becomes available in the next two years.

Table VIII summarizes the evaluation plans for ~ 8 higher mass actinides ($A > 241$) and 75 fission products. Resonance parameters and thermal cross sections will be revised based on the most recent issue of BNL-325 and the analyses using the RESPARFM code.³⁰ For selected nuclei, both measured (n, γ), (n,f), and (n,t) integral cross sections and differential data will be used in the FERRET least-squares data adjustment code.³¹ Other cross sections [(n,n'), (n,2n), etc.] will be calculated using the HAUSER*6 code.³² In all cases, the latest measured data will be incorporated in the evaluations.

An example of the use of this evaluation technique is given for the $^{129}\text{I}(n,\gamma)$ cross section in Fig. 7. In this instance, the influence of the integral data (not shown) is such that the adjusted result (solid curve) is pulled away from the differential data (dashed histogram). The shape of the a priori input (dashed curve) is maintained in the adjustment.

TABLE VIII
CROSS SECTION EVALUATION UPDATE PLANS FOR
ENDF/B-VI FISSION PRODUCTS AND HIGHER ACTINIDES

- o Focus on 75 FP nuclides and 8 higher actinides (having Z greater than or equal to 94)
- o To include new resolved resonance parameter data
 - (a) Use computer code RESPARFM
 - (b) Input primarily from BNL-325 (1982 Z = 1-60, 1984 Z > 60)
 - (c) Obtain D_{obs} and Γ_{γ} from RESPARFM analyses
- o Calculate n_{γ} , n_f , and n_t cross sections using least squares code FERRET for selected nuclei.
 - (a) Use integral and differential data as input
 - (b) Use elemental differential data as constraint on individual isotope cross sections.
 - (c) Use primarily latest CSIRS as source of differential data.
 - (d) Use CFRMF, STEK, EBR-II, and FFTF as source of integral data.
- o Calculate nn' , n_{γ} , n_f , nn , $n2n$, and γ production, etc. for selected nuclei using HAUSER*6 code.
 - (a) Input levels from latest ENSDF files
 - (b) Use optical model parameters obtained from expected HEDL study.
- o Include recent capture measurements of radioactive nuclei (I-129, Pd-107, etc.)--see example figure.
- o Evaluations to be completed May 1986.

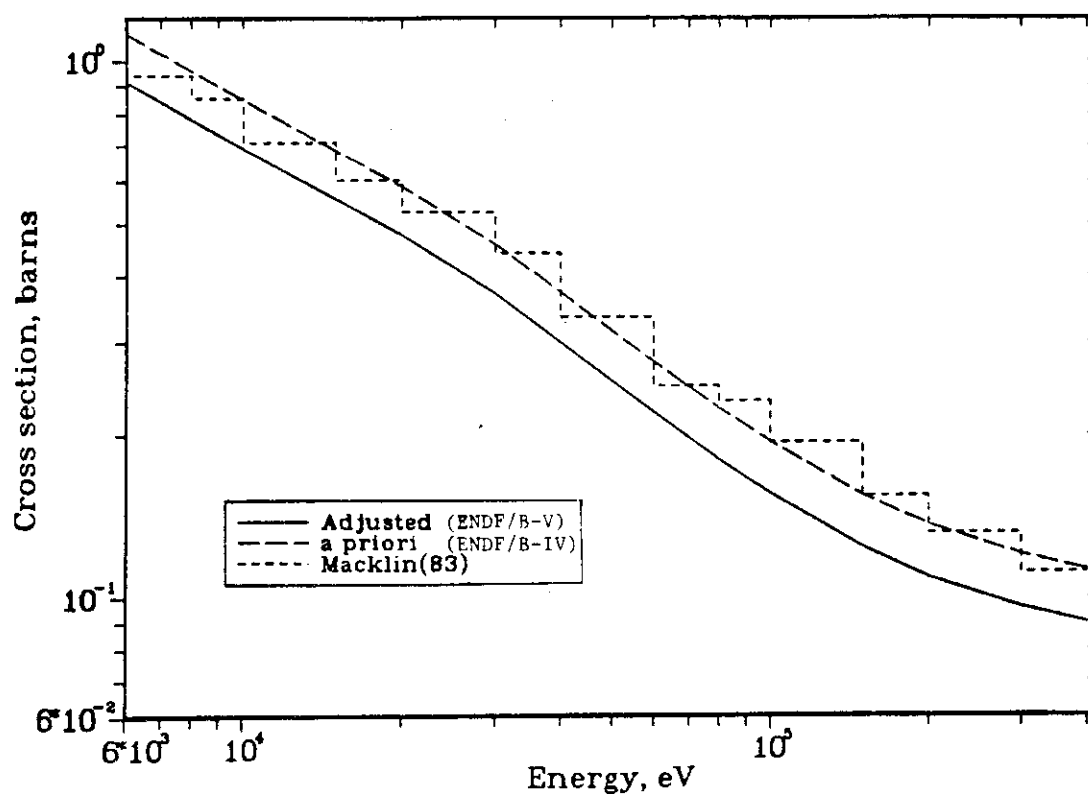


Fig. 7 I-129 Cross section evaluation: an example of the influence of integral data.

V. CONCLUDING REMARKS

We have summarized the fission product and actinide data in ENDF/B-IV and -V, and the needed (and partially planned) improvements in these files. These data have been used in a wide spectrum of studies varying from antineutrino spectra to mundane problems in waste disposal and economic studies of the production of useful radioactive nuclides. The data have been used to calculate some needed integral quantities that had no measurement such as delayed neutrons from several fuels. The economic value of this data base is probably best illustrated by its use in answering many questions during the progress of, and following, the TMI-2 accident.³³ Yet we are very aware of the needed data expansions and improvements for other uses and have attempted to list these in this report.

REFERENCES:

1. The Evaluated Nuclear Data File, Versions IV and V (ENDF/B-IV and -V), available from and maintained by the National Nuclear Data Center at Brookhaven National Laboratory, Upton, New York).
2. R. Kinsey, "Data Formats and Procedures for the Evaluated Nuclear Data File, ENDF, "Brookhaven National Laboratory report BNL-NCS-50496 (ENDF-102) (October 1979).
3. "Fission Product Nuclear Data (FPND)-1977," Proceedings of the Second Advisory Group Meeting on Fission Product Nuclear Data, Energy Centrum Netherlands, Petten, The Netherlands, September 5-9, 1977 (IAEA-213).
4. T. R. England, R. E. Schenter, and F. Schmittroth, "Integral Decay-Heat Measurements and Comparison to ENDF/B-IV and V," Los Alamos Scientific Laboratory report LA-7422-MS [NUREG/CR-0305 (August 1978)]. Also published in Proc. of the Seminar on "Nuclear Data Problems for Thermal Reactor Applications," Brookhaven National Laboratory, May 22-24, 1978. [EPRI-NP-1098, BNL-NC-25047 (ENDF 270), June 1979.]
5. R. E. Schenter, F. Schmittroth, and T. R. England, "Integral Determinations of Fission Product Inventory and Decay Power," Review Paper published in Proc. IAEA Second Advisory Group Meeting on FPND, Petten, The Netherlands, IAEA-213 (September 1977).
6. E. M. Bohm, et. al., Ed., "Benchmark Testing of ENDF/B-IV," Brookhaven National Laboratory report BNL-NCS-21118 (ENDF-230) (March 1976).
7. T. R. England and R. E. Schenter, "ENDF/B-IV Fission-Product Files: Summary of Major Nuclide Data," Los Alamos Scientific Laboratory report LA-6116-MS (ENDF-223) (October 1975).
8. B. F. Rider and M. E. Meek, "Compilation of Fission Product Yields," General Electric Company report NEDO-12154-2(E) (June 1976).
9. P. F. Rose and T. W. Burrows, "ENDF/B Fission Product Decay Data," Brookhaven National Laboratory report BNL-NCS-50545 (ENDF-243) (August 1976).
10. C. W. Reich, "Status of Beta- and Gamma-Decay and Spontaneous-Fission Data from Transactinium Isotopes," Idaho National Engineering Laboratory report ANCR-1299 (April 1976).
11. C. W. Reich, "Application of Fission Product Decay Data," Proc. of Isotope On-Line Separator Workshop, Brookhaven National Laboratory, October 31-November 1, 1977, Brookhaven National Laboratory report BNL 50847 (1978).
12. R. L. Bunting and C. W. Reich, "Evaluation Procedures for Experimental Decay Data," Proc. Conf. on Nuclear Data Evaluation Methods and Procedures, Brookhaven National Laboratory, September 22-25, 1980, Brookhaven National Laboratory report BNL-NCS-51363 (March 1981).
13. F. Schmittroth, "Theoretical Estimates of Decay Information for 'Non-Experimental' Nuclides," Proc. Conf. on Nuclear Data Evaluation Methods and Procedures, Brookhaven National Laboratory, September 22-25, 1980, Brookhaven National Laboratory report BNL-NCS-51363 (March 1981).

14. B. F. Rider, T. R. England, D. G. Madland, J. R. Liaw, and R. E. Schenter, "Evaluation of Fission Product Yields for the U. S. National Nuclear Data Files," Proc. Conf. on Nuclear Data Evaluation Methods and Procedures, Brookhaven National Laboratory, September 22-25, 1980, BNL-NCS-51363 (March 1981).
15. T. R. England and B. F. Rider, "Status of Fission Yield Evaluations," Proc. Specialists' Meeting on Yields and Decay Data for Fission Product Nuclides," Brookhaven National Laboratory, October 24-27, 1983 (sponsored by the OECD/NEA Nuclear Data Committee) (to be published). Los Alamos National Laboratory document LA-UR 83-3531.
16. R. J. LaBauve, T. R. England, and D. C. George, "Integral Data Testing of ENDF/B Fission Product Data and Comparisons of ENDF/B with Other Fission Product Data Files," Los Alamos National Laboratory report LA-9090-MS (ENDF-320) (November 1981).
17. C. R. Weisbin, et al., Ed., "Benchmark Data TEsting of ENDF/B-V," Brookhaven National Laboratory report BNL-NCS-31531 (ENDF-311) (August 1982).
18. R. E. Schenter and T. R. England, "ENDF/B-V Fission Product Cross Section Evaluations," Proc. of NEANDC Specialists' Meeting on Neutron Cross Sections of Fission Product Nuclei, Bologna, Italy, December 12-14, 1979, [NEANDC(E) 209 "L"], p. 253.
19. W. B. Wilson, R. J. LaBauve, and T. R. England, "Calculation of Spent Thermal Reactor Fuel Nuclide Inventories in Comparison with Measurements," Proc. Conf. on Thermal Reactor Benchmark Calculations, Techniques, Results, and Applications, Brookhaven National Laboratory, May 17-18, 1982. Electric Power Research Institute report EPRI NP-2855 (February 1983).
20. T. R. England, W. B. Wilson, R. E. Schenter, and F. M. Mann, "ENDF/B-V Summary Data for Fission Products and Actinides," to be published by the Electric Power Research Institute (ENDF-322) (March 1984).
21. T. Yamamoto, M. Akiyama, Z. Matumoto, and R. Nakasima, "JNDC FP Decay Data File," Japan Atomic Energy Research Institute report JAERI M 9357, February 1981.
22. T. Yoshida, M. Akiyama, Z. Matumoto, J. Katakura, and R. Nakasima, "Decay Heat Data Needs," invited paper to be published in Proc. of the Specialists' Meeting on Yields and Data Decay for Fission Product Nuclides, October 24-27, 1983, Brookhaven National Laboratory (sponsored by the OECD/NEA Nuclear Data Committee).
23. J. C. Hardy, L. C. Carray, B. Johnson, and P. G. Hansen, "The Essential Decay of Pandemonium: A Demonstration of Errors in Complex Beta-Decay Schemes," Phys. Lett. 71B, No. 2 (November 1977).
24. T. Yoshida, "Estimation of Nuclear Decay Heat for Short-Lived Fission Products," Nucl. Sci. Eng. 63, 376-390 (1977). [See also K. Takahashi and M. Yamada, Prog. Theor. Phys. 41, 1470 (1969) and S. Kayama, K. Takahashi, and M. Yamada, Prog. Theor. Phys. 44, 663 (1970).

25. F. M. Mann, C. Dunn, and R. E. Schenter, Trans. Am. Nucl. Soc. 39, 880 (1981). [See also Phys. Rev. C25, 524 (1982).]
26. F. M. Mann, M. Schreiber, R. E. Schenter, and T. R. England, "Evaluation of Neutron Precursor Data," submitted to Nucl. Sci. and Eng. (1984).
27. T. R. England, W. B. Wilson, R. E. Schenter, and F. M. Mann, "Aggregate Delayed Neutron Intensities and Spectra Using Augmented ENDF/B-V Precursor Data," Nucl. Sci. Eng. 62, 139-155 (October 1983).
28. P. G. Young and E. D. Arthur, "GNASH: A Preequilibrium-Statistical Nuclear Model Code for Calculations of Cross Sections and Emission Spectra," Los Alamos Scientific Laboratory report LA-6947 (November 1977).
29. J. Raynal, "Optical Model and Coupled-Channel Calculations in Nuclear Physics," International Atomic Energy Agency report IAEA SMR-9/8 (1970).
30. RESPARFM Code, unpublished. (Private communication from F. M. Mann, Hanford Engineering Development Laboratory, to T. R. England).
31. F. Schmittroth and R. E. Schenter, "Finite Element Basis in Beta Adjustment," Nucl. Sci. Eng. 74, 168 (1980).
32. F. M. Mann, "HAUSER*5, A Computer Code to Calculate Nuclear Cross Sections," Hanford Engineering Development Laboratory report HEDL-TME 78-83, (1978). (HAUSER*6 code is still under development.)
33. T. R. England and W. B. Wilson, "TMI-2 Decay Power: LASL Fission-Product and Actinide Decay Power Calculations for the President's Commission on the Accident at Three Mile Island," Los Alamos Scientific Laboratory report LA-8041-MS (October 1979) (Rev. March 1980). Note: Elemental values are given in Los Alamos National Laboratory report LA-9622-MS.

I-2 EVALUATION OF FISSION PRODUCT NEUTRON CROSS SECTIONS FOR JENDL

Fission-Product Neutron Cross Section Evaluation Working Group
Japanese Nuclear Data Committee

Japan Atomic Energy Research Institute
Tokai-mura, Naka-gun, Ibaraki-ken, Japan

I. Integral Test of JENDL-1 Fission-Product Neutron Cross Sections

JENDL-1 fission product cross section file (including additional library Version 1.5) contains neutron cross sections for 67 nuclides. Details of JENDL-1 and comparison with other recent evaluated data files are described in Ref. 1.

An extensive integral test was performed using the CFRMF sample activation data and STEK sample reactivity data. Results of test for CFRMF activations and for strong absorber reactivities in STEK were reported at the Bologna meeting, 1979. (Ref. 2.)

After that, a tentative analysis was performed for weak absorber samples of STEK measurements by applying the correction to the calculated scattering reactivity component based on the measured reactivities of scatterer samples. The measured (positive) reactivities of scatterer samples such as carbon, aluminum, aluminum oxide, lead and lead oxide, were compared with calculation. The experiment-to-calculation ratios were nearly constant and about 1.2 for all of the above samples and core spectra, except for the lead sample in STEK-1000 and -500 cores. This is shown in Fig. 1.

Since the scattering cross sections of these nuclides are considered as well known, the discrepancy may be regarded as the result of inaccuracy of neutron spectra of STEK cores, or rather that of neutron adjoint spectra used in calculation. Therefore, the factor 1.2 was applied to all of the calculated scattering reactivity component to obtain the corrected total reactivity of weak absorber sample. Examples of results before and after correction are shown in Fig. 2. In most cases, we obtained a better agreement with experiments after applying this correction. The result for Zr-93 shows that JENDL-1 Zr-93 capture cross section is too large by about a factor of 2. (ENDF/B or RCN-2 data are more consistent with STEK integral data.) In case of La, the inelastic cross section is probably overestimated by about 30 %, because the adopted levels at 0.57, 0.83, 0.93 and 1.07 MeV, based on the Nuclear Data Sheets 1974, are not confirmed in a later version of NDS, and therefore have to be discarded. (Ref. 1.)

The results of integral test are summarized in Table 2, together with the observations from the comparison with recent differential capture data.

II. Evaluation of JENDL-2 FP Neutron Cross Sections

Evaluation for JENDL-2 is at a final stage. It will contain 100 nuclides from Kr to Tb. The following improvements in data and method are made compared to JENDL-1.

*) Working group members: Kawai, M. (group leader, NAIG), Iijima, S. (NAIG), Kikuchi, Y. (JAERI), Nakajima, Y. (JAERI), Nakagawa, T. (JAERI), Watanabe, T. (Kawasaki Heavy Industries), Sasaki, M. (MAPI), Aoki, T. (Fuji Electric Co.), Matsunobu, H. (Sumitomo Atomic Industry), Zukeran, A. (Hitachi), Nishigori, T. (Osaka Univ.)

- (1) Integral test results are reflected on evaluation.
- (2) Recent differential capture data are taken into account. Resonance parameters are re-evaluated using recent resonance data.
- (3) The spherical optical model parameters and the level density parameters were re-determined. (Ref. 3 and 4.) The systematics of level density parameters and gamma-ray strength functions were studied in detail to estimate these values for nuclides whose experimental data were lacking.
- (4) Level scheme data were revised based on the evaluation by Nakasima, R. and Matsumoto, Z. (priv. comm.), and on Table of Isotopes, 7-th ed.
- (5) The maximum energy of unresolved resonance region was extended from 50 keV to 100 keV, where self-shielding factor can be calculated from unresolved resonance parameters.
- (6) An auxiliary program JOBSETTER (Ref. 5) for the statistical model calculation was developed which utilizes the input parameter data base to a maximum extent. This is to simplify the input procedure and improve the quality control of the evaluation.

III. Near-Future Scope

Integral test is scheduled using the data at CFRMF, STEK and EBR-II. Adjustment of cross section is also planned, especially for nuclides for which differential capture data are not available. These are, Zr-93, some of Xe isotopes, Ce-142, Pm-147, Eu-152 and -154. Cross section covariance will be generated by the statistical theory calculation using the method of Gruppelaar. Both capture cross section and the statistical model parameters will be adjusted.

References :

- (1) Kikuchi, Y., Nakagawa, T., Matsunobu, H., Kawai, M., Igarasi, S., Iijima, S.: JAERI-1268 (1981). See also, Iijima, S.: IAEA-213 (1978)p.165
- (2) Iijima, S., Watanabe, T., Yoshida, T., Kikuchi, Y., Nishimura, H.: NEANDC(E)209"L"(1979) p.317
- (3) Iijima, S., Kawai, M.: J.Nucl.Sci.Technol. 20(1983)77
- (4) Iijima, S., Yoshida, T., Aoki, T., Watanabe, T., Sasaki, M.: J.Nucl.Sci.Technol. 21(1984)10
- (5) Nakagawa, T.: Nuclear Data Center, Internal Memo. (1980)

Table 1 Summary of Comparison of JENDL Fission Product Neutron Cross Sections with Integral and Differential Data^{a)}

	STEK Reactivity Data	CERMF Activation Data	Recent Differential Data	Discre- pancy
Zr 91	CVE (ρ : small)		~ 1.2	
93	capture: too large (factor of 2)			
Nb 93	1.0-1.06	0.68 ($\pm 50\%$)	~ 1.0	
Mo nat	0.97-1.1			
95	0.95-1.05		~ 1	
97	0.95-1.1		~ 1	
98	capture: too large	1.24 ($\pm 6\%$)	$\sim 1 \sim 1.2$	
100	~ 1 (ρ : small)	0.89 ($\pm 17\%$)	~ 0.8	
Tc 99	0.85-0.9	1.21 ($\pm 15\%$)	~ 0.9	\times
Ru 101	0.95-1.1		~ 1.2	
102	capture: too large	1.58 ($\pm 7\%$)	~ 1.5	
104	CVE (ρ : small)	1.17 ($\pm 6\%$)	~ 1	\times
Rh 103	~ 1.0	0.98 ($\pm 24\%$)	~ 1	
Pb 105	0.8		~ 0.8	
107	0.8 (low enrichment)			
108	1.1-1.3 (ρ : small)*	0.82 ($\pm 7\%$)*	~ 0.8	
110	CVE (ρ : small)		~ 0.6	
Ag 107		0.99 ($\pm 19\%$)	$\sim 1 \sim 1.1$	
109	~ 1 (scattering among exp. data)	1.03 ($\pm 10\%$)	~ 1.4	\times
I 127	0.95-1.05	1.23 ($\pm 10\%$)	~ 1	
129	1.3-1.5	1.49 ($\pm 7\%$)	$\sim 1.1 \sim 1.2$	\times
Xe 131	1.04 \sim 1.30			
132		1.11 ($\pm 7\%$)*		
134		1.15 ($\pm 7\%$)*		
Cs 133	0.8-0.9	1.01 ($\pm 7\%$)	~ 1.0	solved
135	0.9-1.0 (low enrich- ment)			
137		not yet analyzed		
La 139	CVE (ρ : small)	1.21 ($\pm 5\%$)	$\sim 1 \sim 1.2$	

a) Table gives the ratio of JENDL or JENDL calculation to measurement.

*) ENDF/B-4 cross sections were used.

JAERI-M 84-182
Table 1 (continued)

	STEK Reactivity Data	CFRMF Activation Data	Recent Differential Data	Discre- pancy
Ce 140	capture: too large (ρ : small)			
142	capture: too large (ρ : small)	2.05($\pm 7\%$)		
Pr 141	C/E (ρ : small)	0.92($\pm 15\%$)	$\approx 0.9 \sim 1.0$	
Nb 142	capture: too large (ρ : small)*			
143	0.9		≈ 0.85	
144	C/E (ρ : small)		≈ 1.1	
145	0.7*		$\approx 0.6 \sim 0.7$	
146	C/E (ρ : small)	1.00($\pm 7\%$)	≈ 0.85	x
148	capture: too large (ρ : small)	1.49($\pm 14\%$)	≈ 1.2	x
150	C/E (ρ : small)	1.84($\pm 12\%$)	1.2 \sim 2	
Pm 147	0.95	1.13($\pm 13\%$)		x
Sm 147	0.95-1.05		0.85 \sim 1.0	
148	1.0-1.5		1 \sim 1.2	
149	0.9-1.1		≈ 0.75	x
150	0.9-1.2		≈ 1.0	
151	1.0-1.1 (low enrich- ment)			
152	≈ 0.9 -1.1	1.19($\pm 6\%$)	1 \sim 1.2	
154	≈ 1 (scattering among exp. data)	1.25($\pm 5\%$)	1 \sim 1.3	
Eu nat	0.8-1.05			
151		0.87($\pm 6\%$)	0.6-0.8	x
153	0.9-1.05*	0.96($\pm 7\%$)*	0.6-1.1	x
Gd 156	0.9 \sim 1.4 (scattering among exp. data)			
157	≈ 1.1			
158		1.01($\pm 12\%$)*		
160		1.51($\pm 9\%$)*		
Pu 239	$\approx 1.0^{**}$	0.97(n,f)**		
U 235	1.0-1.1**	[1.000(n,f)]		
U 238		1.04(n,f)**		
		1.07(n, γ)**		
B nat	≈ 1.0			

**) JENDL-2A (preliminary version of JENDL-2) values.

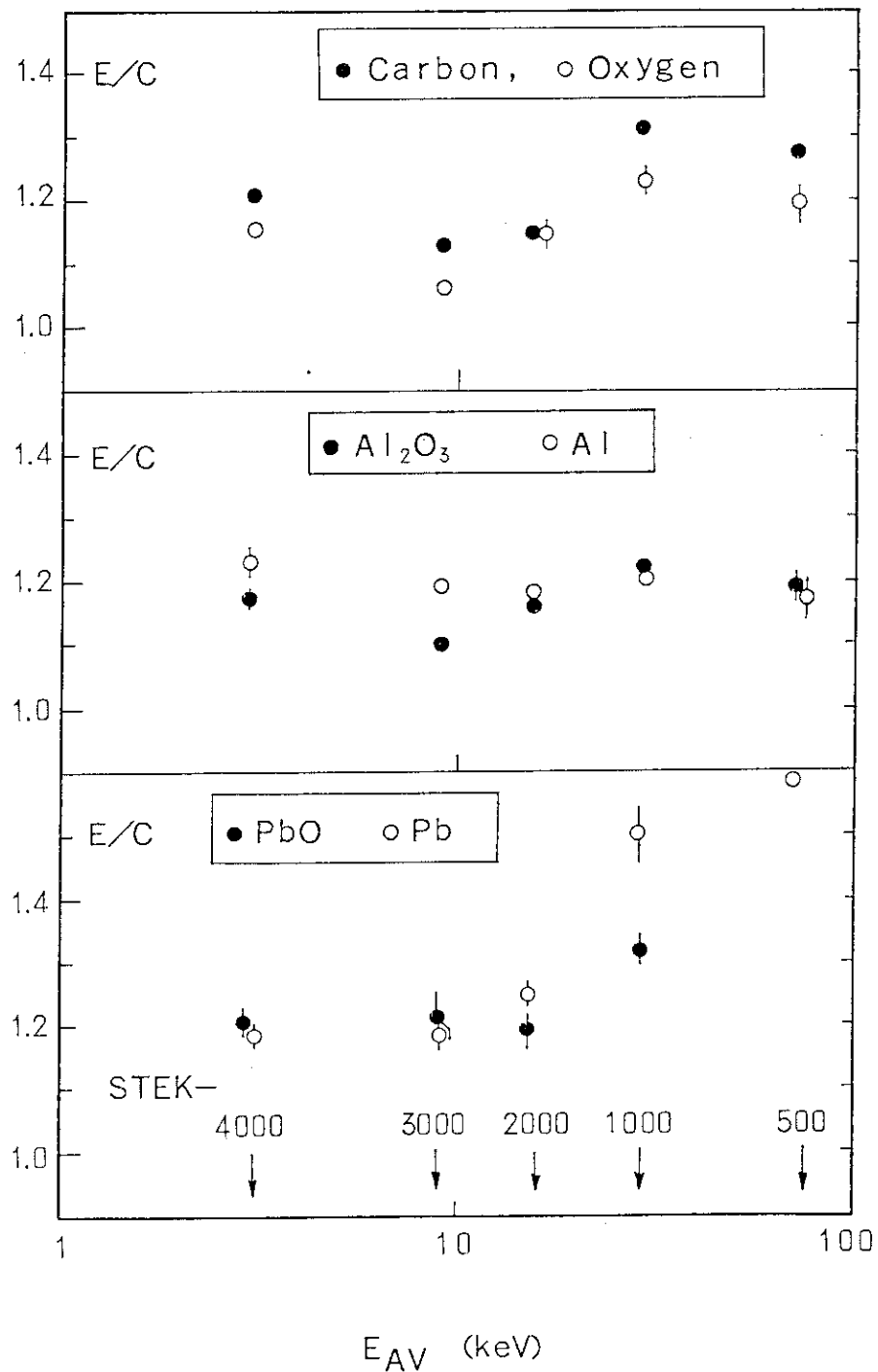


Fig. 1 Experiment-to-calculation ratios for scatterer sample reactivities in STEK cores. Each STEK core is designated by the arrow at the bottom of figure, which indicates the average energy E_{AV} of the neutron spectrum of the core, defined by,

$$1/\sqrt{E_{AV}} = \int (1/\sqrt{E}) \phi(E) dE / \int \phi(E) dE .$$

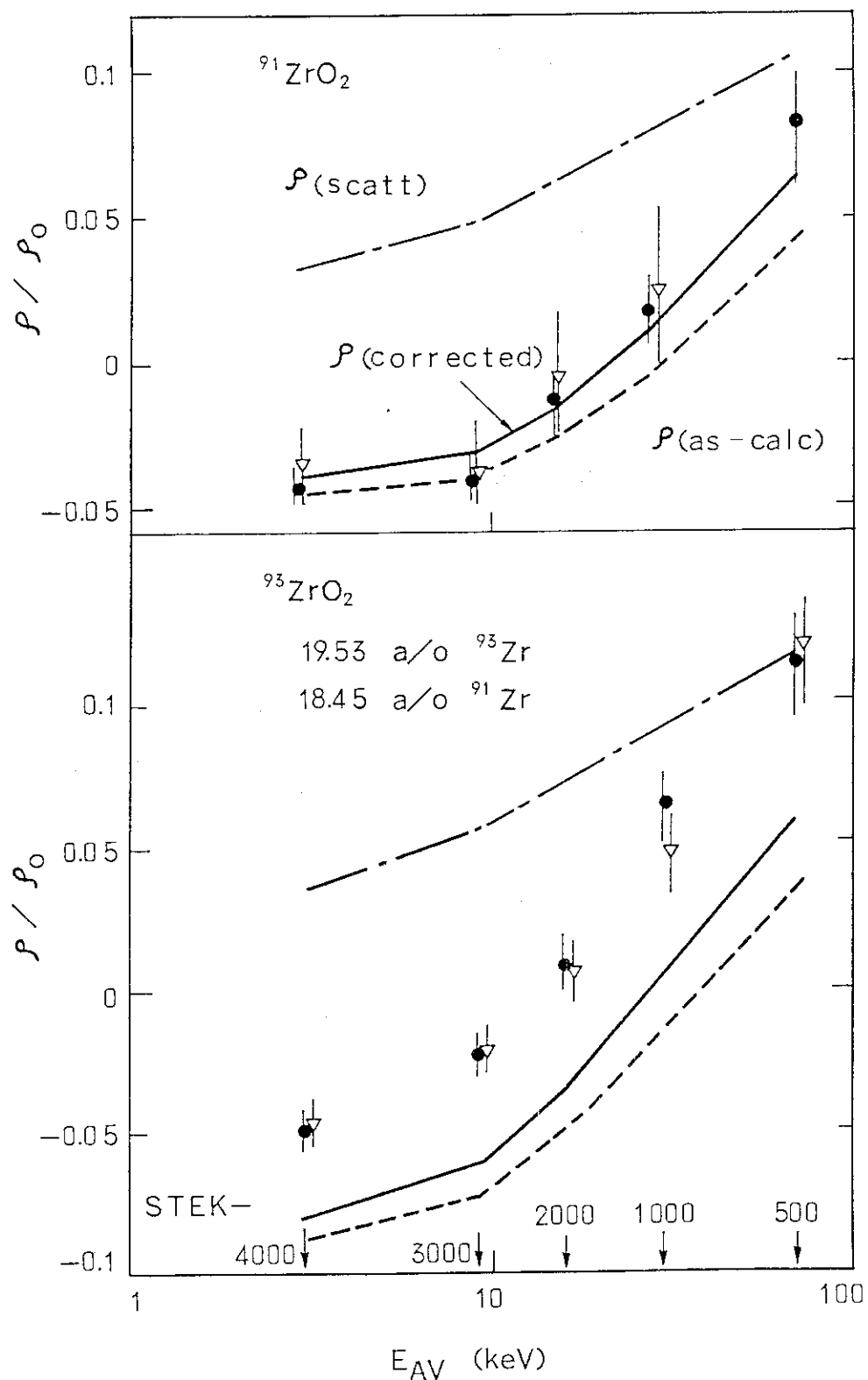


Fig. 2 Comparison of calculation and experiment of weak absorber sample reactivities in STEK cores. Experimental data are shown only for samples of typical sizes. The broken and dashed lines are the as-calculated values of scattering and total reactivities, resp. The solid line is the corrected total reactivity obtained by multiplying the scattering reactivity component by a factor of 1.2. The calculation-to-experiment ratios for available CFRMF activation data are also given.

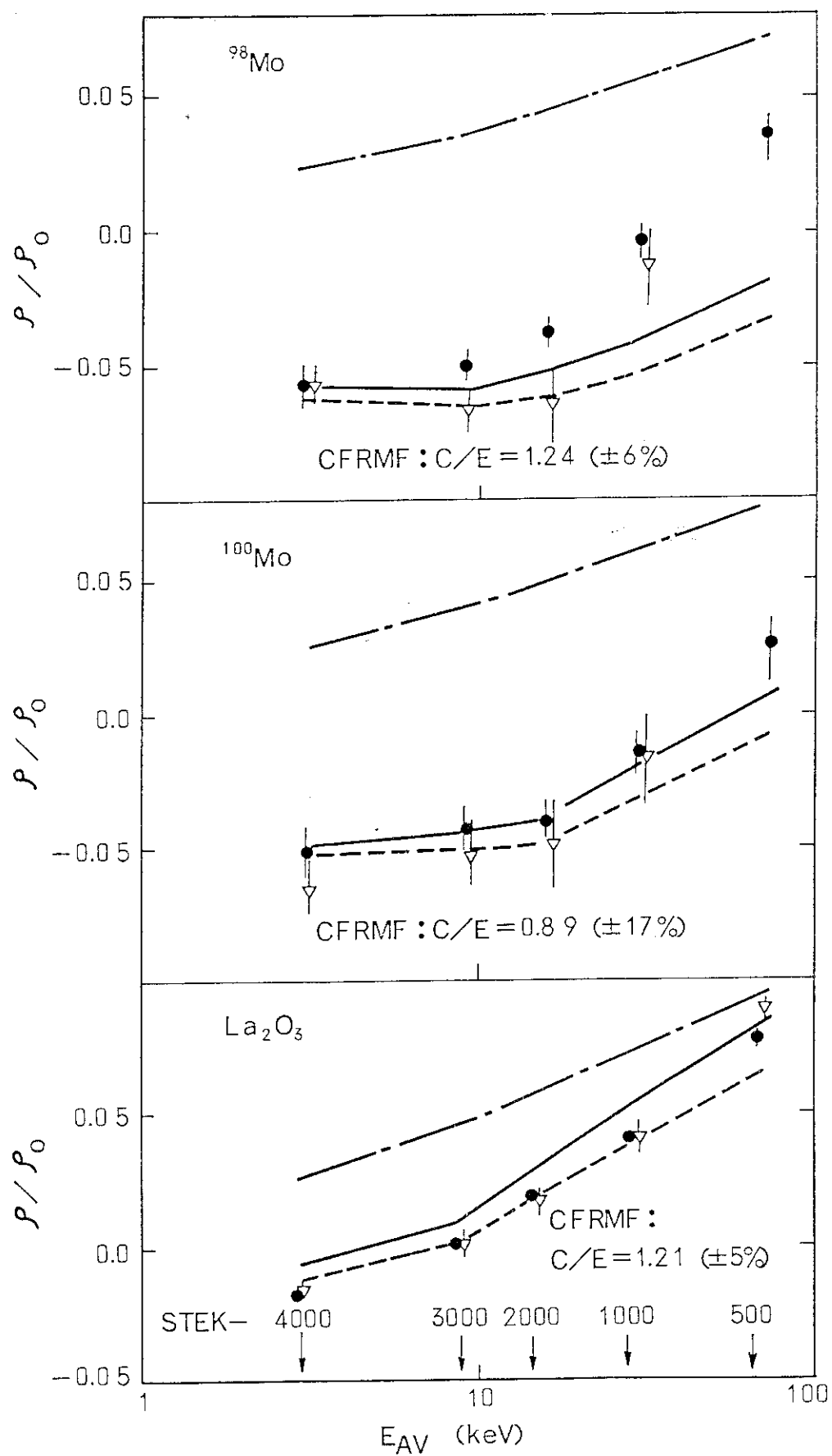


Fig. 2 (continued)

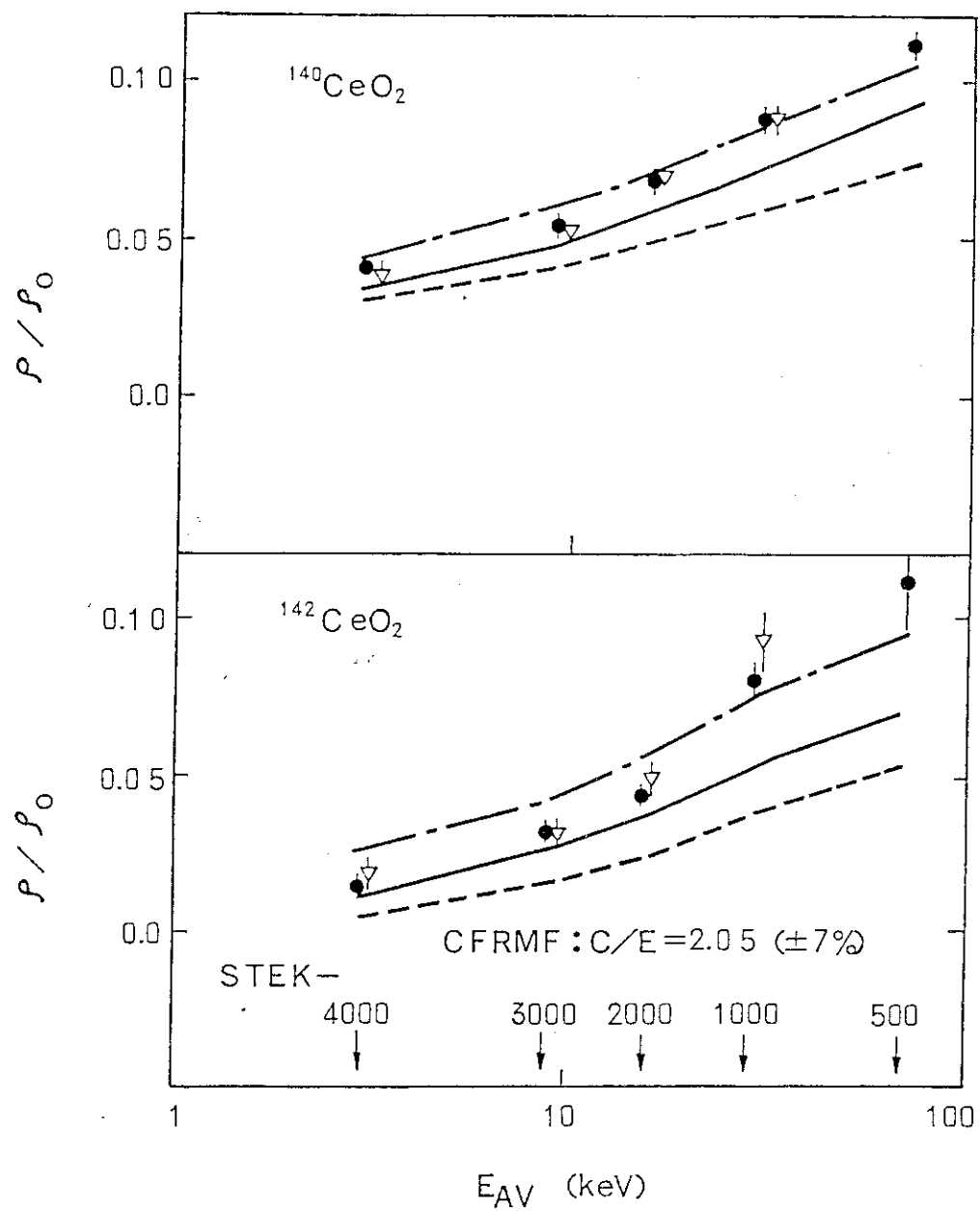


Fig. 2 (continued)

I-3 PRESENT STATUS AND FUTURE PROGRAMS OF EVALUATION OF DECAY HEAT FOR FISSION PRODUCTS IN JAPAN

Decay Heat Evaluation Working Group
Japanese Nuclear Data Committee

Japan Atomic Energy Research Institute
Tokai-mura, Naka-gun, Ibaraki-ken, Japan

I. JNDC Decay Data File, Version 1

JNDC Version 1 file contains the decay data and fission yield data for 1172 nuclides and the neutron cross section data for 80 nuclides in fission product mass region. Details of this file and the results of comparison of decay heat calculation with recent measurements (Refs. 1-3) have been reported in Refs. 4-7. The file is based on recent measurements and compilation of decay data and fission yields. A particular feature is the full use of the gross theory of beta-decay to estimate the energy-release data of all nuclides (except Y-96) with Q-values larger than 5 MeV. (Ref. 8,9.)

Calculated decay powers for fission pulse from U-235 and Pu-239 are shown in Figs. 1 through 4 in comparison with the experimental data at YAYOI. The agreement is generally very good for a wide range of fissile nuclides from Th-232 to Pu-241, especially at short cooling time and for beta decay powers. However, the gamma decay heat is underestimated for all fissile nuclides by 5 to 15 % at cooling times between 200 sec and 2000 sec, and overestimated for Th-232, U-233 and U-235 by 5 to 15 % at longer cooling time than about 2000 sec.

The calculated decay heat was fitted by 31 exponential terms. The fitted parameters are given in Table 1 for major fissile nuclides. (Ref. 6.)

II. JNDC Decay Data File, Version 1.5

To seek for the possible sources of the above-stated disagreement between calculation and experiment, an extensive sensitivity study and the comparison with other decay data files (ENDF/B-V, UKFPDD-2, ENSDF) and experimental data were made, particularly for nuclides with Q-values greater than 5 MeV and/or half-lives longer than a few tens of sec. (Ref. 7, 10).

Although significant discrepancies among the data files were noted for a number of nuclides concerning the energy-release data, the experimental data were often too uncertain for most of these nuclides to revise the evaluated data with convince. As the result, Version 1.5 was made by revising only the energy-release data of Rb-88(1068s) and La-143(852s).

In the beta-decay of Rb-88, a strong transition to the ground state is observed experimentally. The JNDC value of gamma energy-release for Rb-88 based on the gross theory was in overestimation by a factor of 4. As to the La-143 average gamma-ray energy data, JNDC value was smaller than that of ENSDF and ENDF/B-V by a factor of 3 and 20, respectively. Recent measurement at Nagoya University (Ref. 11) gives the value close to that of ENSDF. We adopted temporarily the ENSDF value as Version 1.5 data.

*) Working group members: Matumoto, Z. (Group leader, JAERI), Akiyama, M. (Tokyo Univ.), Nakasima, R. (Hosei Univ.), Tasaka, K. (JAERI), Katakura, J. (JAERI), Ihara, H. (JAERI), Yoshida, T. (NAIG), Iijima, S. (NAIG)

The calculated decay powers after revision are also shown in Figs. 1 through 4 for U-235 and Pu-239 fissions. The agreement of the calculated U-235 gamma decay power with experiment was improved significantly for cooling time longer than 2000 sec. The same is true for the case of Th-232 and U-233 fissions. Revision of Rb-88 decay data was the dominant cause of improvement. There still remains the discrepancy for cooling time between 200 sec and 2000 sec., the solution to which is not yet found successfully.

Incidentally, the gamma decay powers for 14MeV neutron fissions of U-235, U-238 and Th-232 were also measured at YAYOI (Ref. 2). These data are of interest not only for the application to a fusion-fission hybrid reactor, but as a basic application of high energy fission yield data. Figures 5 and 6 compare the measured data for fast and 14 MeV fissions of U-238 and Th-232, respectively, together with the calculation using JNDC 1.5 file. Very large disagreement between calculation and experiment for fast fission of thorium at intermediate cooling time is striking. It was found very recently that the disagreement disappeared almost completely after correcting the experimental data for the decay of Th-233 (22.3m) produced by neutron capture of Th-233 (13).

III. Future Scope

The following works are planned for the near future.

- (1) Identification of the discrepancy source of gamma decay heat for cooling time between 200 sec and 2000 sec.
- (2) Addition and elaboration of decay data of short-lived nuclides.
- (3) Evaluation of gamma-ray spectrum based on the measured data (Ref.12) and calculation.
- (4) Re-evaluation of delayed neutron data.

References :

- (1) Akiyama,M., Furuta,T., Ida,T., Sakata,K., An,S. : J. At. Energy Soc., Japan, 24 (1982) 709, and 803 (in Japanese)
- (2) Akiyama,M., An,S. : Paper present at OECD/NEANDC Mtg. on Yield and Decay Data of Fission Product Nuclides, Brookhaven (1983)
- (3) Dickens, J.K., Love,T.A., McConnel,J.W., Peele,R.W.: Nucl. Sci. Eng. 74 (1980) 106, and 78 (1981) 126
- (4) Yamamoto,T., Akiyama,M., Matumoto,Z., Nakasima,R: "JNDC FP Decay Data File", JAERI-M 9357 (1981)
- (5) Ihara,H., et al.: "JNDC FP Decay and Yield Data", JAERI-M 9715 (1981)
- (6) Tasaka,K., et al.: "JNDC Nuclear Data Library of Fission Products", JAERI 1287 (1983)
- (7) Yoshida, T. et al.: Paper presented at OECD/NEANDC Mtg., Brookhaven (1983), loc. cit.
- (8) Yoshida,T.: Nucl.Sci.Eng. 63(1977)376
- (9) Yoshida,T., Nakasima,R.: J.Nucl.Sci.Technol. 18(1981)393
- (10) Katakura,J., et al.: JAERI-M report (1984) (to be published)
- (11) Yamamoto, H., et al. : J. Inorg. Nucl. Chem. 43 (1981) 855
- (12) Akiyama,M. : Private communication
- (13) Akiyama,M. : Comment in this Topical Discussion.

Table 1 Exponential fit parameters for the calculated beta, gamma, and total sensible decay powers after a fission pulse

U-235 (T)				U-238 (T)				Pu-239 (T)					
NO.	LAMBDA	ALPHA		(B+G)		BETA	GAMMA	ALPHA	(B+G)		BETA	GAMMA	(B+G)
		BETA	GAMMA	BETA	GAMMA				BETA	GAMMA			
1	3.290E+00	5.255E-02	3.121E-02	8.376E-02	2.278E-01	1.436E-01	3.714E-01	1.603E-03	5.259E-04	2.129E-03	1.603E-03	5.259E-04	2.129E-03
2	2.210E+00	7.112E-02	4.500E-02	1.161E-01	3.848E-02	3.203E-02	7.051E-02	3.868E-02	3.467E-02	7.335E-02	3.868E-02	3.467E-02	7.335E-02
3	1.001E+00	2.145E-01	1.288E-01	3.433E-01	4.858E-01	2.589E-01	7.447E-01	1.093E-01	5.217E-02	1.615E-01	1.093E-01	5.217E-02	1.615E-01
4	5.157E-01	9.898E-02	7.654E-02	1.755E-01	1.655E-01	1.698E-01	3.353E-01	1.071E-01	8.151E-02	1.887E-01	1.071E-01	8.151E-02	1.887E-01
5	2.951E-01	1.183E-01	7.821E-02	1.965E-01	2.656E-01	1.194E-01	3.849E-01	6.652E-02	2.204E-02	8.856E-02	6.652E-02	2.204E-02	8.856E-02
6	1.959E-01	8.540E-02	5.550E-02	1.409E-01	1.379E-01	1.277E-01	2.657E-01	5.950E-02	5.547E-02	1.150E-01	5.950E-02	5.547E-02	1.150E-01
7	1.037E-01	1.008E-01	5.269E-02	1.535E-01	1.402E-01	6.154E-02	2.018E-01	7.194E-02	2.981E-02	1.018E-01	7.194E-02	2.981E-02	1.018E-01
8	3.488E-02	2.441E-02	2.173E-02	4.614E-02	2.874E-02	2.947E-02	5.821E-02	1.907E-02	1.679E-02	3.586E-02	1.907E-02	1.679E-02	3.586E-02
9	1.330E-02	9.589E-03	1.328E-02	2.287E-02	1.125E-02	1.540E-02	2.665E-02	8.878E-03	1.112E-02	2.000E-02	8.878E-03	1.112E-02	2.000E-02
10	5.004E-03	1.796E-03	2.160E-03	3.956E-03	2.639E-03	3.025E-03	5.664E-03	1.492E-03	1.104E-03	2.596E-03	1.492E-03	1.104E-03	2.596E-03
11	3.591E-03	5.027E-04	6.555E-04	1.158E-03	1.955E-04	2.385E-04	4.340E-04	6.189E-04	7.177E-04	1.337E-03	6.189E-04	7.177E-04	1.337E-03
12	1.357E-03	6.026E-04	4.945E-04	1.097E-03	6.907E-04	5.162E-04	1.207E-03	6.595E-04	3.732E-04	1.033E-03	6.595E-04	3.732E-04	1.033E-03
13	5.645E-04	3.274E-04	3.220E-04	6.495E-04	3.320E-04	3.391E-04	6.711E-04	3.175E-04	3.699E-04	6.873E-04	3.175E-04	3.699E-04	6.873E-04
14	1.850E-04	5.409E-05	1.490E-04	2.031E-04	5.054E-05	1.385E-04	1.890E-04	4.589E-05	1.237E-04	1.696E-04	4.589E-05	1.237E-04	1.696E-04
15	5.435E-05	5.784E-06	3.753E-05	3.174E-05	-7.489E-06	2.093E-05	1.344E-05	-2.793E-06	9.851E-06	7.058E-06	1.259E-05	2.019E-06	1.461E-05
16	4.918E-05	1.982E-05	-1.812E-05	1.696E-06	1.889E-05	-6.124E-06	1.277E-05	1.259E-05	2.019E-06	1.461E-05	1.259E-05	2.019E-06	1.461E-05
17	1.922E-05	3.969E-06	4.361E-06	8.329E-06	3.422E-06	4.002E-06	7.424E-06	3.058E-06	3.366E-06	6.424E-06	3.058E-06	3.366E-06	6.424E-06
18	8.422E-06	8.295E-07	8.308E-07	1.660E-06	8.285E-07	7.838E-07	1.612E-06	8.798E-07	9.349E-07	1.815E-06	8.798E-07	9.349E-07	1.815E-06
19	2.443E-06	1.643E-07	2.972E-07	4.615E-07	1.863E-07	3.634E-07	5.497E-07	1.938E-07	3.831E-07	5.769E-07	1.938E-07	3.831E-07	5.769E-07
20	6.925E-07	8.885E-09	1.151E-07	1.240E-07	6.507E-09	7.620E-08	8.271E-08	1.300E-08	7.003E-08	8.304E-08	1.300E-08	7.003E-08	8.304E-08
21	6.202E-07	5.200E-08	8.412E-09	6.041E-08	4.998E-08	4.144E-08	9.143E-08	4.240E-08	4.280E-08	8.520E-08	4.240E-08	4.280E-08	8.520E-08
22	1.503E-07	1.076E-08	-1.336E-08	-2.597E-09	8.811E-09	-5.920E-09	2.891E-09	7.477E-09	-4.420E-09	3.057E-09	7.477E-09	-4.420E-09	3.057E-09
23	1.277E-07	1.645E-09	2.799E-08	2.964E-08	5.529E-10	2.005E-08	2.060E-08	-2.934E-10	1.855E-08	1.826E-08	-2.934E-10	1.855E-08	1.826E-08
24	2.714E-08	2.387E-09	-7.006E-12	2.381E-09	1.768E-09	1.002E-11	1.778E-09	1.294E-09	-4.360E-12	1.290E-09	1.294E-09	-4.360E-12	1.290E-09
25	2.251E-08	-2.527E-10	7.682E-11	-1.759E-10	6.596E-10	1.478E-10	8.074E-10	1.391E-09	2.280E-10	1.619E-09	1.391E-09	2.280E-10	1.619E-09
26	8.985E-09	1.983E-11	-3.418E-12	1.642E-11	2.383E-11	1.100E-12	2.493E-11	2.373E-11	5.261E-12	2.899E-11	2.373E-11	5.261E-12	2.899E-11
27	4.366E-09	1.648E-12	9.831E-13	2.631E-12	8.320E-13	5.263E-13	1.358E-12	3.966E-13	3.050E-13	7.015E-13	3.966E-13	3.050E-13	7.015E-13
28	7.707E-10	5.217E-11	5.572E-15	5.217E-11	2.795E-11	1.557E-13	2.811E-11	1.929E-11	7.101E-13	2.000E-11	1.929E-11	7.101E-13	2.000E-11
29	7.280E-10	8.944E-12	2.527E-11	3.422E-11	9.108E-12	2.415E-11	3.326E-11	1.022E-11	2.630E-11	3.652E-11	1.022E-11	2.630E-11	3.652E-11
30	2.430E-10	2.599E-14	1.970E-15	2.796E-14	4.349E-14	2.396E-15	4.589E-14	4.410E-14	8.124E-15	5.223E-14	4.410E-14	8.124E-15	5.223E-14
31	9.550E-15	4.677E-16	1.211E-16	5.888E-16	4.741E-16	1.382E-16	6.124E-16	5.692E-16	4.311E-16	1.000E-15	5.692E-16	4.311E-16	1.000E-15

Fitting formula is $f(t) = \sum_{i=1}^{31} \alpha_i e^{-\lambda_i t}$, where $f(t)$ is the decay power after a fission pulse at $t = 0$. α_i 's are in unit of MeV/s/fiss.

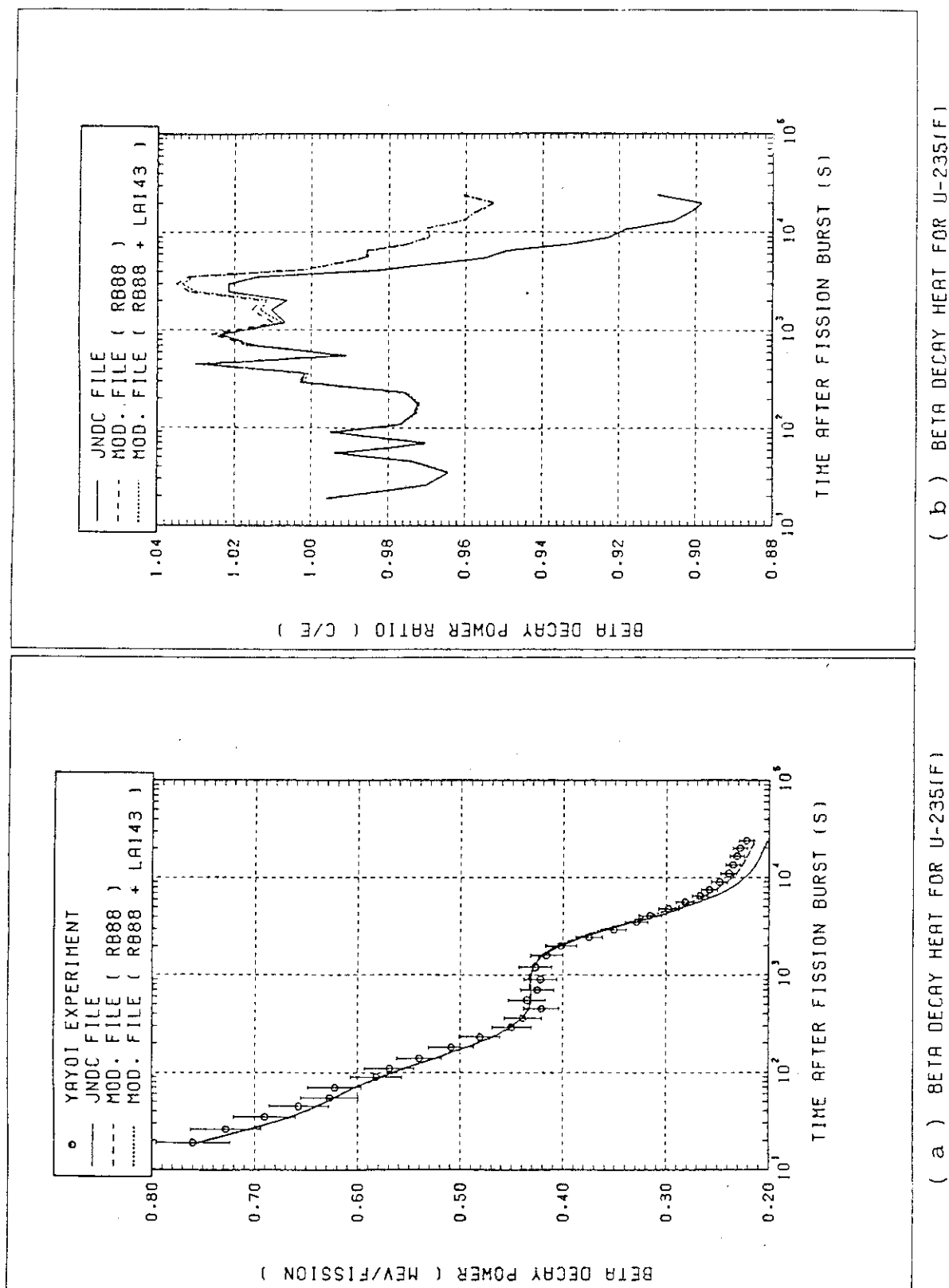


Fig. 1 Comparison of calculated beta decay power with measured results at University of Tokyo (YAYOI) for the fast neutron fission pulse of U-235. (a) Beta decay power \times time. (b) Ratio of calculation to experiment.

Solid, broken and dashed curves correspond to calculation with JNDC Version 1 library, after revision of Rb-88 data, and after revision of Rb-88 and La-143 data (Version 1.5), respectively.

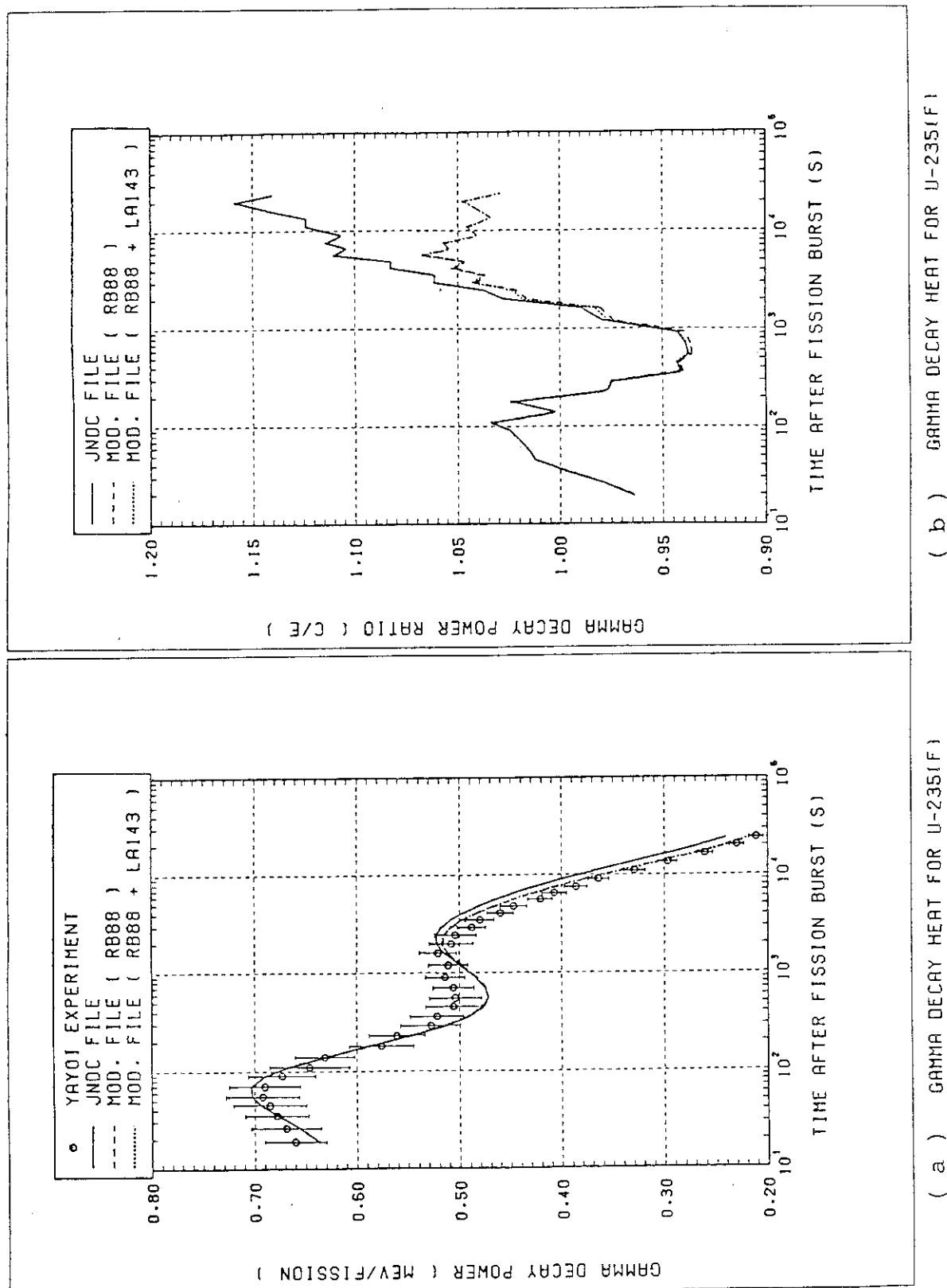


Fig. 2 Comparison of calculated gamma decay power with measured results at University of Tokyo (YAYOI) for the fast neutron fission pulse of U-235. (a) Gamma decay power \times time. (b) Ratio of calculation to experiment. See the caption to Fig. 1 for explanation of curves.

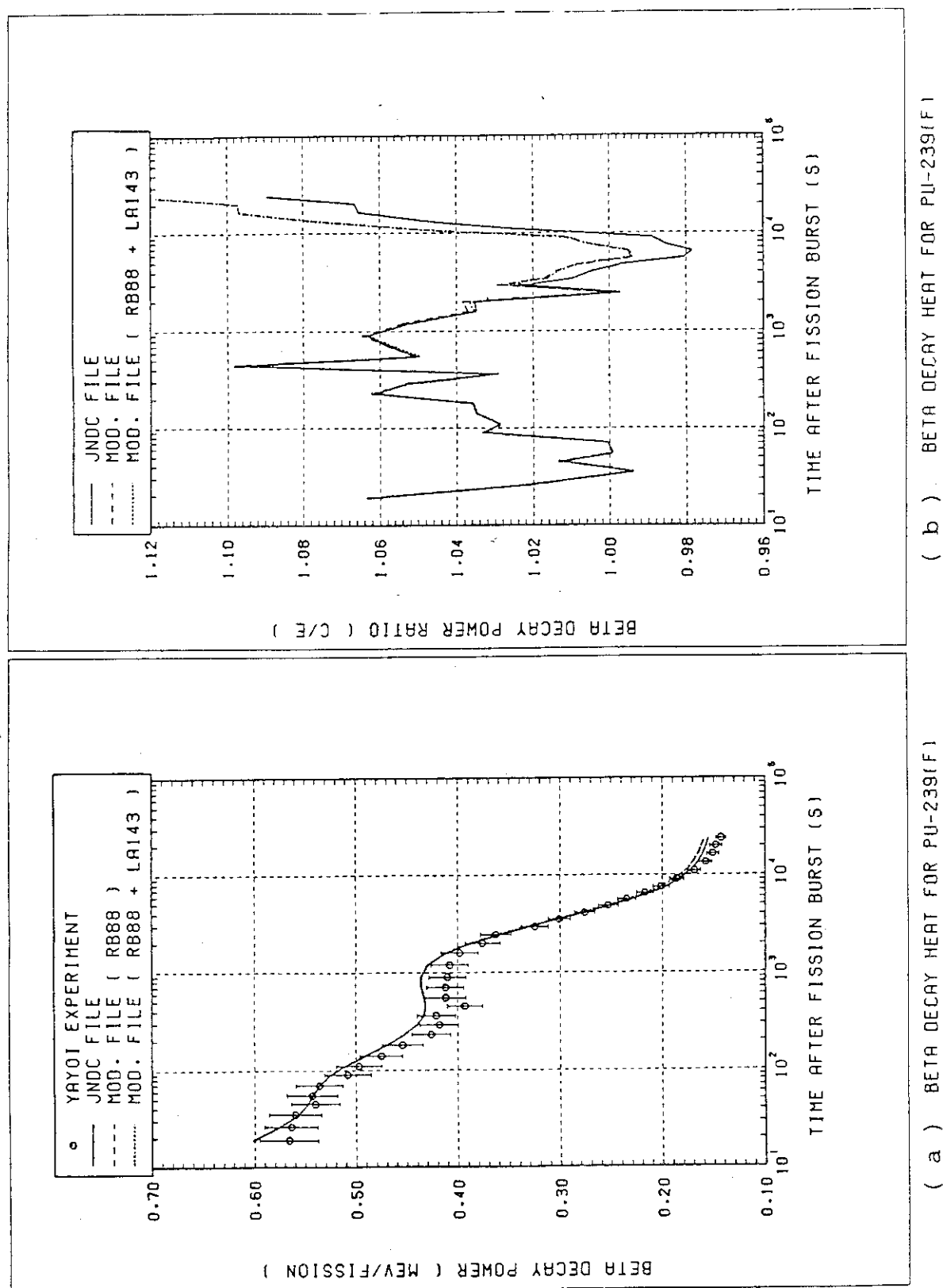


Fig. 3 Comparison of calculated beta decay power with measured results at University of Tokyo (YAYOI) for the fast neutron fission pulse of Pu-239. (a) Beta decay power x time. (b) Ratio of calculation to experiment. See the caption to Fig. 1 for explanation of curves.

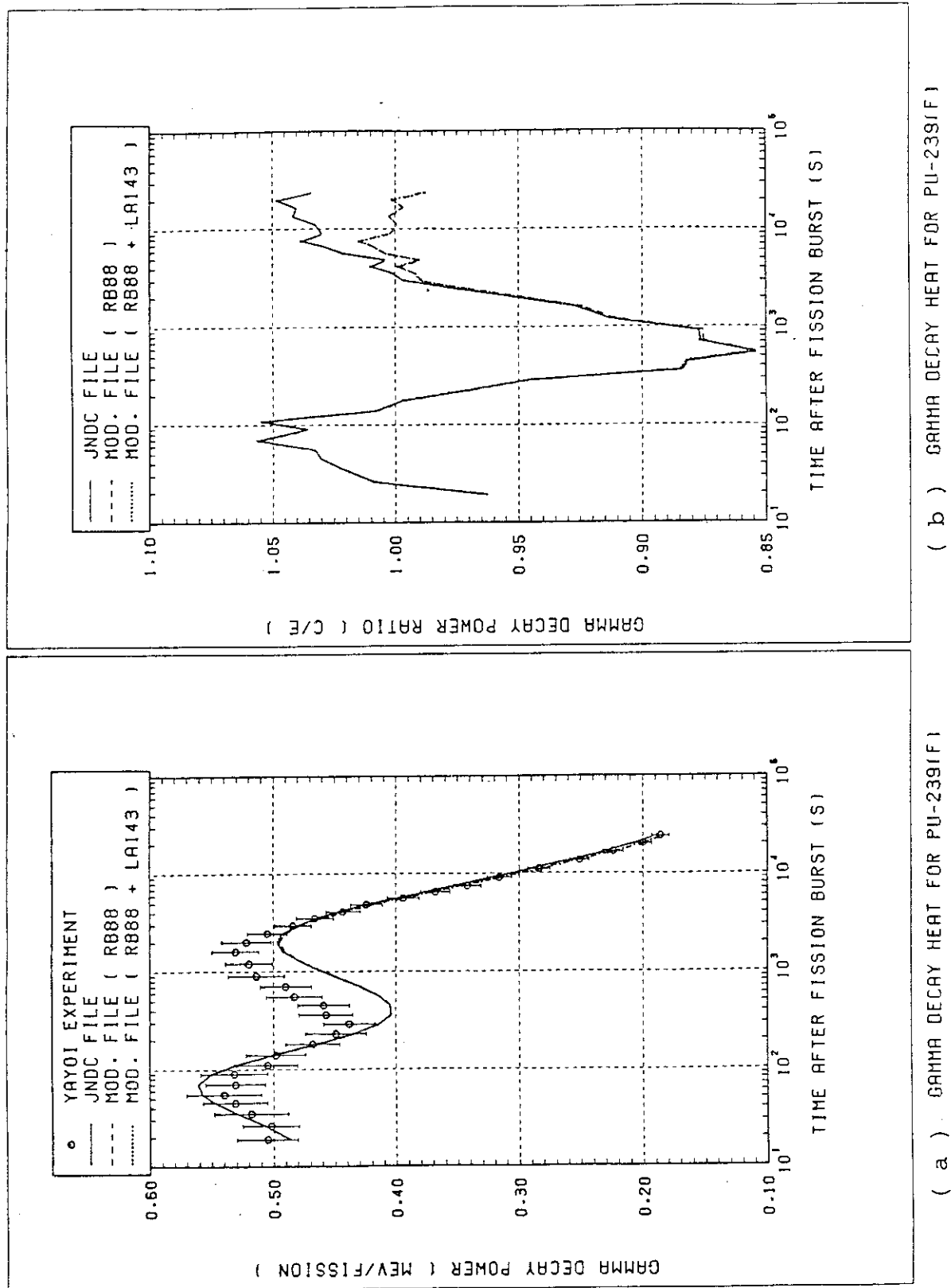


Fig. 4 Comparison of calculated gamma decay power with measured results at University of Tokyo (YAYOI) for the fast neutron fission pulse of Pu-239. (a) Gamma decay power x time. (b) Ratio of calculation to experiment. See the caption to Fig. 1 for explanation of curves.

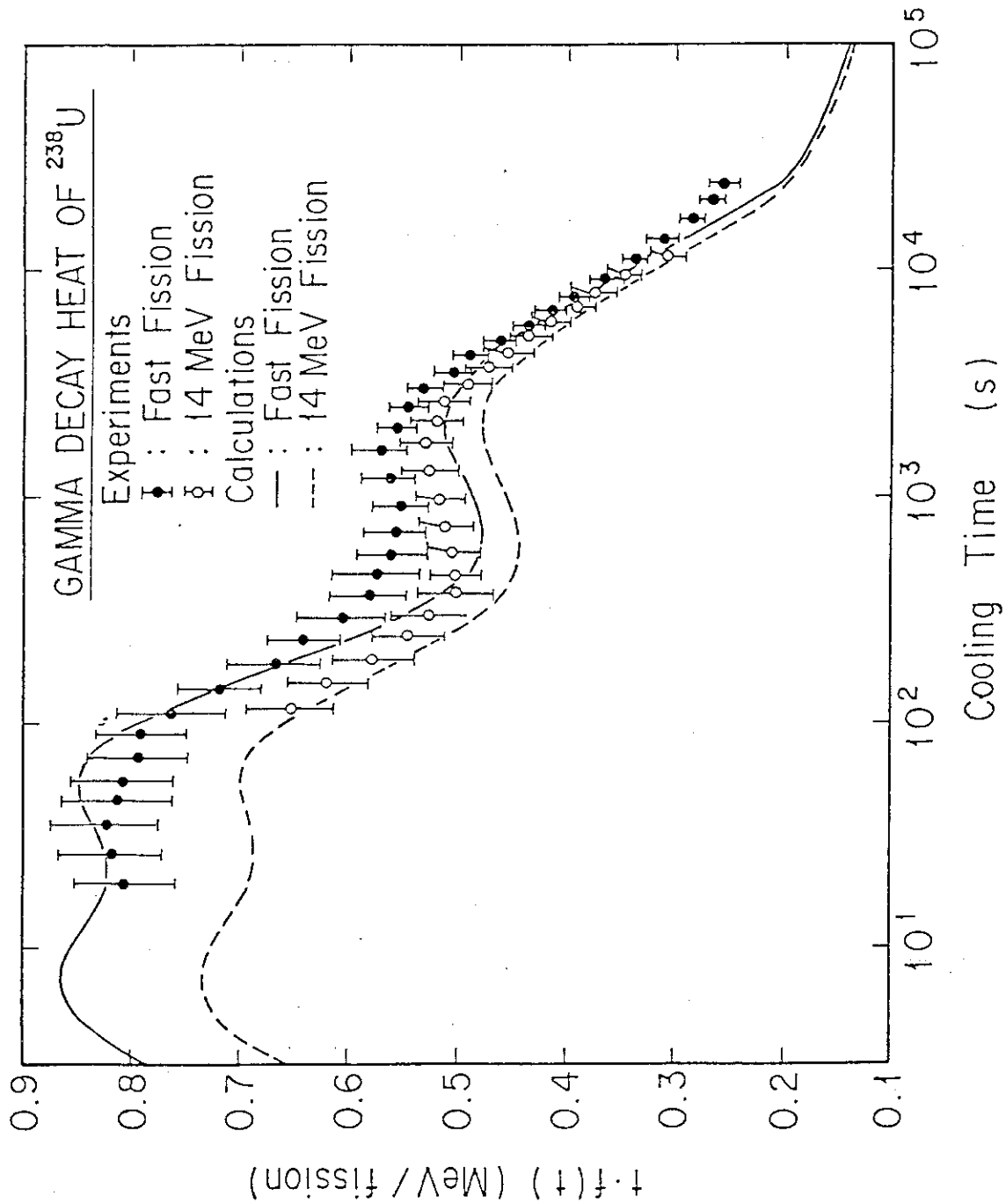


Fig. 5 Comparison of gamma decay heat for fast and 14 MeV neutron fissions of ^{238}U .

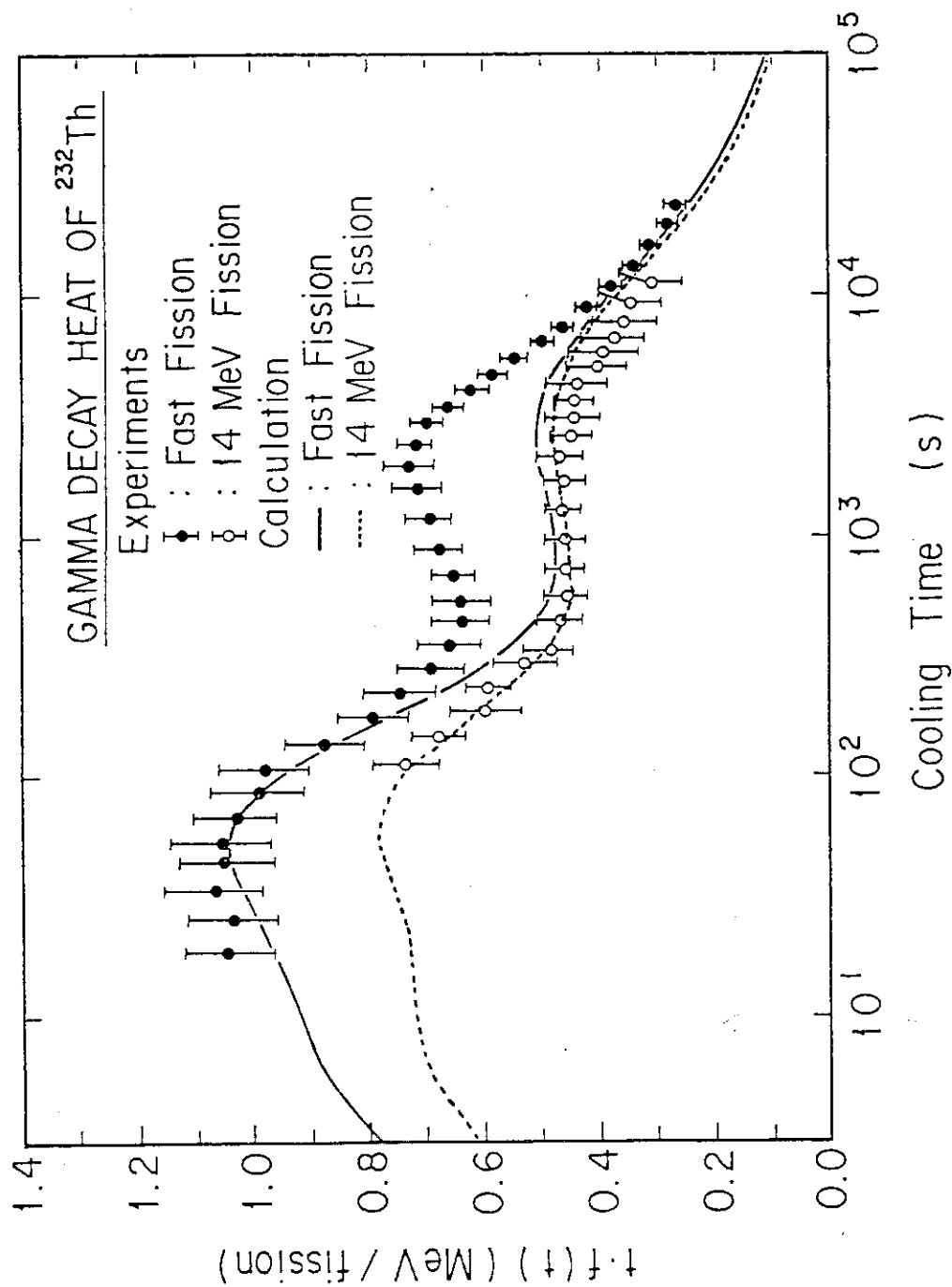


Fig. 6 Comparison of gamma decay heat for fast and 14 MeV neutron fissions of ^{232}Th .

I-4 Fission Product Nuclear Data Measurements and Evaluations at the Studsvik Science Research Laboratory

G. Rudstam

The Studsvik Science Research Laboratory,
S-611 82 Nyköping, Sweden

The group for nuclear physics and chemistry at the Studsvik Science Research Laboratory has at its main tool an isotope separator ("OSIRIS") attached to the 1 MW nuclear reactor R2-0. An integrated target-ion source system is used where the target material forms a cylinder consisting of uranium oxide/carbide on a matrix of graphite cloth which is placed in the discharge chamber of the ion source. The target is irradiated with thermal neutrons from the reactor with a maximum flux of 4×10^{11} n/cm²s. All elements volatile in the ion source temperature of $\sim 1500^\circ\text{C}$ are released from the target and processed as elementary ions by the separator. In this way isotopes of the elements Zn, Ga, Br, Kr, Rb, Ag, Cd, In, Sb, Te, I, Xe, and Cs, and their daughter products, become available for study. By the addition of carbon tetrafluoride a further set of elements - Sr, Y, Zr, Ba, lanthanides - become volatile as fluorides and may be processed as molecular ions. This means an almost complete coverage of fission products down to half-lives about a tenth of a second.

The experimental programme is focussed on fundamental studies of short-lived fission products. This programme comprises measurements of specific properties such as total beta decay energies, half-lives, and the emission of delayed neutrons. More complete spectroscopic investigations are carried out for especially interesting nuclides. Because of the great importance of macroscopic effects of the fission products in nuclear fuel the group is also engaged in applied research with the view to measure certain quantities and to evaluate integrated effects. Examples of this is the beta part of the decay heat, the delayed-neutron energy spectrum and its time dependence, and the fission yields. The decay heat problem is also attacked by integral measurements of the beta and gamma spectra emitted from irradiated fissile nuclides using a Van de Graaff-accelerator.

A summary of the experimental programme is given below in the form of a table

A. Measurements

1. Delayed neutrons
 - 1.1 Branching ratios
 - 1.2 Energy spectra
2. Decay data
 - 2.1 Total decay energies
 - 2.2 Half-lives
 - 2.3 Gamma branching ratios
 - 2.4 Gamma spectroscopy
3. Research related to the decay heat problem
 - 3.1 Measurement of the complete beta spectrum for individual fission products and determination of the average beta energy emitted per decay

- 3.2 Integral measurements of decay heat from
 - ^{235}U (thermal fission; beta and gamma part)
 - ^{238}U (fast fission; gamma part)
 - ^{239}U (thermal fission; beta and gamma part)
- 4. Fission yields
 - 4.1 Yields of thermal fission of ^{235}U (many isomeric yield ratios determined for the first time)
 - 4.2 Yields of fast fission of ^{238}U (new project planned)

B. Evaluations

- 5. Energy spectra of delayed-neutron groups and their time variation
- 6. Decay heat in nuclear fuel
- 7. Abundance pattern of fission products in nuclear fuel
- 8. Antineutrino energy spectrum around a nuclear reactor

Participants in the programme:

P. Aagaard
K. Aleklett
B. Fogelberg
P.I. Johansson
E. Lund
G. Rudstam

and the technical staff of OSIRIS.

SESSION II

II-1 DECAF HEAT CALCULATION WITH THE
C.E.A. RADIOACTIVITY DATA BANKB. DUCHEMIN¹, J. BLACHOT², B. NIMAL¹,
J.C. NIMAL¹, J.P. VEILLAUT¹

COMMISSARIAT A L'ENERGIE ATOMIQUE FRANCE

1 SERMA/LEPF - CEN.SACLAY - 91191 GIF SUR YVETTE CEDEX -

2 DRF/CPN - CEN.GRENOBLE - 38041 GRENOBLE CEDEX -

SUMMARY

For a long time the French CEA has developed a radioactivity data bank. This bank is updated using ENSDF and some recent experimental results.

The fission product part of this library is currently used for shielding source and decay heat calculations. A computer code called PEPIN, using direct summation method has been developed and is briefly described. A comparison is made with other calculations and available experiments.

INTRODUCTION

In this report we recall briefly how our PEPIN code, which computes residual heat and source terms for shielding calculations, due to fission products, works, using the summation method. We also show how, by comparing our results with available experiments and other calculations, we are able to improve them.

DATA

To make summation calculations many data are necessary : fission yields, spectroscopic data by nuclide, capture cross sections and branching ratio,...

Fission yields

The fission yields are computed using the well-known Wahl(1), formula

$$Y_{if}(Z,A) = \frac{Y_f(A) * KP_f(Z,A) * NF_f(A)}{\sqrt{\pi c}} \int_{Z-0.5}^{Z+0.5} e^{-\frac{(Z-ZP)^2}{c}} dz$$

where :

Z : atomic number
 A : atomic mass
 $Y_f(A)$: cumulative fission yields after RIDER (2)
 $ZP(A)$: more probable Z value for A chain after RIDER (2)
 $NF_f(A)$: normalisation coefficient
 c : gaussian parameter
 $KP_f(Z,A)$: pairing coefficient after Wahl (1) with EOZ and EON values selected by J. BLACHOT

For isomeric states, $Y_{if}(Z,A)$ is distributed using the MADLAND (3) method. The nuclide spins are taken from our radioactivity data bank.

Spectroscopic data

The spectroscopic data are taken from the CEA radioactivity data bank (4).

The library is currently updated using ENSDF and recent available experiment. We use now the May 82 version which contains 699 nuclides.

Capture cross sections

The effective capture cross sections, resonance integrals and branching ratio are taken from several sources (5).

CALCULATION METHODOLOGY

Our PEPIN code solves analytically the Bateman equations for irradiation

$$\frac{dC_i(t)}{dt} = \sum_f Y_{if} \tau_f + \sum_j C_j(t) \tau_j b_{j \rightarrow i} - \tau_i C_i(t) \\ + \sum_k C_k(t) \lambda_k b_{k \rightarrow i} - \lambda_i C_i(t)$$

with

$C_i(t)$: nuclide i concentration at time t
 τ_f : $C_f \sigma_f \varphi$: fission rate
 σ_f : fission cross section of nuclide f
 φ : neutron flux
 τ_i : $\sigma_i \varphi$: capture rate
 σ_i : nuclide i capture cross section
 $b_{j \rightarrow i}$: branching ratio of nuclide j towards nuclide i
 λ_i : decay constant.

Our method which assumes that the fission rate is constant during an irradiation step allows us to get analytical solutions at any cooling time without too much computer cost.

COMPARISON WITH EXPERIMENTS

Many comparisons have been made with available experiments and other calculations. As an example we show in figure 1 to 4 such comparisons for fission pulse of ^{235}U (total, β and γ decay heat) and ^{239}Pu (total decay heat). Our results (PEPIN 699) are compared with DICKENS experiments (6), LOTT et FICHE experiments (7), our earlier calculations (PEPIN 635) and calculations made by the CINDER code with ENDF/BV (8).

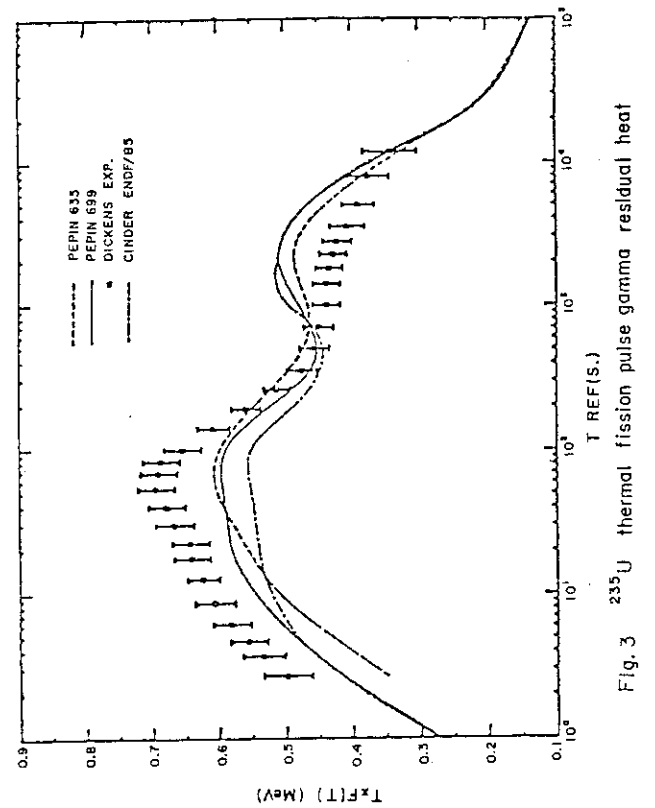
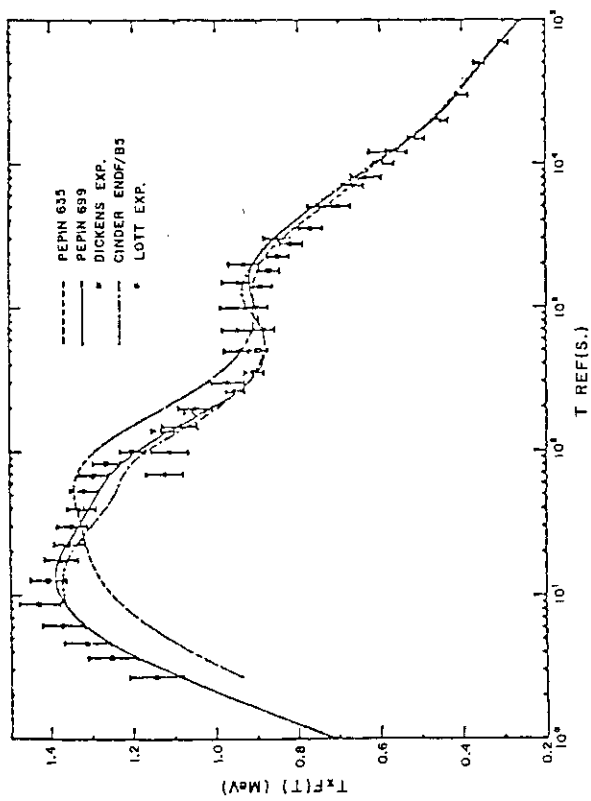
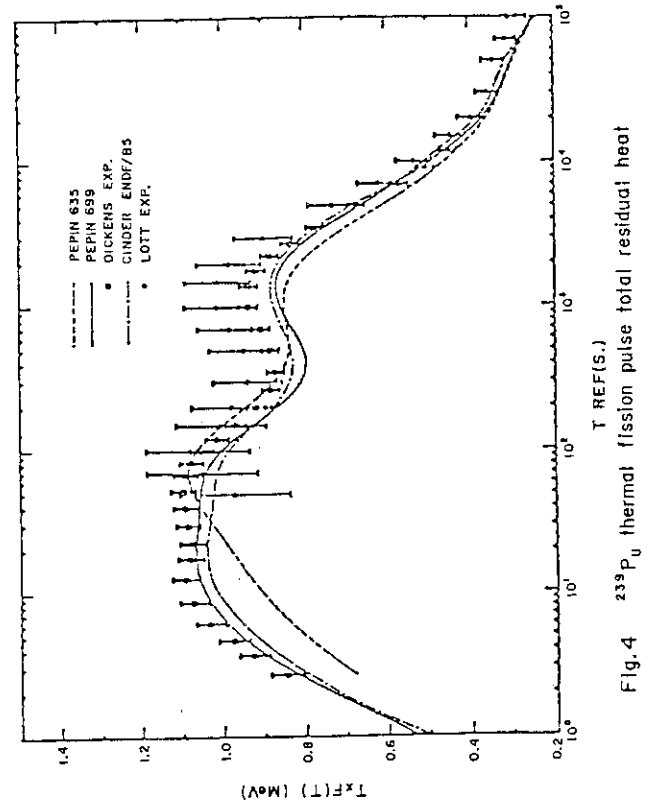
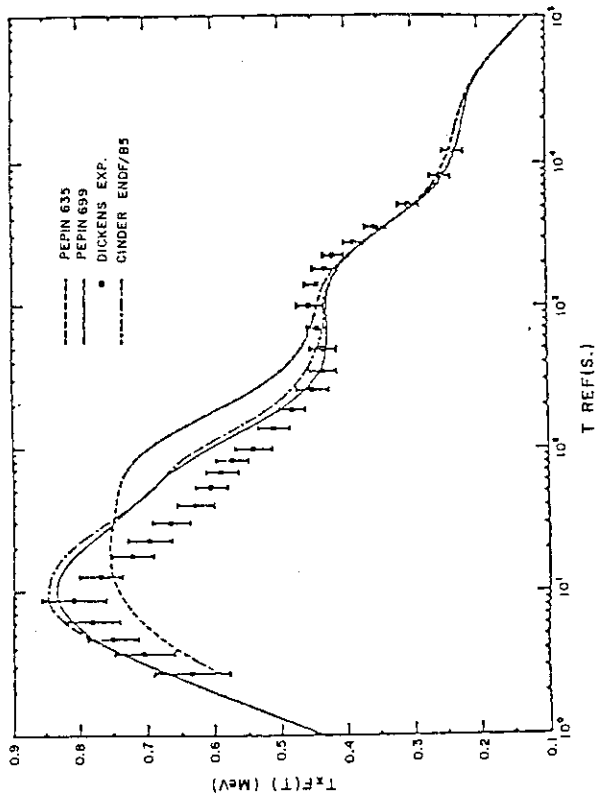
These figures show that the total residual heat is well reproduced either if some underestimations appear for ^{239}Pu around 1000 sec cooling time. But for β and γ residual heat the comparisons are not so good. Some improvements of these results were obtained using Aleklett and Rudstam values (9) for mean β energy.

In fig. 5 and 6 some gamma spectra comparisons are made between our results and the Dickens experiment for thermal fission pulse of ^{235}U . These figures show that the highest energy gamma are not found in the calculation. We are currently working to improve this result.

In conclusion it seems to us that although these results are satisfactory, some improvements have to be made in our knowledge of nuclides with large Q value or short decay time.

REFERENCES

- 1 A.C. WAHL - Journal of Radioanalytical Chemistry Vol. 55 n° 1 (1980)
- 2 B.F. RIDER Nedo 12154-3C (1981)
- 3 D.G. MADLAND - LA-6595-MS (ENDF 241) (1976)
- 4 J. BLACHOT - C. FICHE - Harwell 1978 p 216 and J. BLACHOT - C. FICHE ANPHAJ 6 (suppl.) (1981)
- 5 W.H. WALKER AECL-3037 (1969) and Chart of the nuclides (1977)
- 6 J.K. DICKENS et al - ORNL-NUREG 39 (1978) and ORNL-NUREG 66 (1980)
- 7 M. LOTT et al J.N.E. 27 597 (1973) and C. FICHE NEACRP/L 212 (1976)
- 8 R.J. LABAUVE et al LA 9090 MS (1981)
- 9 K. ALEKLETT, C. RUDSTAM Nucl.Sci.Eng. 80 74 (1982).



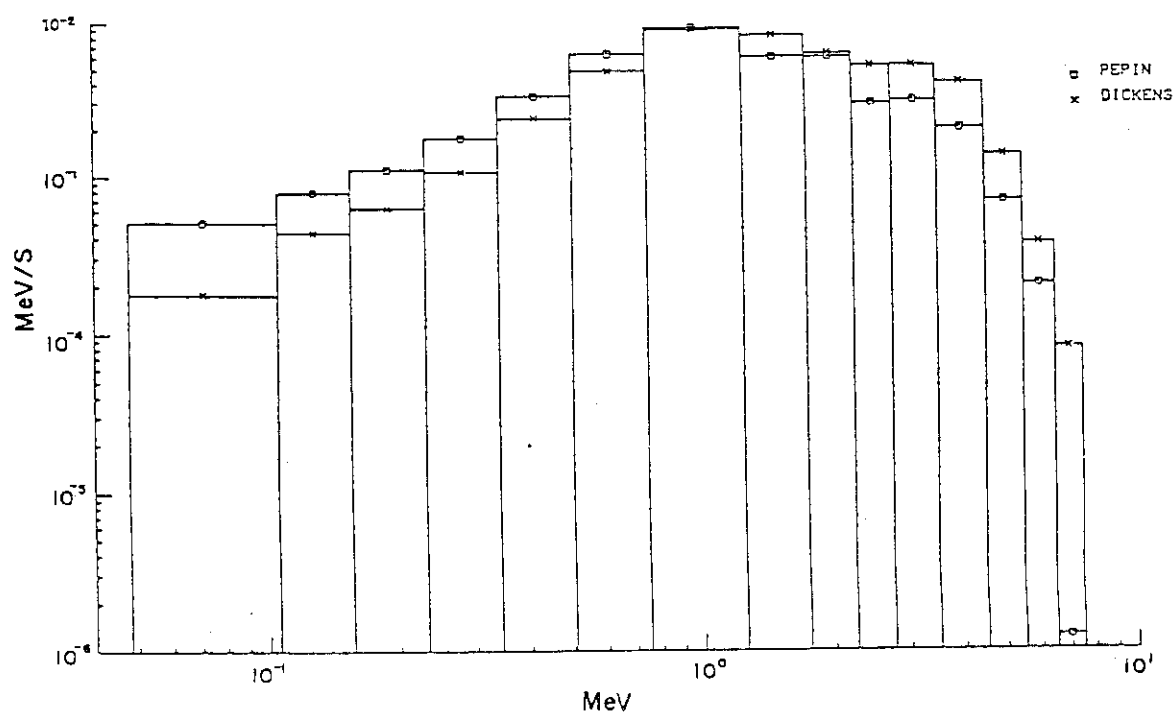


Fig. 5 ^{235}U thermal fission pulse residual heat gamma spectra cooling time 12.7 sec.

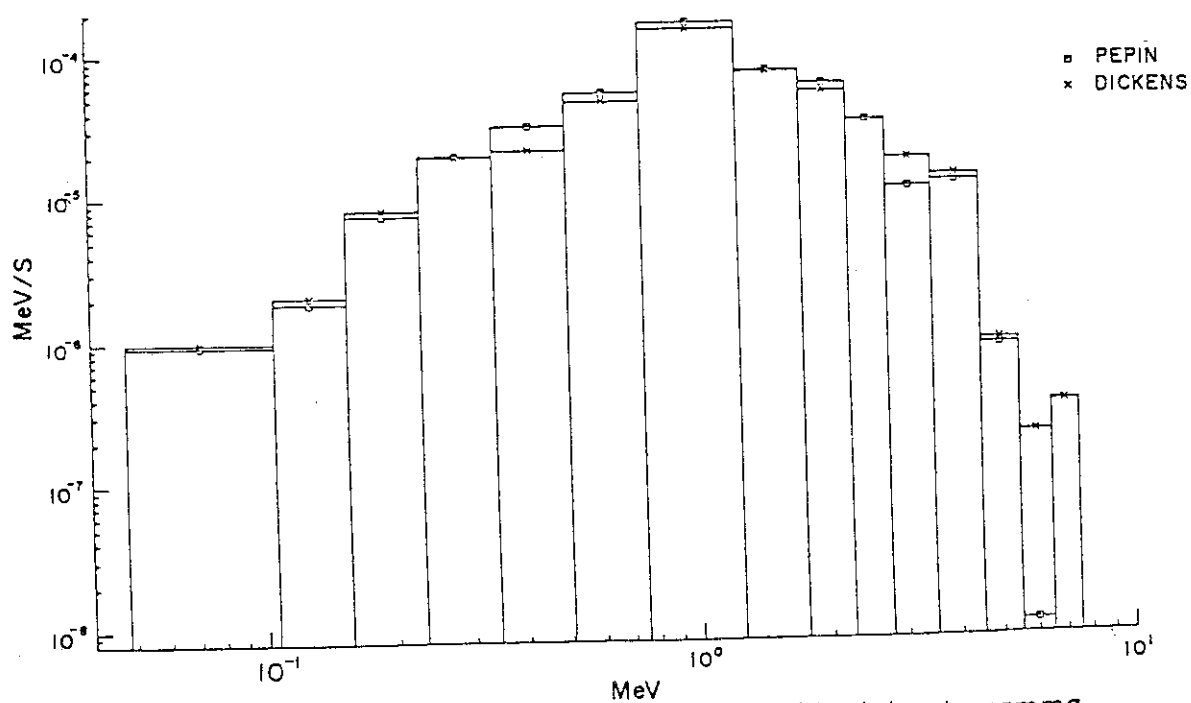


Fig. 6 ^{235}U thermal fission pulse residual heat gamma spectra cooling time 1000 sec.

II-2 MEASUREMENTS OF GLOBAL
FISSION PRODUCTS CROSS SECTIONS
IN PWR SPECTRUM

P. GAUCHER, L. MARTIN DEIDIER

Commissariat à l'Energie Atomique

Département des Réacteurs à Eau

*Centre d'Etudes Nucléaires de CADARACHE
B.P n° 1 13115 SAINT-PAUL-LEZ-DURANCE*

MEASUREMENTS OF GLOBAL FISSION PRODUCTS CROSS SECTIONS IN PWR SPECTRUM

Ph. GAUCHER, L. MARTIN-DEIDIER

Fission product absorption is very important in power reactors: for a large part, the reactivity loss during irradiation is due to the fission product capture. With the exception of ^{135}Xe , this absorption leads during one reactor cycle to a loss of around 3000-3500 pcm in reactivity, whereas the total loss due to fuel spending is of around 6000 pcm.

72 % of this effect comes from the following nuclides: ^{147}Pm , ^{149}Sm , ^{152}Sm , ^{95}Mo , ^{99}Tc , ^{103}Rh , ^{131}Xe , ^{133}Cs , ^{143}Nd , ^{145}Nd . The remaining 28% comes from a very large number of nuclides.

In fact, for power reactor calculations, only global fission product absorption is needed. Experimental programs developed in France are therefore based on direct measurements of the global effects of spent fuel fission products, in order to qualify calculation means.

A comparison between this method and integral measurements on separated nuclides shows the following advantages:

- The fission product effects are measured in conditions closely related to a PWR's, in terms of neutronic spectrum and self-shielding. It will therefore be easy to obtain the true effect in a power reactor through the interpretation of the measurements.
- To obtain the global effect, there is no need to use such data as fission yields or accumulation parameters in fuel, in which uncertainties are still important today.

1 Experimental methods:

From an experimental point of view, global fission products absorption measurements are realised by an oscillation method. The reactivity effects of spent fuel samples are compared to the ones of non-irradiated samples. These experiments are realised in the Minerve reactor, at the Centre d'Etudes Nucleaires de Cadarache (France). The measurements by the oscillation method are performed in the center of the experimental assembly MELODIE, composed of a lattice of 800 UO₂ rods with a ²³⁵U 3% enrichment, similar in characteristics to power reactor rods. The neutronic spectrum obtained is therefore very close to the PWR's. Figure 1 gives a view of the Melodie assembly.

Experimental samples of about 100 mm long are cut in special labs from spent fuel rods and re-clad. In each sample, there is about .4 g of fission products. ¹³⁵Xe, which has a great importance in reactors because of a large absorption cross section (200 barns), has disappeared because of a very short half-life (9.17 hours). But the data concerning this nuclide can be checked precisely in power reactors.

The compositions in heavy nuclides (Uranium, Plutonium, Americium), are measured through analysis of pellets taken at each end of the spent fuel sample. The quantity of fission products is obtained through measurements of ¹⁴⁸Nd concentration, which is a classical burn-up indicator./1/

There are two solutions to interpret spent fuel measures:

- Comparison by oscillation of two samples, one consisting of spent fuel, the other of the same non-irradiated fuel. The global loss in reactivity due to irradiation is thus directly obtained. But to reach fission products absorption, we have to take into account the evolution of heavy nuclides during irradiation, and the final precision is lessened.
- Comparison by oscillations of the spent fuel sample with a standard sample, the uranium and plutonium concentrations of which are close to the studied sample's. Corrections due to heavy nuclides are reduced, and the final precision on fission products absorption is improved.

2 Experimental program:

During the years 1973/1974, a program of measurements on PWR spent fuels was realised /2/. The samples were taken from the SENA reactor assemblies after one, two and three cycles of irradiation; the burn-up was between 5000 and 30000 MWD/T. The results obtained have shown that global absorption of fission products was correctly predicted, for the concerned burn-up, by the APOLLO code (used in the C.E.A. for light water reactors calculation)/3/. The uncertainties and discrepancies between calculation and experiment are given in the following table.

	sample with one cycle	sample with two cycles	sample with three cycles
E-C / C	+ 12 ± 12 %	-1 ± 12 %	+1 ± 12 %

Because of the modifications of the French reactors, these results are no longer sufficient:

- The burn-up scale studied is too narrow compared with the current PWR burn-up of unloading (33 GWD/T in average, 38 GWD/T for the most burnt fuels), and the problem will become even more serious with the future unloading burn-up of 45 GWD/T in average./4/
- Neutronical characteristics of the SENA's core are not typical of modern reactors: fuel assemblies are in tubes, rods are steel-clad, whereas French PWR reactors are mainly 17x17 with zircaloy cladding.

To solve these problems, a new program of measurements is to take place in the Minerve reactor at the end of 1984. The spent fuel samples come from BUGEY III and FESSENHEIM II reactors (PWR 17x17). Samples and associated burn-up are listed in the following table.

REACTOR	Number of cycles	Burn-up (GWD/T)	number of samples
BUGEY III	1.5	22.	1
	2.	27	1
	3	36-39	2
FESSENHEIM II	4	38-48	3

In figure 2, the absorption of the fission products is shown according to the burn-up for a typical PWR reactor, and the investigated burn-up scales are represented.

With this program, the uncertainty on the global absorption of fission products should be restrained to less than 6%, concerning PWR calculations and the present or future unloading burn-up.

To complete this program, oscillations on $\text{UO}_2\text{-PuO}_2$ samples, irradiated in the SENA reactor, will be done. Thus, informations on global capture of fission products issued from that kind of fuel will be obtained. These measures are part of the studies the C.E.A. is presently carrying out on Plutonium recycling in P.W.R.

REFERENCES

=====

/1/ M. ROBIN- " Specific burn-up determination and qualification of fuel irradiation dosimetry calculations based on post-irradiation measurements". Symposium ASTM/EURATOM, PALOALTO(1977).

/2/ L. MARTIN-DEIDIER and Al.- " Mesures intégrales de la capture des produits de fission dans les spectres de réacteurs à eau et de réacteurs à neutrons rapides". International conference on neutron physics and nuclear data, HARWELL(september 1978).

/3/ J. BOUCHARD and Al. - "Neptune: un système modulaire pour le calcul des réacteurs à eau ordinaire". (Conférence Nucléaire Européenne, PARIS (1975).

/4/ C. DEHON and Al.- " Expérience acquise, progrès accomplis et perspectives d'évolution dans la conception et les performances des combustibles P.W.R. du programme électronucléaire français". Conférence AEA sur l'expérience acquise dans le domaine nucléo-énergétique, VIENNE (september 1982)

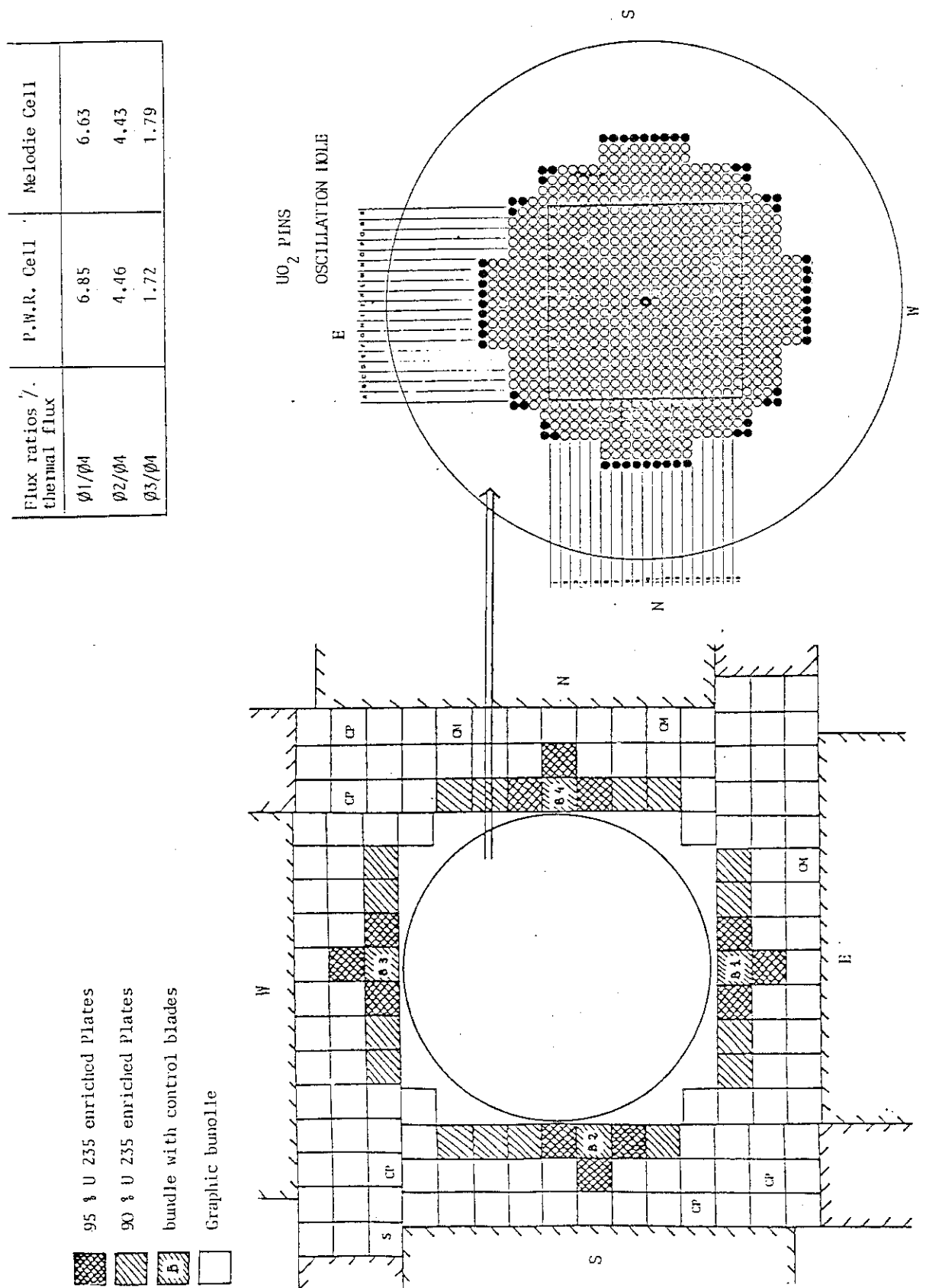


Fig. 1 The melody assembly

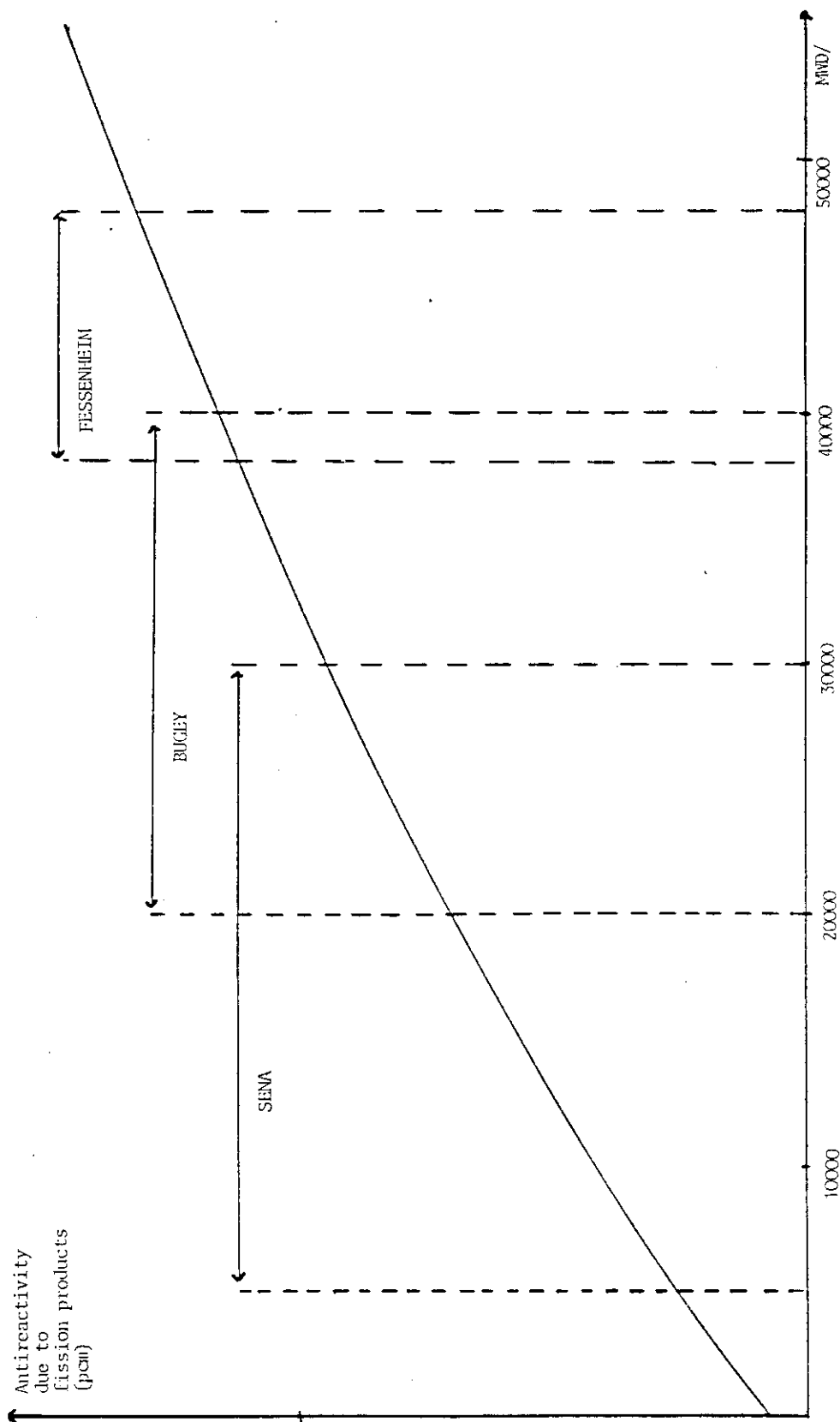


Fig. 2 Antireactivity due to fission products (except ^{135}Xe) and investigated burn-up scales

II-3 SOME INVESTIGATIONS ON THE CONTRIBUTION
OF THE INTERNAL CONVERSION PROCESS
TO THE DECAY HEAT OF A LMFB

Nicole KAROUBY-COHEN
IRDI/DRNR/SPCI/LEPh - bât. 230
Centre d'Etudes Nucléaires de CADARACHE
Boîte Postale N°1
F.13115 - SAINT-PAUL-LEZ-DURANCE
(France)

ABSTRACT

The internal conversion process contributes not negligibly to the total decay heat. The contribution of this phenomenon has been investigated using BLACHOT-FICHE data /Ref. 1/.

This study has allowed to show the importance of internal conversion process for the calculation of the decay heat of fission products, i.e. up to 10 ÷ 15%.

It has allowed, also to show the need of reliable and precise data on the internal conversion process in this type of decay data libraries.

1 - INTRODUCTION

The calculation of fission products decay heat is necessary for fuel cycle studies. The internal conversion process contributes not negligibly to the total results. The contribution of this phenomenon has been investigated using BLACHOT-FICHE data /réf. 1/.

2 - PART OF THE DECAY HEAT PRODUCED BY THE FISSION PRODUCTS

About 70 % of the decay heat for a fuel assembly in a fast reactor core is originated by fission products gamma and beta desintegration (see table I, relative to SUPER-PHENIX). When studying the gamma emission, we have been interested by the internal conversion process as a complementary desexcitation mode.

This process is related to the gamma emission. When the excitation energy is small, this is the principal phenomenon of desexcitation. The excitation energy is transmitted to an inner-shell (mainly k and L) electron, the conversion electron, which is emitted by the atom. The created hole originates an electron cloud rearrangement with characteristic x-ray emission.

The internal conversion coefficient α_T is defined as :

$$\alpha_T = \frac{N_e}{N_\gamma}$$

where N_e is the number of conversion electrons and N_γ the number of photons by unit time. The total α_T may be decomposed on partial factors corresponding to each electron shell

$$\alpha_T = \alpha_K + \alpha_L + \alpha_M + \dots$$

3 - DECAY HEAT CALCUL

In the BLACHOT-FICHE data library, the actual intensity of a gamma transition is increased by a factor $(1 + \alpha_T)$ to take into account the internal conversion process. The decay heat has been

calculated for a SUPER PHENIX 1 type fast reactor, for an average neutron flux of $4.16 \cdot 10^{15}$ n/cm²/s and different cooling times (3 months to 3 years), considering 273 fission products.

At present an assessment based on the BLACHOT-FICHE library data, indicates that the internal conversion process represents a 10 to 15 % contribution to the total decay heat generated by fission products.

These values may be by far and large dependent on which isotope is considered. For example, for the Ce 144 (11.4 % of the decay heat produced by fission products), 45 % of gamma ray decay heat is originated by internal conversion.

4 - INTERNAL CONVERSION IN THE BLACHOT-FICHE LIBRARY

This library contains 707 fission products. A code makes the energy balance for all the fission products for the internal conversion process. For every fission product we have calculated the αT energy ($E_{\alpha T}$), the conversion electron energy (E_{EC}) and the x-ray energy (E_x).

However for 10 % of fission products in BLACHOT-FICHE data the equality : $E_{\alpha T} = E_x + E_{EC}$ is not verified.

We can see the importance of this difference in the table II.

The 8 isotopes in the table II contribute to 95 % of total decay heat of fission products for a core fuel assembly in SUPER PHENIX 1 after 3 years of cooling.

These rather large differences must be considered having in mind that internal conversion represents at most 15 % of total decay heat, reducing their impact on global values.

Nevertheless, for a better reliability of the library, the internal conversion treatment ought to be improved.

4 - CONCLUSION

This study has permitted to show the importance of internal conversion process for the calculation of decay heat of fission products, i.e. up to 10 ÷ 15 %.

It has allowed, also, to show the need of reliable and precise data on the internal conversion process in this type of decay data libraries.

REFERENCES

/Réf.1/ - Table of radioactive isotopes and of their main decay characteristics by J. BLACHOT and CH. FICHE.

TABLE I

DECAY HEAT FOR A CORE FUEL STANDARD SUBASSEMBLY IN

SUPERPHENIX 1*

(percentage contributions)

Times of cooling	Fission products Decay heat ($\beta + \gamma$)	Heavy Nuclides (α)	Steel ($\beta + \gamma$)
3 months	87 %	7 %	6 %
6 months	82 %	11 %	7 %
1 year	73 %	20 %	7 %
6 years	23 %	68 %	9 %

* Irradiation time : 160 days

TABLE II
INTERNAL CONVERSION ENERGY
IN BLACHOT-FICHE DATA

	% P _{FP} T = 3 years	Ex + E _{EC} (KeV)	E α T (KeV)
Y 90 F (1)	4.1 %	2.816 10 ⁻¹	0
RH 106 F (2)	42.3 %	8.101 10 ⁻¹	8.484 10 ⁻¹
SB 125 (3)	0.5 %	2.587 10 ¹	2.697 10 ¹
TE 125 M (4)	7.3 %	3.179 10 ¹	1.419 10 ²
BA 137 M (5)	7.5 %	2.494	6.662 10 ¹
PR 144 (6)	20.1 %	4.967 10 ⁻²	4.967 10 ⁻²
CE 144 (7)	11.4 %	1.307 10 ¹	1.307 10 ¹
PM 147 (8)	1.3 %	3.423 10 ⁻³	3.490 10 ⁻³

(1) For Y 90 F the $\alpha T = 0$

(4) For TE 127 M

Gamma of 35.46 KeV	$\alpha T = 14.02$	$\sum \alpha_i = 13.92$
		$i = K, L$
Gamma of 109.27 KeV	$\alpha T = 353$	no sum over α_i
Gamma of 144.78 KeV	$\alpha T = 252$	$\sum \alpha_i = 199.0$
		$i = K, L$

(5) This data does not give the conversion electron spectrum.

(6) and (7): the library gives the αT coefficient but does not give x-ray and conversion electron spectrum. However all their energies are given as a comment.

II-4 A Model for Fission-Product Calculations^{*,1}

by

A. B. Smith

Argonne National Laboratory

Argonne, Illinois, U.S.A.

Many fission-product cross sections remain unmeasurable thus considerable reliance must be placed upon calculational interpolation and extrapolation from the few available measured cross sections. The vehicle, particularly for the lighter fission products, is the conventional the optical-statistical model.² The applied goals generally are: capture cross sections to 7-10% accuracies and inelastic-scattering cross sections to 25-50%. Comparisons of recent evaluations and experimental results indicate that these goals have too often are far from met, particularly in the area of inelastic scattering, and some of the evaluated fission-product cross sections are simply physically unreasonable. An example of these discrepancies is shown in Fig. 1. The evaluated inelastic-scattering cross sections of palladium are nearly a 100% discrepant with observation and the isotopes are prominent fission products with large inelastic-scattering cross sections at relatively low energies. It is difficult to avoid the conclusion that the models employed in many of the evaluations are inappropriate and/or inappropriately used.

^{*}This work supported by U. S. Department of Energy.

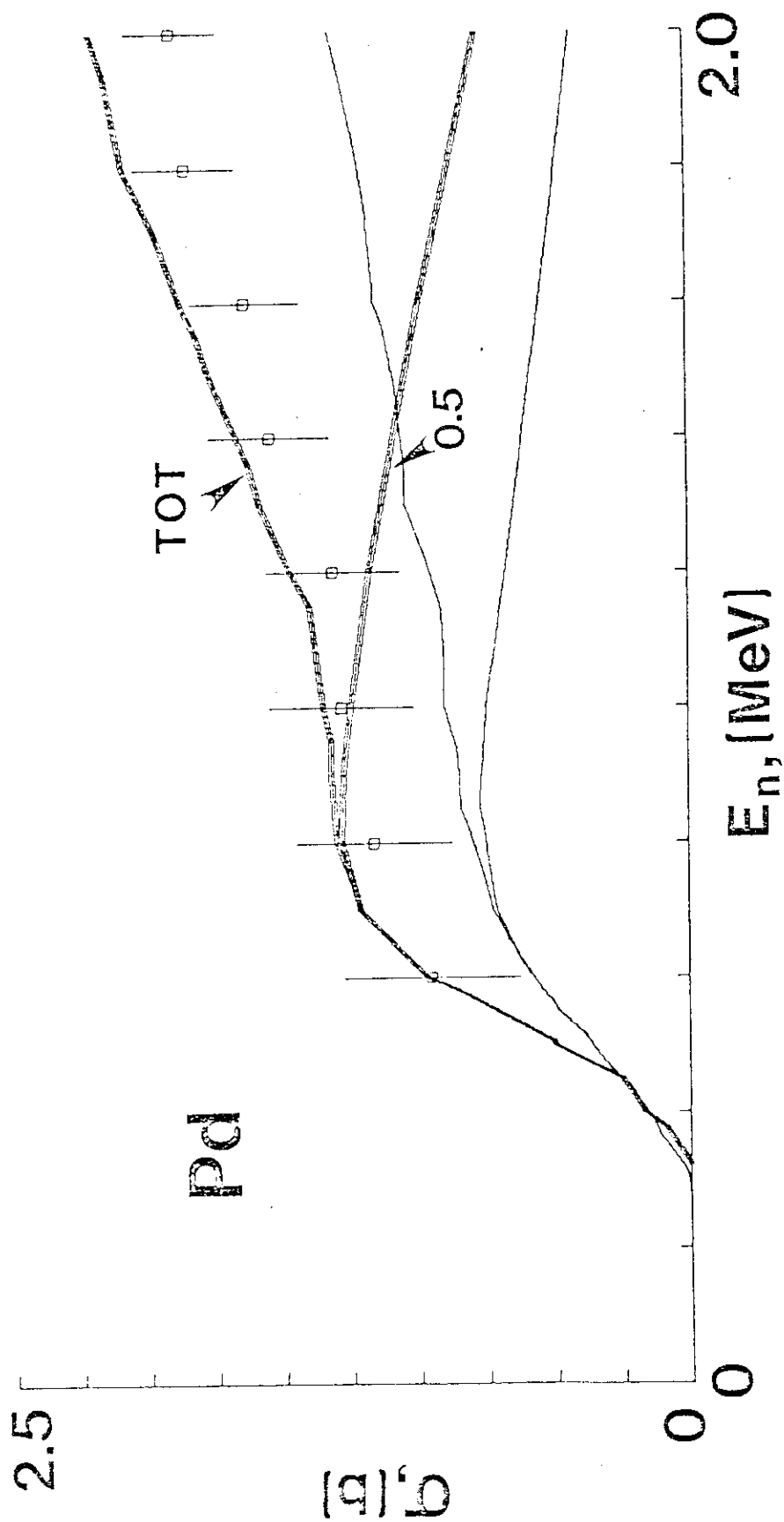


Fig. 1 Comparison of Measured and Evaluated Inelastic-Scattering Cross Sections of Elemental Palladium. The heavy curves indicate the total inelastic scattering cross sections and the cross sections for the excitation of all levels up to excitation energies of 580 keV taken from the experimental measurements. The light curves represent the corresponding quantities taken from ENDF/B-V. The data symbols are representative non-elastic cross-section values implied by measurements.

Objective and Methodology

In order to alleviate the above unfortunate situations, a "regional" optical-statistical (OM) model was sought with the goal of quantitative prediction of the cross sections of the lighter-mass ($Z=39-51$) fission products. The first step toward that goal was the establishment of a reliable experimental data base consisting of energy-averaged neutron total and differential-scattering cross sections. The second step was the deduction of a "regional" model from the experimental data. It was assumed that a spherical OM is appropriate: a reasonable and practical assumption. The resulting OM then was verified against the measured data base. Finally, the physical character of the "regional" model was examined.

Total Neutron Cross Section Measurements³

The neutron total cross sections of all elemental targets in the region $Z=39-51$ (excepting Tc and Ru) were measured from 0.05 to 20.0 MeV with the emphasis on energies below 5 MeV: i.e. the region of primary fast-breeder-reactor interest. The broad resolution accuracies were generally 1-2%. The results form a high-quality and internally consistent data base, and provide an essential model bench mark (the total cross section is one of the few reasonably unambiguously calculable quantities). Illustrative experimental results are given in Fig. 2.

Differential-Scattering-Cross-Section Measurements

The differential scattering cross sections were obtained for the same $Z=39-51$ targets as above. Incident-energy resolutions were intentionally

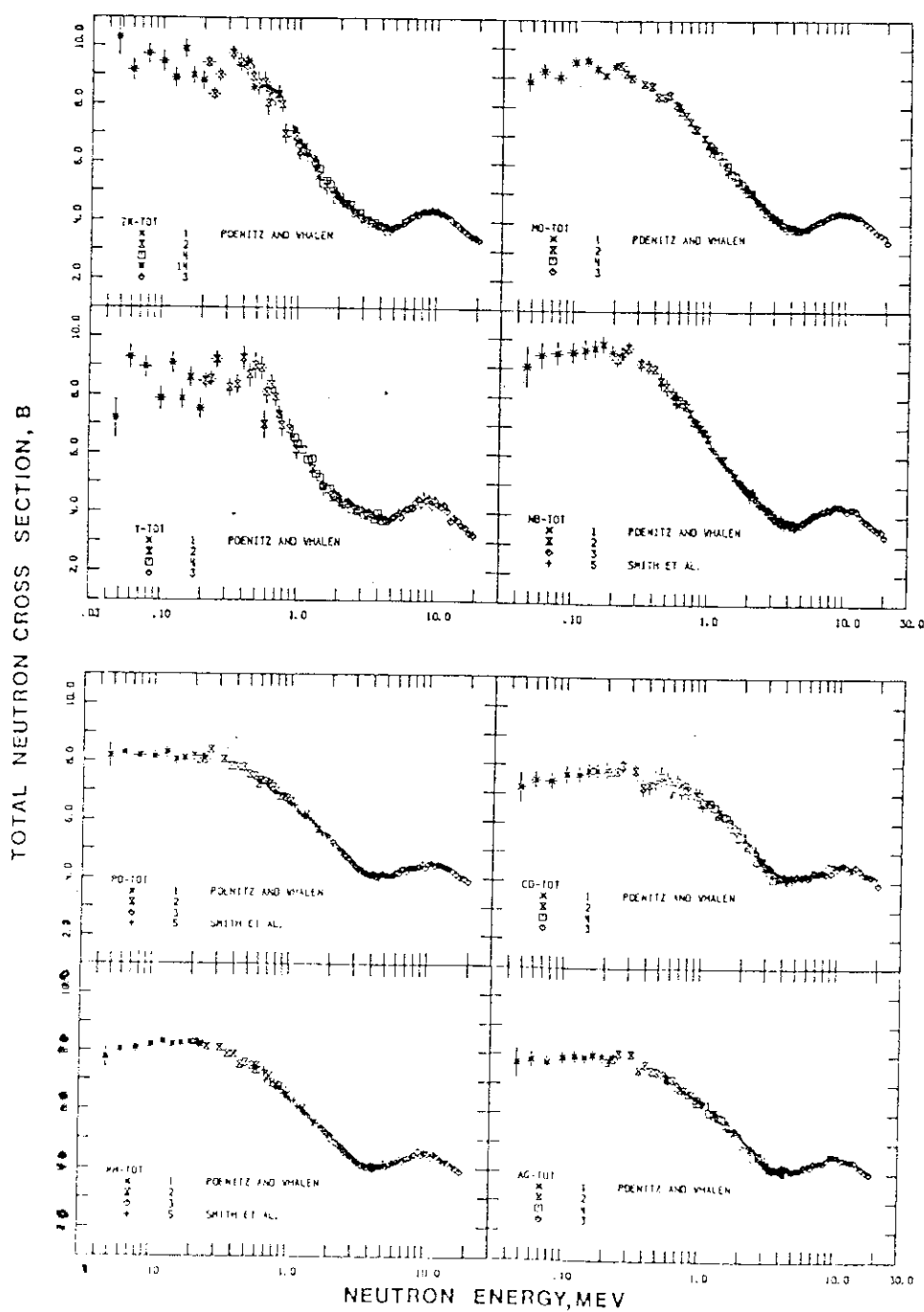


Fig. 2 The present results for the neutron total cross sections of Yttrium, Zirconium, Niobium, Molybdenum, Rhodium, Palladium, Silver and Cadmium.

relatively broad (e.g. 50 keV) in order to provide energy-averaged results reasonably consistent with the concept of the OM. Particular attention was given to elastic scattering over the energy range 1.5-4.0 MeV. Lower-energy results tend to fluctuate in a manner that is difficult to interpret within the OM context. The scattering-angle range was 20-160 deg. and the differential-elastic-scattering accuracies generally 3-5%. All magnitudes were obtained relative to the neutron total cross section of carbon in the manner described in ref. 4. The experimental elastic-scattering results spanned a region from strong compound-elastic (CE) scattering to one where the elastic process is due primarily to shape-elastic (SE) scattering. The experimental scattering results are illustrated in Figs. 3A-3D.

Model Deduction

The experimental elastic-scattering results for each target were concurrently χ^2 -square fitted with the OM potential. Neutron total cross sections were also introduced into the fitting procedure to assure reasonable cross section behavior down to 0.1 MeV and to energies above 4.0 MeV. Six-parameters were varied in the fitting: real and imaginary strengths, radii and diffusenesses. The results were "best" parameter sets for each target. The details of the fitting procedure, the potential form and the resulting parameter values for each target are given in ref. 1. The "regional" model was derived from the mass-dependent trends of the parameters obtained for the individual targets. That "regional" model was then used to calculate the observed quantities. The calculated results were in remarkably good agreement with the experimental values as illustrated by the graphical comparisons of Fig. 4. Rather generally, the calculated values are consistent with the observed quantities to within the experimental uncertainty alone.

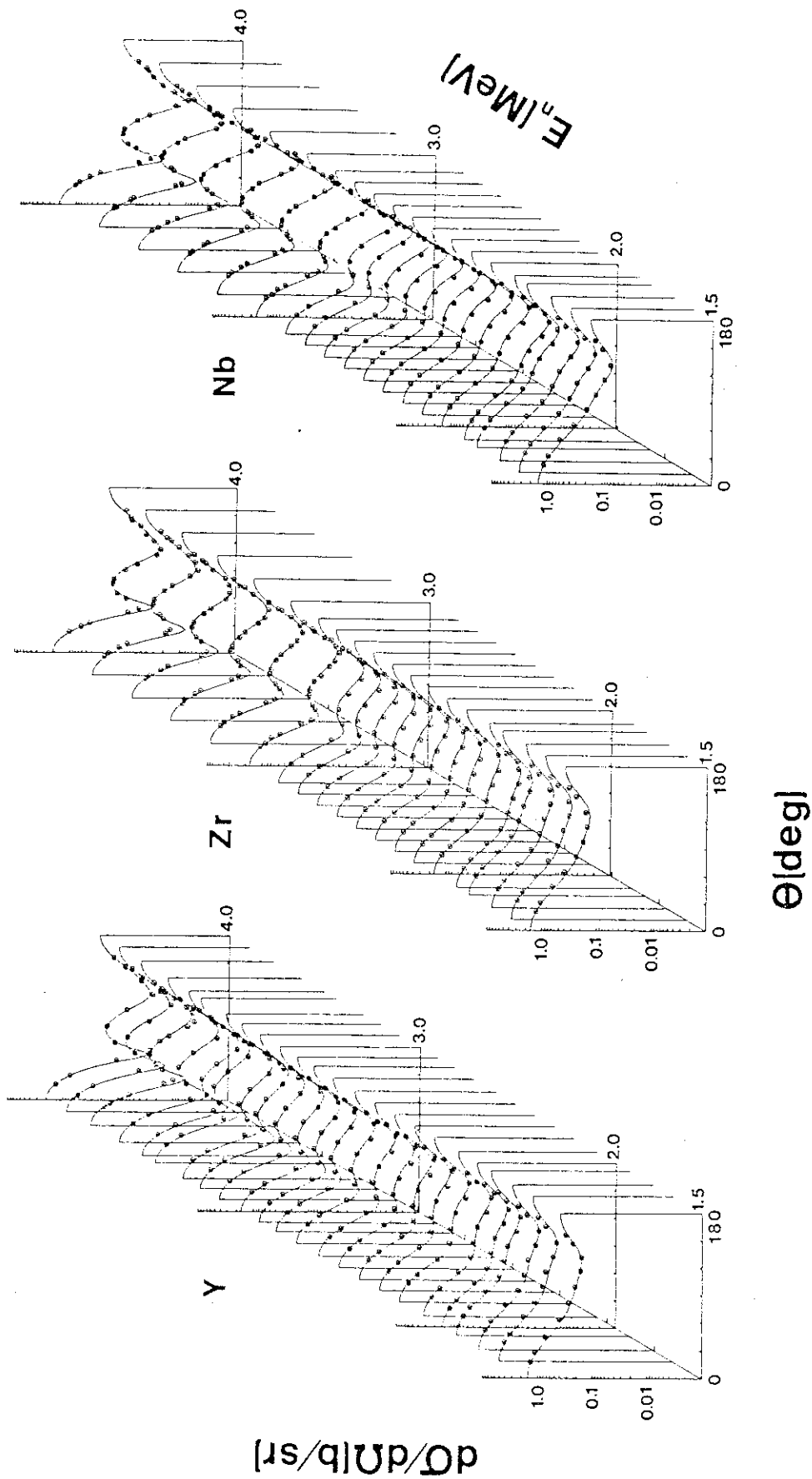


Fig. 3A Illustrative elastic-scattering results. The measured values are indicated by data symbols and the results of calculation (as described in the text) by curves.

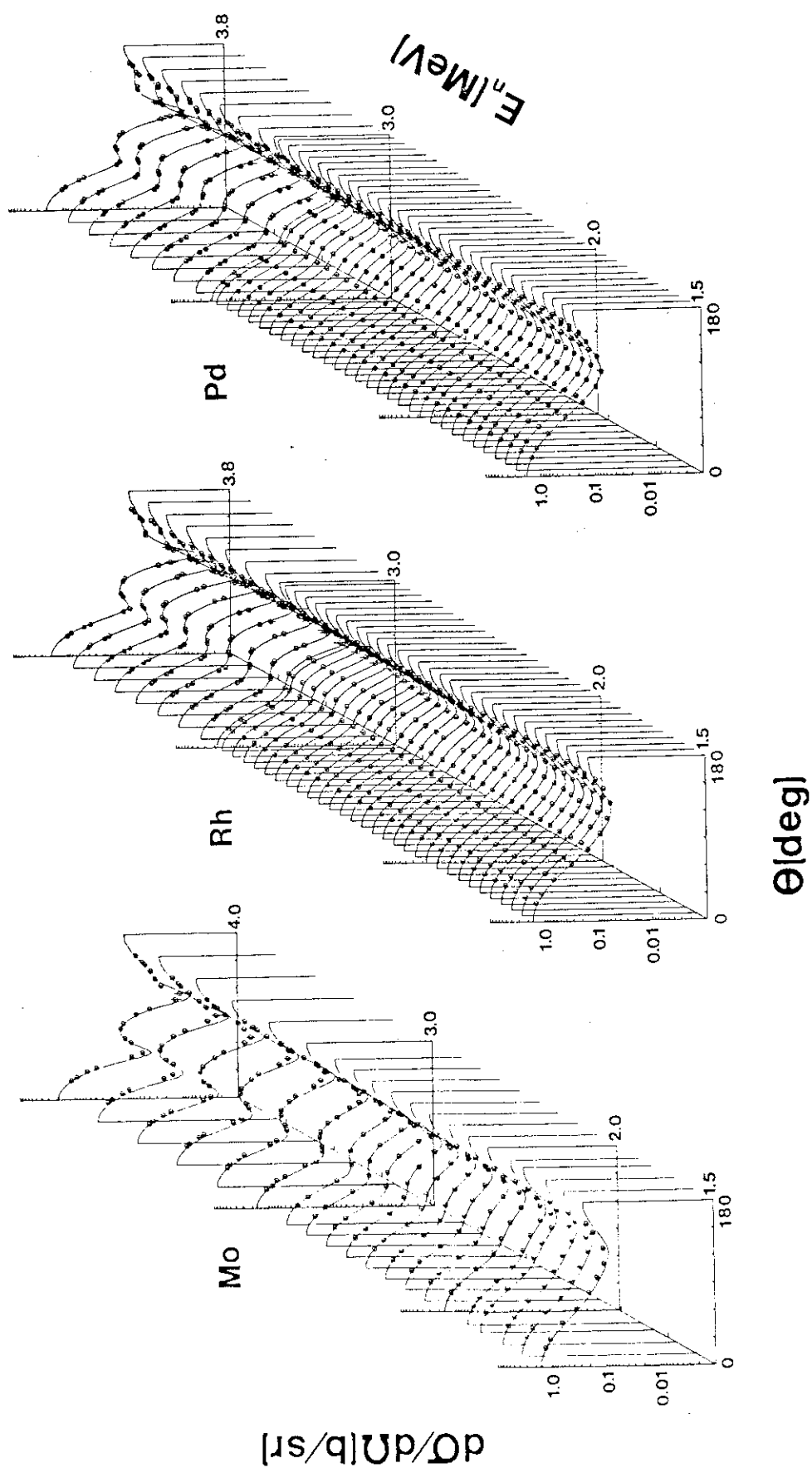


Fig. 3B Illustrative elastic-scattering results. The measured values are indicated by data symbols and the results of calculation (as described in the text) by curves.

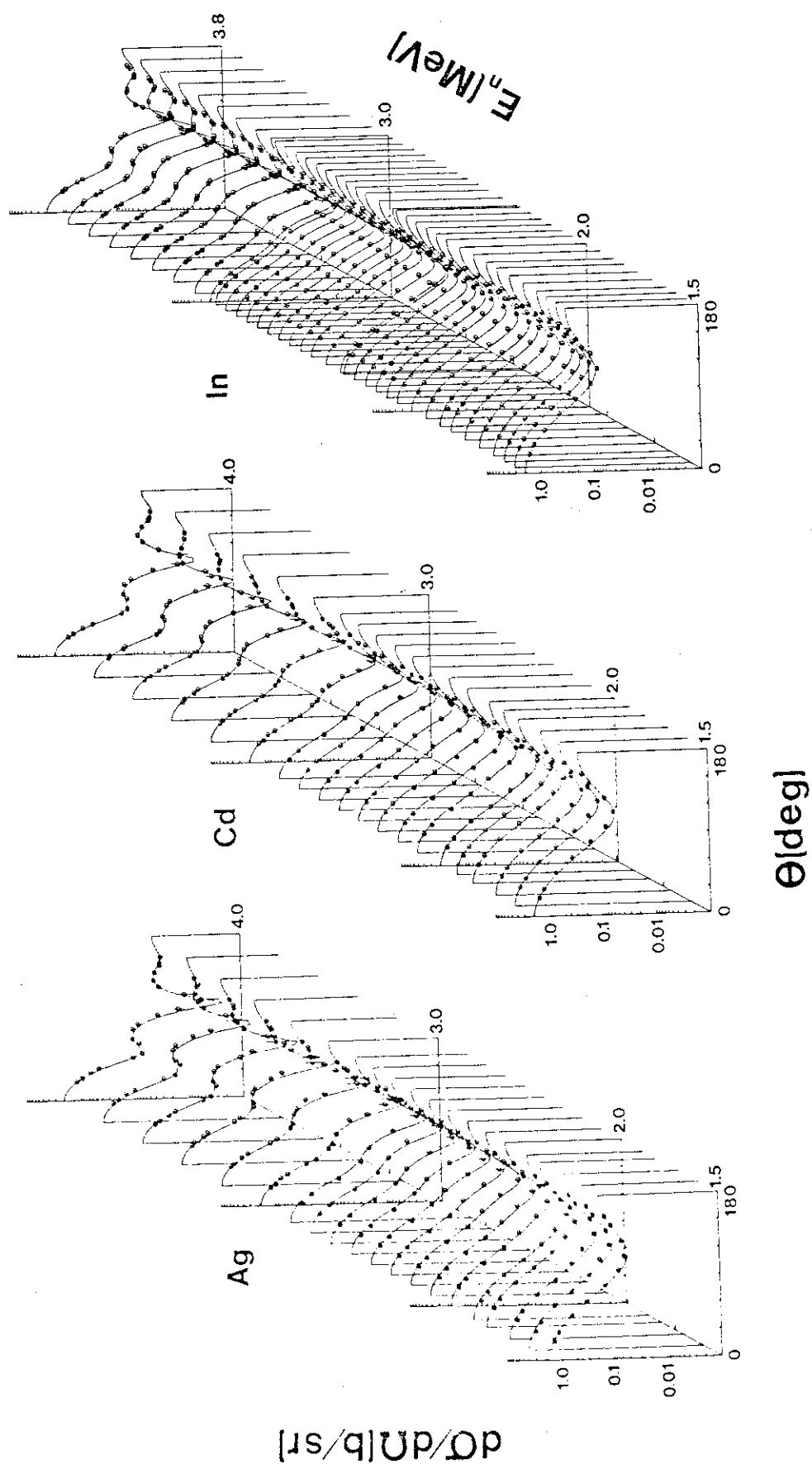


Fig. 3C Illustrative elastic-scattering results. The measured values are indicated by data symbols and the results of calculation (as described in the text) by curves.

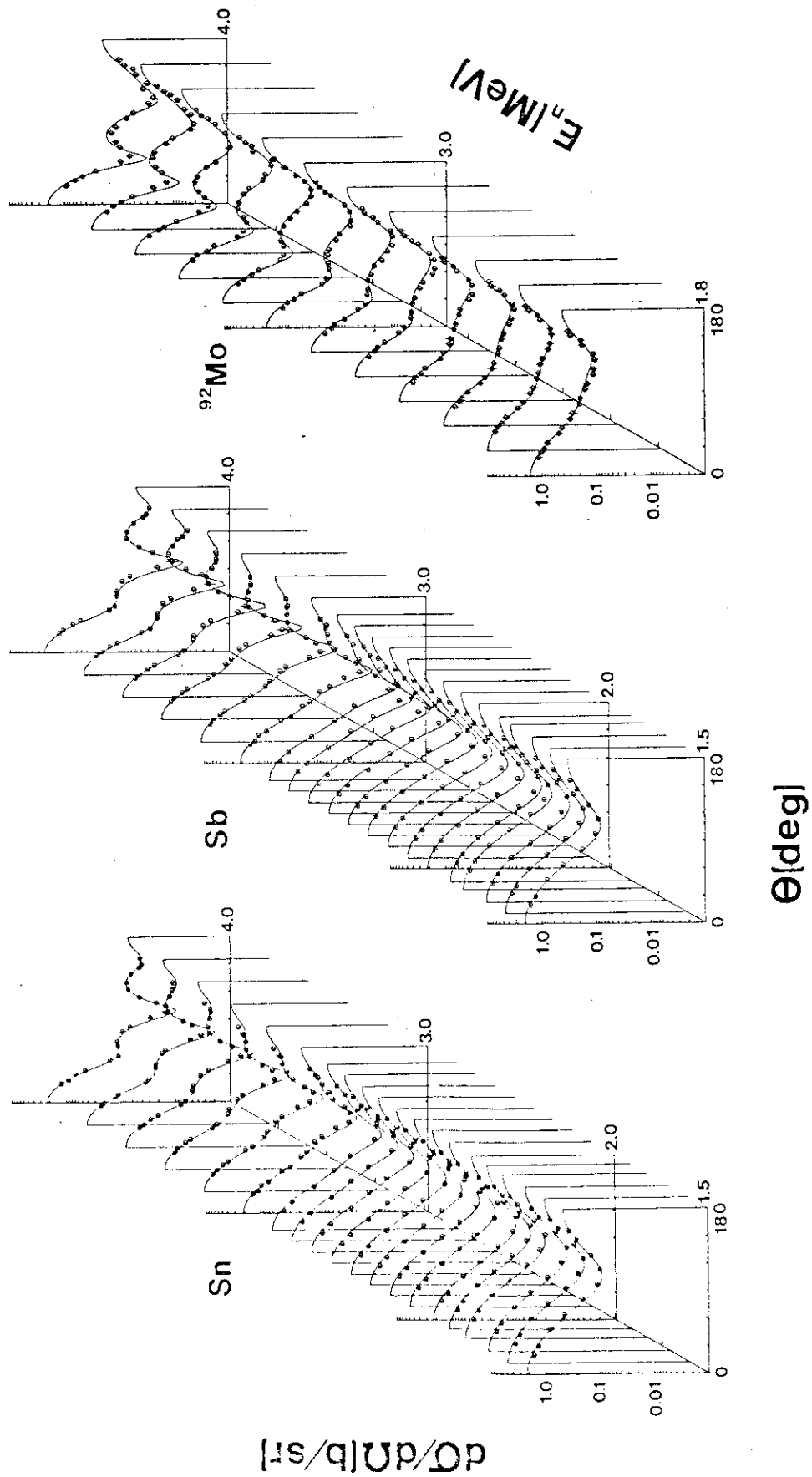


Fig. 3D Illustrative elastic-scattering results. The measured values are indicated by data symbols and the results of calculation (as described in the text) by curves.

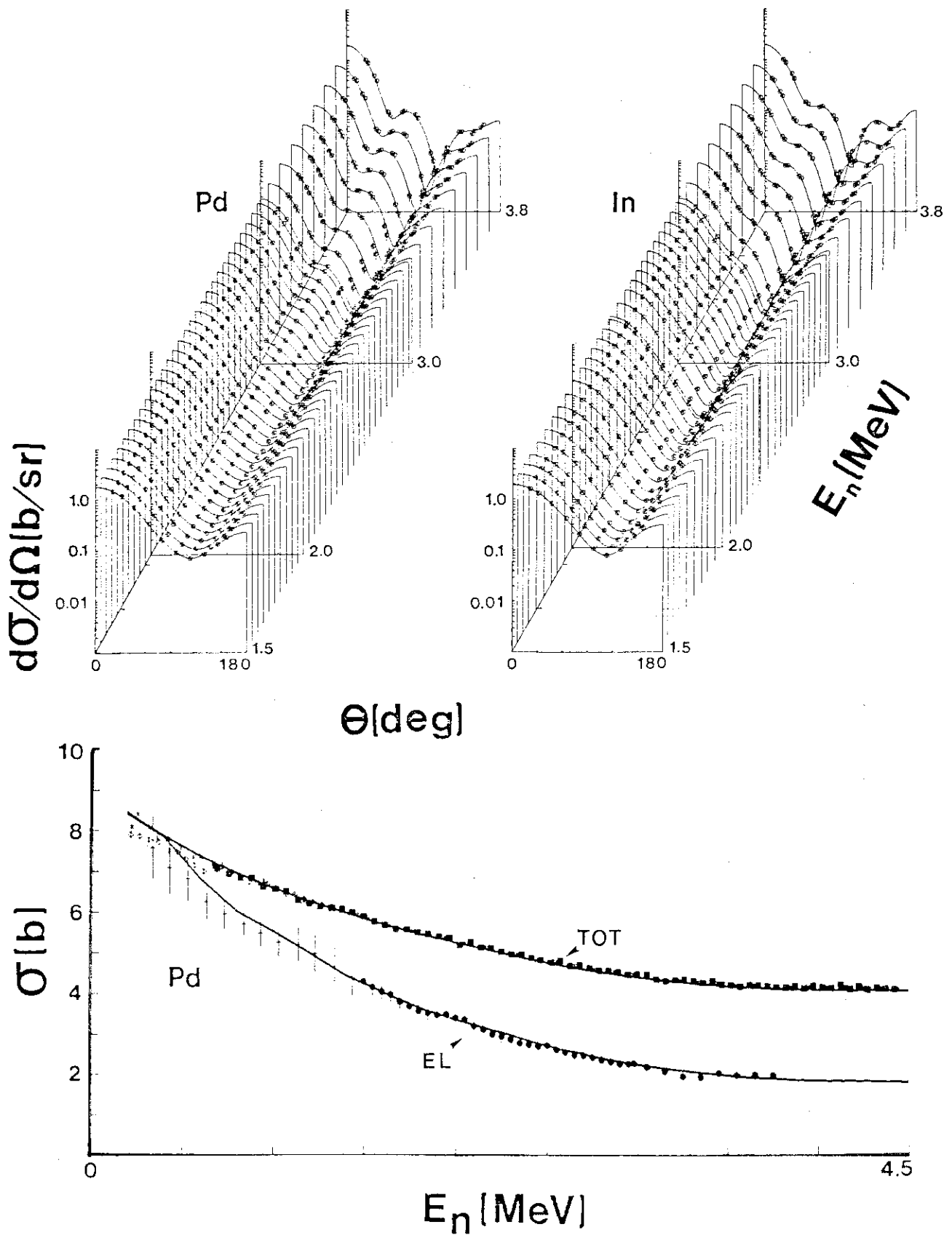


Fig. 4 Comparisons of the experimental data (symbols) with the results of calculations (curves) based upon the "regional" model.

Character of the "Regional" Model

The real portion of the "regional" potential is relatively conventional. In particular, the dependence on isospin is very similar to that encountered in "global" representations¹, as illustrated in Fig. 5. More interesting is the "anomalous" absorption strength indicated in Fig. 6. The absorption has sharp minima at the N and P=50 shell closures as suggested by Lane et al.⁵ Only a modest portion of the effect is attributable to deformation, as shown by detailed studies of extreme cases; e.g. of the effect of the strong vibration character of the palladium isotopes¹. Similar anomalous absorption has been noted in low-energy (p,n) measurements⁶ and there it has been attributed to a modulation of the density of intermediate states⁷, although the suggestion is largely qualitative. Certainly, the absorption evident in the present "regional" OM is inconsistent with the "global" model concept by very considerable amounts that will be manifest as corresponding differences in calculated cross sections. The "regional" OM model does predict reasonable $\ell=0$ and $\ell=1$ strength functions though those quantities were not an input to the model deduction.

Summary Comments

A quantitative "regional" OM has been obtained. Results calculated with it alleviate many of the observed discrepancies between evaluated and measured light-fission-product cross sections. The next step is a similar study of the complimentary heavy fission products. Toward that end: neutron-total-cross-section measurements have been largely completed, scattering measurements are in progress, and model development has started. The latter portion of the endeavor is difficult as the targets are generally rotators with large static deformations. As a consequence, the experimental interpretation and the model development is far more complex than for the simple spherical OM treatment discussed above.

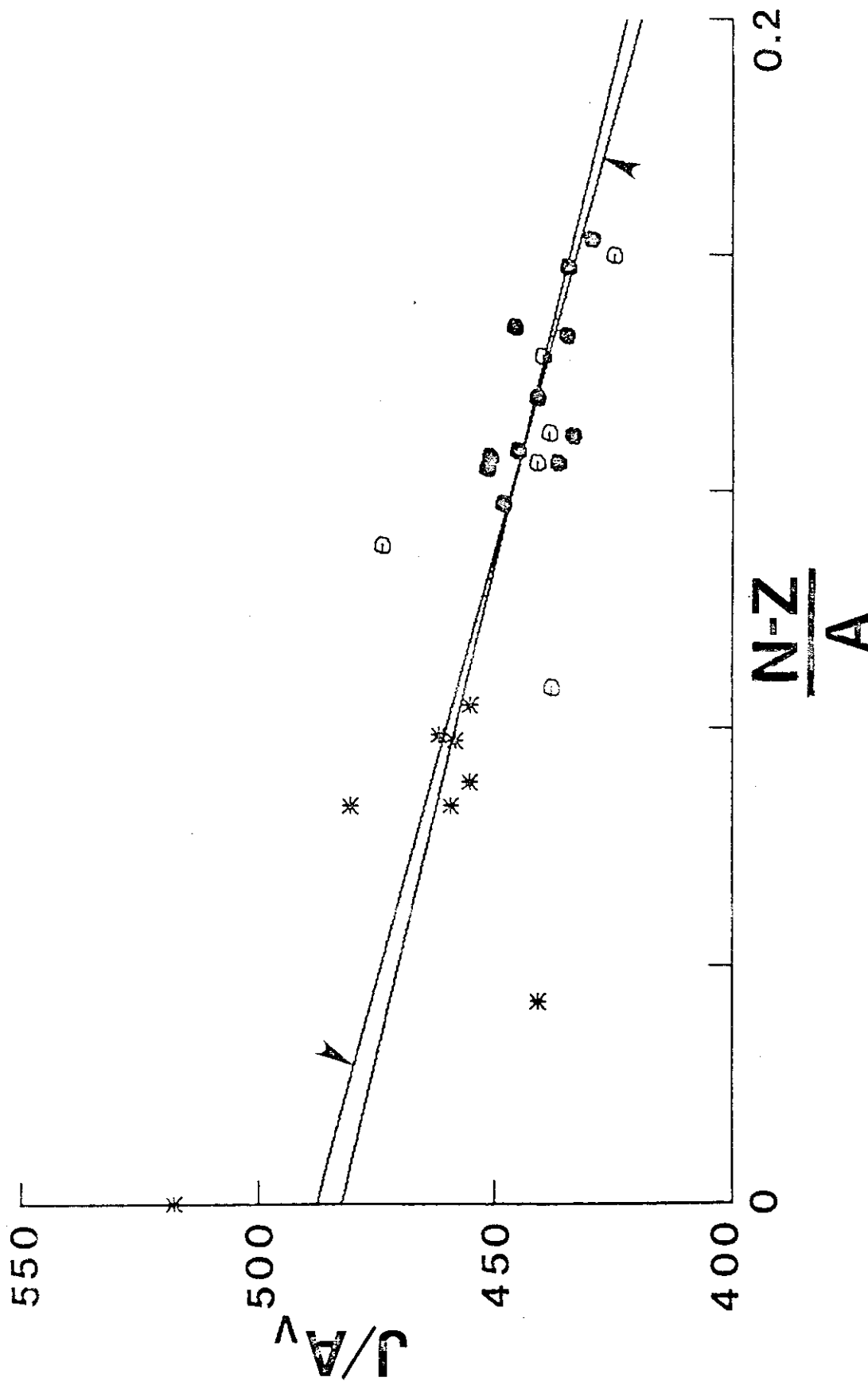


Fig. 5 The real potential strength (expressed as integral per nucleon, J/A) as a function of asymmetry $((N-Z)/A)$. Detailed specification of the figure and its interpretation are given in ref. 1

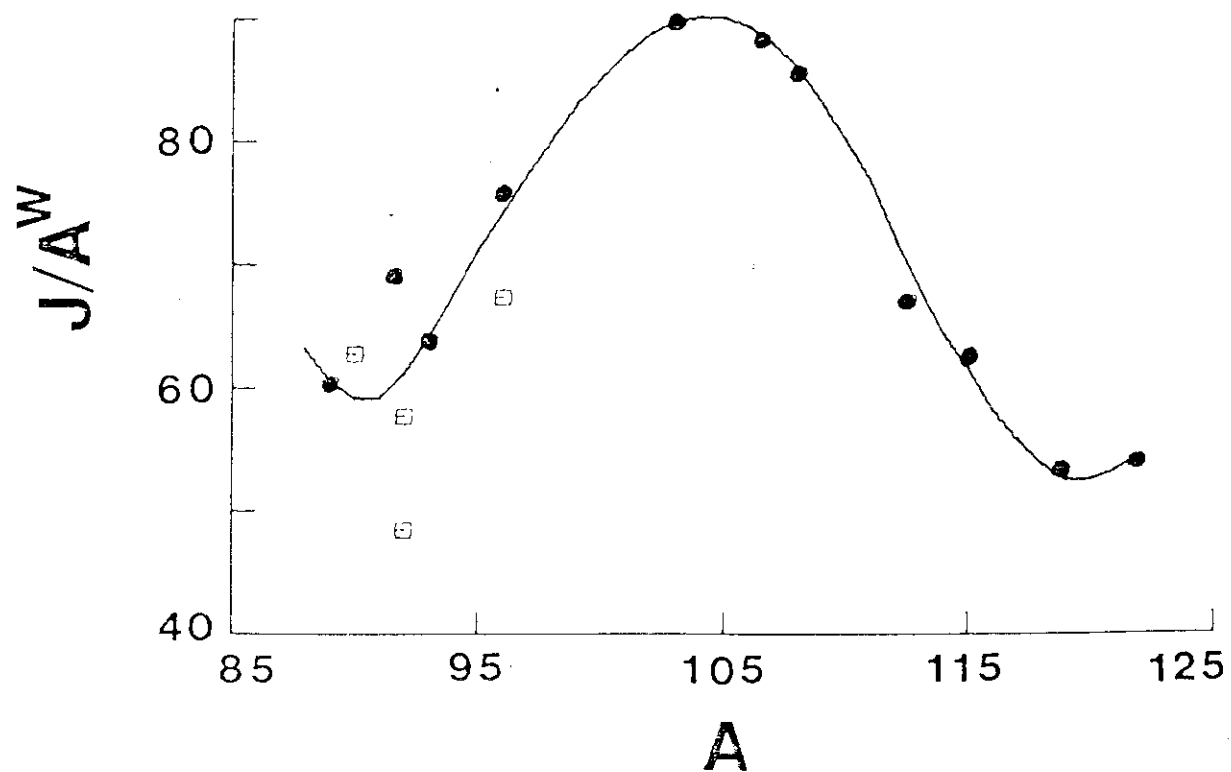


Fig. 6 The absorption strength (J/A) of the "regional" OM as a function of target mass (A). The "regional" values are noted by the curve while the results obtained for the individual targets are noted by data symbols. Details are given in ref. 1.

The author would be pleased to respond to any questions that might be directed to his office.

Argonne 3/15/84

References

1. The details of this work are found in a number of Argonne National Laboratory Reports and, particularly, in "The Optical Model of Few-MeV Neutron Elastic-scattering from Z=39 to 51 Targets", A. Smith, P. Guenther and J. Whalen, Nucl. Phys., in press.
2. P. Hodgson, Nuclear Reactions and Nuclear Structure, Clarendon Press, Oxford (1971).
3. See W. Poenitz and J. Whalen, Argonne National Laboratory Report, ANL/NDM-80 (1984).
4. A. Smith, P. Guenther and R. McKnight, Proc. Conf. on Nuclear Data for Science and Technology, Antwerp (1982).
5. A. M. Lane et al., Phys. Rev. Lett., 8 171 (1962).
6. C. Johnson, A. Galonsky and R. Kernell, Phys. Rev., C20 2052 (1979).
7. S. Grimes, Phys. Rev., C22 436 (1980).

II-5 Fission product nuclear data measurements at the JAERI LINAC

M. Mizumoto, Y. Nakajima, M. Ohkubo
M. Sugimoto, Y. Furuta and Y. Kawarasaki

Japan Atomic Energy Research Institute
Tokai-mura, Naka-gun, Ibaraki-ken, Japan

I. Introduction

Neutron cross sections of fission products are of great importance for reactor application, although it seems that the emphasis on the needs of more accurate data is gradually decreasing partly due to financial problems for fast reactor development program. But, average capture cross sections in the keV region have been still requested in WRENDA with high priority. A systematic study of the average properties of resonance parameters, strength functions and level spacings provides valuable information in order to understand neutron interaction mechanism with nuclei. The measurements of fission product cross sections carried out at the JAERI Linac were reviewed by Yamamuro and Asami (1) in the 1979 Bologna FP specialist meeting. In the present report, the only recent results since 1980 will be summarized. Some of these experimental results have been already published elsewhere.

II Experiments

A block diagram of the experimental arrangement is shown in Fig. 1. The 120 MeV electron linear accelerator has been used with the parameters and performances listed in Table 1. Neutrons are produced in a laminated water-cooled Ta target surrounded by a 5 cm thick boron-loaded polyethylene. Six evacuated neutron flight paths are available for measurements. The 100 m and 190 m stations have been used mainly for high energy resolution transmission experiments with five 11.1 cm diameter x 1.25 cm thick ^6Li -glass detector or NE110 plastic detector. The 45 m and 55 m stations are also used for transmission experiments.

Capture cross section measurements are made either with a large scintillation detector at 55 m or with a Moxon-Rae detector at 45 m. Recently an old 3500 l scintillator tank was replaced by a smaller 500 l tank. The new tank is optically separated into halves by thin aluminized mirror, so that background counts are reduced by operating the two halves of the tank in coincidence. Neutrons captured by hydrogens in liquid are reduced by adding tri-methylborate. Neutron flux is measured with a ^6Li -glass scintillation detector or with a ^{10}B -NaI

detector. A time dependent background is determined by a modified black resonance method, by inserting black resonance filters such as Na, Al, Mn and Co in the beam. The computer programs used for resonance analyses are a modified Harvey-Atta code and a SIOB for transmission data and a CAFIT and a TACASI for capture data. Several enriched samples for separated isotope measurements were borrowed from the Isotope Division of the Oak Ridge National Laboratory.

III. Results and discussion

1) Resonance parameter experiments.

Resonance parameter experiments of fission product nuclei performed at the JAERI Linac are listed in Table 2.1), along with the covered energy range and the flight path length used. In general, most of the old resonance parameter measurements for FP nuclei are limited to the low energy region, say 1 keV and the quality of data in the high energy region is rather poor, even when they are available. On the other hand, high resolution capture cross section measurements have been extensively carried out at ORELA for last ten years only above 2.5 keV for fast reactor application. They measured resonance capture areas for many FP nuclei. We have tried to measure also neutron widths with high resolution transmission experiments and to fill up this energy gap in order to obtain complete sets of accurate resonance parameters.

The radiative capture cross section of La-139 was measured in the energy range of 70 - 2540 eV, and capture areas for 20 resonances and radiative widths for 5 resonances were newly obtained. (2)

Neutron resonance parameters of Rb-85 and Rb-87 were determined for 138 resonances up to 18.5 keV and for 30 resonances up to 48.6 keV, respectively. Average parameters listed in Table 3a show large difference in average level spacing and radiative widths due to the different neutron binding energy for these nuclei. Cumulative sum of the resonance levels and reduced neutron widths for Rb-87 are shown in Figs. 2 and 3 with several curves with different cut-off values of reduced neutron widths. Four large s-wave resonances, which have 37 % of the strength below 50 keV, are found in this experiment. (3)

Resonance energies and neutron widths for silver isotopes were obtained in the energy region of 400 eV - 7 keV. Average parameters deduced are $S_0 = (0.43 \pm 0.05) \times 10^{-4}$, $D_0 = 20 \pm 2$ eV for Ag-107 and $S_0 = (0.45 \pm 0.05) \times 10^{-4}$, $D_0 = 20 \pm 2$ eV for Ag-109. In these nuclei, admixture of p-wave resonances are expected to be observed in small s-wave resonances due to the large p-wave

strength functions as shown in Fig. 5. For the analysis of missing resonances, the procedure proposed by Moore was adopted, which uses the moments of the reduced neutron widths. (4) The detectability of small resonances for our experiments are indicated as the curve in Fig. 6. The large differences between strength functions of Ag-107 and Ag-109 observed below 1 keV disappeared in the higher energy range. (5)

Very recently, resonances of Sn-122 were measured up to 30 keV and average resonance parameters are newly obtained, being $S_0 = (0.30 \pm 0.12) \times 10^{-4}$, $D_0 = 1.17 \pm 0.27$ keV and $R' = 0.60 \pm 0.05$ fm. Cumulative plot of reduced neutron widths are shown in Fig. 8. The transmission and capture measurements of several other isotopes such as Sb-121, Sb-123, Ba-135, Ba-137 and Ba-138 have been recently completed and the analyses are in progress. Fig. 4 shows a cumulative values of $g\Gamma_n^0$ of Sb-123 vs. neutron energy, with several cut-off values in $g\Gamma_n^0$.

2) Average capture data

The measurements of average capture cross sections are listed in Table 2.2). These cross section data were used to deduce average resonance parameters by fitting the data with the energy independent strength function model.

The average capture cross sections for odd isotopes of gadolinium were measured from 1.1 keV to 220 keV with a 500 l liquid scintillator tank. Figs. 9 and 10 show our results for Gd-155 and Gd-157, respectively. Previous measurements for these isotopes in keV region were only made by Shorin et al. (6), while recent data by Voignier et al. (7) cover only above 500 keV. The slope of the data by Shorin et al. are slightly steeper than our data. The solid curves are calculated with the preliminary values of strength functions given in Table 3b.

Capture cross section measurements for Ag-107, Ag-109 and Ag-nat were carried out with a 3500 l liquid scintillation detector. ^6Li and ^{10}B were used to determine relative neutron flux and normalization was made by the saturated resonance method. Numerical values of cross sections are listed in Table 4 together with statistical uncertainties in percentage. We tried to fit the three kinds of data simultaneously with consistent strength functions, by taking into account the correlation of the input data in the different energy and with the different isotopes. The sources of systematic uncertainties, which might correlate the data points, are given in Table 5. The shape of time dependent background is expressed by the power of neutron energy. Uncertainties caused by sample thickness and normalization correlates the data in different energy bin by 100 % for each sample. The correlation matrices for our standard cross section $B(n, d\gamma)$ are taken from the ENDF/B-V. In the low energy region where standard cross section is inversely proportional to neutron velocity, correlation of these cross sections is assumed to be 100 %. The standard deviations of the

systematical uncertainties, that are the square roots of diagonal elements of the covariance matrices, are listed in Table 6. Energy bins are adapted from the JAERI Fast Set used for fast reactor calculation. The computer program was developed to calculate correlation matrix of uncertainty by error propagation rules. (8) Table 7a-7c show the deduced correlation matrices of systematic uncertainties for Ag-107 itself in the different energy and between Ag-nat and Ag-109. Six similar matrices are calculated in the same manner. Uncorrelated uncertainties due to counts statistics and width fluctuations from Porter-Thomas and Wigner distribution of resonance are also taken into account. A least squares method to fit the data with the strength function model is based on the similar procedure proposed by Perey. (9) By assuming that experimental values D^0 and initial parameters P are independent of each other, the determination of new parameters P' is given by minimizing with

$$X^2 = (P - P')^T M^{-1} (P - P') + (D^0 - D')^T V^{-1} (D^0 - D') ,$$

where M specifies the uncertainties of P and V is covariance matrix of data, and $D' = D + G (P' - P)$, G is a sensitivity matrix with the element $g_{ij} = \partial d_i / \partial p_j$, D is a vector of calculated values using P . In the calculation, only diagonal parts were considered in the covariance matrix M for parameters. The initial values for parameters and their standard deviations are listed in the fourth column of Table 8a, by using our results of resonance analyses, and the recent BNL-325, 4th edition. Fig. 11 shows the cross section data and the fitted curves. Calculated curves for Ag-109 and Ag-nat are obviously low in the low energy region compared with the experimental values. This might be interpreted as the influence of small initial values of s-wave strength function of Ag-109.

In the 6th column of Table 8a, results which obtained with the conventional method are listed. In this method, fit was made separately for Ag-107 and Ag-109 capture cross sections assuming no correlations. As the result, the very similar average resonance parameters are obtained from two different methods. Table 8b shows the correlation matrices of the fitted average parameters. The strong correlations between s-wave and p-wave and between p-wave and d-wave strength functions calculated with the conventional method is somewhat unrealistic. These correlations disappear in the result when the correlations of the input data are considered.

IV Acknowledgement

The authors wish to thank Dr. S. Tanaka for his continuous interest and encouragement. Thanks are also due to Dr. I. Tsubone and Professor Y. Kanda of Kyushu Univ. for their cooperation. The technical assistances of Messrs. T. Shoji and K. Mashiko and other Linac staff are greatly acknowledged.

References

- (1) N. Yamamuro and A. Asami, NEANDC Specialist's Meeting on Neutron Cross Sections of Fission Product Nuclei, 1979, Bologna, Italy Report NEANDC(E)-209, p19.
- (2) Y. Nakajima et al., J. Nucl. Sci. Technol. 20 (1983) 183
- (3) M. Ohkubo, M. Mizumoto and Y. Kawarasaki, to be published in J. Nucl. Sci. Technol. 21 (1984)
- (4) M. Moore, A. Thompson and P. Ribon, NEANDC-160-U, (1982)
- (5) M. Mizumoto et al., Proc. Int. on Nuclear Data for Science and Technology, 1982, Antwerp, Belgium, p982 J. Nucl. Sci. Technol. 20 (1983) 883
- (6) V.S. Shorin, V.N. Kononov and E.D. Poletaev, Soviet J. of Nucl. Phys. 19 (1974) 2
- (7) J. Voignier et al., Int. Conf. on Nuclear Cross Sections for Technology, Knoxville, 1979, p323
- (8) M. Sugimoto, to be published.
- (9) F.G. Perey, Int. Conf. on Neutron Physics and Nuclear Data for Reactors and Other Applied Purposes, AERE Harwell, 1978, p104

Table 1 JAERI linac parameters and performances.

Electron energy	120 MeV
Operating frequency	2857 MHz (s-band)
Pulse repetition rate	12.5 - 450 pps
Pulse width	10 ns - 2 μ s
Maximum peak current	6 A (20 ns) - 600 mA (1 μ s)
Maximum beam power	4.5 kW (short pulse)
Neutron target	Laminated water-cooled Ta
Moderator thickness	5 cm
Number flight paths	5 (18.5 - 190 m)

Table 2 Recent measurements of fission product nucleus cross sections at the JAERI Linac

1) Resonance parameter measurements

Target nucleus	Energy range (eV)	Flight path length (m)
La-139	700 - 2540	52
Ag-107, Ag-109	1.5 - 7000	52, 56, 190
Rb-85, Rb-87	200 - 18500 (Rb-85) 200 - 48600 (Rb-87)	47, 190
Sb-121, Sb-123	20 - 6000	47, 190
Sn-122	100 - 3000	47, 190
Gd-155, Gd-157	a)	190
Ba-135, Ba-137	a)	52, 56, 190
Ba-138		

2) Average capture cross section measurements at 52 m.

Target	Energy (keV)	Uncertainty (%)
Ag-107, Ag-109	3.2 - 700	4 - 7
Gd-155, Gd-157	1.1 - 220	5 - 8
Sb-123, Sb-123	a)	
Ba-135	a)	

a) Experiments have been completed, and analyses are in progress.

Table 3a Average resonance parameters of Rb-85 and Rb-87.

Average parameter	Rb-85	Rb-87
$S0 \cdot 10^{**4}$	0.94 ± 0.11	1.15 ± 0.3
$D0$ (eV)	133 ± 11	1380 ± 250
$\langle \Gamma_r \rangle$ (meV)	328 ± 18	166 ± 30

Table 3b Average resonance parameters of Gd-155 and Gd-157
(preliminary values)

Average parameter	Gd-155	Gd-157
$S0 \cdot 10^{**4}$	3.00 ± 0.28	2.4 ± 0.2
$\langle \Gamma_r \rangle$ (meV)	120 ± 30	109 ± 6
$S1 \cdot 10^{**4}$	3.7 ± 1.1	2.3 ± 0.2
$\langle \Gamma_f \rangle$ (meV)	140 ± 60	130 ± 9
$S2 \cdot 10^{**4}$	1.0 ± 0.5	

Table 4 Average capture cross sections of Ag-107, Ag-109 and Ag-nat.

En (keV)	Ag-107 (barn)	Ag-109 (barn)	Ag-nat (barn)
	a)	a)	a)
3.2 - 4	1.810 (0.9)	1.851 (1.0)	2.221 (1.1)
4 - 5	1.765 (0.5)	1.713 (0.5)	1.973 (0.6)
5 - 6	1.568 (0.5)	1.629 (0.5)	1.778 (0.6)
6 - 7	1.490 (0.5)	1.671 (0.6)	1.737 (0.6)
7 - 8	1.246 (0.6)	1.391 (0.6)	1.455 (0.6)
8 - 9	1.407 (0.5)	1.637 (0.5)	1.620 (0.6)
9 - 10	1.352 (0.6)	1.320 (0.6)	1.445 (0.7)
10 - 12	1.186 (0.4)	1.349 (0.4)	1.345 (0.5)
12 - 14	1.138 (0.5)	1.171 (0.5)	1.207 (0.6)
14 - 16	1.068 (0.5)	1.309 (0.6)	1.101 (0.6)
16 - 18	1.062 (0.5)	1.075 (0.6)	1.112 (0.7)
18 - 20	1.037 (0.5)	1.061 (0.6)	1.068 (0.7)
20 - 25	0.963 (2.6)	1.010 (2.7)	0.988 (3.1)
25 - 30	0.911 (2.8)	0.855 (3.2)	0.888 (3.4)
30 - 35	0.825 (3.5)	0.816 (3.8)	0.814 (4.3)
35 - 40	0.762 (3.9)	0.748 (4.3)	0.732 (4.9)
40 - 45	0.683 (4.1)	0.681 (4.4)	0.696 (5.0)
45 - 50	0.679 (3.8)	0.623 (4.4)	0.667 (4.7)
50 - 60	0.593 (3.1)	0.575 (3.3)	0.586 (3.7)
60 - 70	0.554 (3.0)	0.518 (3.3)	0.536 (3.7)
70 - 80	0.525 (3.8)	0.477 (4.3)	0.502 (4.8)
80 - 90	0.484 (4.0)	0.438 (4.5)	0.441 (5.1)
90 - 100	0.451 (3.9)	0.419 (4.4)	0.439 (5.1)
100 - 120	0.403 (2.8)	0.375 (3.2)	0.382 (5.2)
120 - 140	0.366 (3.0)	0.337 (3.4)	0.344 (5.5)
140 - 160	0.347 (3.5)	0.316 (4.0)	0.309 (6.7)
160 - 180	0.314 (3.6)	0.291 (4.0)	0.293 (6.6)
180 - 200	0.292 (3.7)	0.285 (4.1)	0.268 (6.6)
200 - 250	0.271 (2.6)	0.257 (2.9)	0.249 (4.6)
250 - 300	0.246 (2.8)	0.232 (3.1)	0.233 (4.4)
300 - 350	0.230 (3.0)	0.213 (3.3)	0.213 (4.6)
350 - 400	0.193 (3.5)	0.179 (4.0)	0.171 (5.6)
400 - 450	0.177 (4.0)	0.157 (4.5)	0.153 (6.2)
450 - 500	0.142 (4.0)	0.133 (4.5)	0.135 (5.0)
500 - 600	0.113 (3.3)	0.109 (3.6)	0.110 (5.1)
600 - 700	0.094 (3.9)	0.091 (4.3)	0.101 (6.1)

a) Statistical standard deviations given in percentage.
Systematic uncertainties are discussed separately.

Table 5 The sources of uncertainties in the measured capture cross section of silver isotopes.

Source of uncertainty	Neutron energy region (keV)		
	10 - 20 (%)	80 - 100 (%)	300 - 400 (%)
Background of capture yield	1.4	2.5	1.0
Normalization	2.2	2.2	2.2
Background of neutron flux	0.0	0.6	1.4
Relative efficiency of flux detector	1.0	1.4	2.6
Sample thickness	2.0	2.0	2.0
Sample thickness corrections	2.4	2.6	2.8
Total	4.2	4.9	5.1

Table 6 Systematic uncertainties of measured capture cross sections of silver isotopes for each group.

Group No.	Energy (keV)	Ag-107 (%)	Ag-109 (%)	Ag-nat (%)
1	630 - 500	5.72	5.77	5.88
2	500 - 400	5.33	5.40	5.51
3	400 - 310	5.08	5.16	5.32
4	310 - 250	4.95	5.05	5.25
5	250 - 200	4.86	5.01	5.27
6	200 - 150	4.74	4.98	5.31
7	150 - 120	4.56	4.95	5.14
8	120 - 100	4.51	5.03	5.13
9	100 - 77.3	4.59	5.45	5.59
10	77.3 - 59.8	4.49	5.10	5.44
11	59.8 - 46.5	4.55	5.31	5.93
12	46.5 - 36.0	4.69	5.51	6.35
13	36.0 - 27.8	4.70	5.61	6.96
14	27.8 - 21.5	4.69	5.15	7.09
15	21.5 - 16.6	4.81	5.24	7.20
16	16.6 - 12.9	4.36	4.49	5.14
17	12.9 - 10.0	4.43	4.54	5.17
18	10.0 - 7.73	4.50	4.65	5.34
19	7.73 - 5.98	4.68	4.85	5.63
20	5.98 - 4.65	4.68	5.07	6.13
21	4.65 - 3.60	5.12	5.17	5.71

Table 7a Correlation matrix (x100) for capture cross sections of Ag-107 isotope.

Group	1	2	3	4	5	6	7	8	9	10	11	12	13	14	15	16	17	18	19	20	21
1	100																				
2	92	100																			
3	87	95	100																		
4	85	93	99	100																	
5	83	92	97	99	100																
6	83	90	96	97	99	100															
7	86	90	94	96	97	98	100														
8	86	90	93	95	97	98	99	100													
9	84	88	92	93	95	97	99	99	100												
10	82	86	91	92	95	97	98	99	100	100											
11	79	85	88	90	93	95	97	98	99	99	100										
12	76	81	85	86	90	92	94	96	98	98	98	100									
13	73	78	82	83	87	90	92	94	97	97	98	99	100								
14	69	75	78	81	84	88	90	92	95	96	97	98	99	100							
15	65	70	74	76	81	84	87	89	92	93	96	97	98	99	100						
16	60	65	68	70	71	73	77	78	77	79	78	77	77	78	76	100					
17	59	64	67	68	70	72	75	77	76	78	77	76	76	77	75	100	100				
18	59	63	66	68	69	71	75	76	75	77	76	75	75	76	75	100	100	100			
19	57	61	64	65	67	69	72	73	73	75	74	73	73	74	72	99	100	100	100		
20	57	61	64	66	67	69	72	74	73	75	74	73	73	74	73	99	100	100	100	100	
21	52	56	58	60	61	63	66	67	67	69	68	67	67	68	67	97	98	98	99	99	100

Table 7b Correlation matrix (x100) for capture cross sections of
Ag-109 and AC-107 isotopes.

Group	1	2	3	4	5	6	7	8	9	10	11	12	13	14	15	16	17	18	19	20	21
1	49	39	32	29	25	24	24	23	20	18	15	13	10	6	3	0	0	0	0	0	0
2	39	43	36	33	29	26	24	22	20	18	16	13	10	7	4	0	0	0	0	0	0
3	32	35	38	35	32	28	24	22	20	18	15	13	10	7	4	0	0	0	0	0	0
4	28	32	35	34	31	28	24	21	19	18	15	13	10	7	4	0	0	0	0	0	0
5	25	29	31	31	30	27	22	20	18	17	14	12	9	7	4	0	0	0	0	0	0
6	23	25	27	27	26	25	21	19	17	16	13	11	9	6	4	0	0	0	0	0	0
7	22	22	23	22	21	20	19	17	15	14	12	10	8	5	3	0	0	0	0	0	0
8	20	20	20	20	19	18	16	15	14	12	11	9	7	5	3	0	0	0	0	0	0
9	17	17	17	17	16	15	14	13	12	11	9	8	6	4	2	0	0	0	0	0	0
10	16	16	16	16	15	14	13	12	11	10	9	7	6	5	2	0	0	0	0	0	0
11	13	13	13	13	13	12	11	10	9	9	8	6	5	4	2	0	0	0	0	0	0
12	11	11	11	11	11	10	9	9	8	7	6	6	4	3	2	0	0	0	0	0	0
13	8	8	8	8	8	8	7	7	6	6	5	4	4	3	1	0	0	0	0	0	0
14	6	6	6	6	6	6	5	5	5	5	4	3	3	3	1	0	0	0	0	0	0
15	3	3	4	4	4	3	3	3	3	3	2	2	2	1	1	0	0	0	0	0	0
16	0	0	0	0	0	0	0	0	0	0	0	0	0	0	0	0	0	0	0	0	0
17	0	0	0	0	0	0	0	0	0	0	0	0	0	0	0	0	0	0	0	0	0
18	0	0	0	0	0	0	0	0	0	0	0	0	0	0	0	0	0	0	0	0	0
19	0	0	0	0	0	0	0	0	0	0	0	0	0	0	0	0	0	0	0	0	0
20	0	0	0	0	0	0	0	0	0	0	0	0	0	0	0	0	0	0	0	0	0
21	0	0	0	0	0	0	0	0	0	0	0	0	0	0	0	0	0	0	0	0	0

Table 7c Correlation matrix (xl00) for capture cross sections of Ag-nat and AG-107 isotopes.

Group	1	2	3	4	5	6	7	8	9	10	11	12	13	14	15	16	17	18	19	20	21
1	41	33	27	24	22	20	21	20	19	17	15	13	10	7	4	2	2	2	2	2	1
2	33	38	32	29	27	23	22	21	19	18	16	13	10	8	5	2	2	2	2	2	1
3	26	31	34	32	29	26	23	21	19	18	16	14	11	8	5	2	2	2	2	2	1
4	23	29	31	31	29	25	22	21	19	18	16	13	11	8	5	2	2	2	2	2	1
5	20	25	28	28	28	24	21	20	18	17	15	13	10	8	5	2	2	2	2	2	1
6	19	22	24	24	24	23	19	18	17	16	14	12	10	7	5	2	2	2	2	2	1
7	19	20	21	21	20	19	18	17	15	14	13	11	9	7	4	2	2	2	2	2	1
8	19	19	19	19	19	18	17	16	15	14	12	11	8	6	4	2	2	2	2	2	1
9	16	16	17	16	16	15	14	14	13	12	11	9	8	6	4	2	2	2	2	2	1
10	15	15	16	15	15	14	14	13	12	12	10	9	7	6	4	2	2	2	2	2	1
11	12	13	13	13	12	12	11	11	10	9	9	7	6	5	3	2	2	2	1	1	1
12	10	10	10	10	10	10	9	9	8	8	7	6	5	4	3	2	2	1	1	1	1
13	7	7	8	8	7	7	7	7	6	6	5	4	3	3	2	1	1	1	1	1	1
14	5	5	5	6	5	5	5	5	5	5	4	4	3	3	2	1	1	1	1	1	1
15	3	3	3	4	4	3	3	3	3	3	3	3	2	2	2	1	1	1	1	1	1
16	2	2	2	2	2	2	2	2	2	2	2	2	2	2	2	2	2	1	1	1	1
17	2	2	2	2	2	2	2	2	2	2	2	2	2	2	2	2	1	1	1	1	1
18	2	2	2	2	2	2	2	2	2	2	2	2	2	1	1	1	1	1	1	1	1
19	2	2	2	2	2	2	2	2	2	2	2	1	1	1	1	1	1	1	1	1	1
20	1	1	1	1	1	1	1	1	1	1	1	1	1	1	1	1	1	1	1	1	1
21	1	1	1	1	1	1	1	1	1	1	1	1	1	1	1	1	1	1	1	1	1

Table 8a Average resonance parameters ;1) fitted simultaneously for Ag-107, Ag-109 and Ag-nat capture cross sections taking into account correlations between measured data. ;2) fitted separately for Ag-107 and Ag-109 capture cross sections assuming no correlations.

Number	Isotope	Average parameter	Initial guess	1) Final values (simultaneous)	2) Final values (separated)
1	Ag-107	S0x10**4	0.43 ± 0.05	0.47 ± 0.04	0.46 ± 0.05
2		S1x10**4	3.8 ± 0.6	3.7 ± 0.2	3.6 ± 0.2
3		S2x10**4	1.0 ± 0.2	1.3 ± 0.2	1.1 ± 0.3
4		Sr	0.0072 ± 0.0005	0.0061 ± 0.0003	0.0069 ± 0.0004
5	Ag-109	S0x10**4	0.45 ± 0.05	0.51 ± 0.04	0.55 ± 0.07
6		S1x10**4	3.8 ± 0.6	3.3 ± 0.2	3.4 ± 0.3
7		S2x10**4	1.0 ± 0.2	1.2 ± 0.2	1.3 ± 0.3
8		Sr	0.0073 ± 0.0005	0.0060 ± 0.0004	0.0063 ± 0.0004

Table 8b Correlation matrix (x1000) of average resonance parameters

Number	1	2	3	4	5	6	7	8
1) 1	1000							
2	-175	1000						
3	461	-317	1000					
4	-267	682	-4	1000				
5	27	-59	-80	-64	1000			
6	-80	3	75	-9	-150	1000		
7	-87	77	92	66	460	-385	1000	
8	-74	-7	58	-7	-228	663	-72	1000
2) 1	1000							
2	-741	1000						
3	737	-941	1000					
4	-606	160	-189	1000				
5					1000			
6					-761	1000		
7					765	-952	1000	
8					-644	232	-263	1000

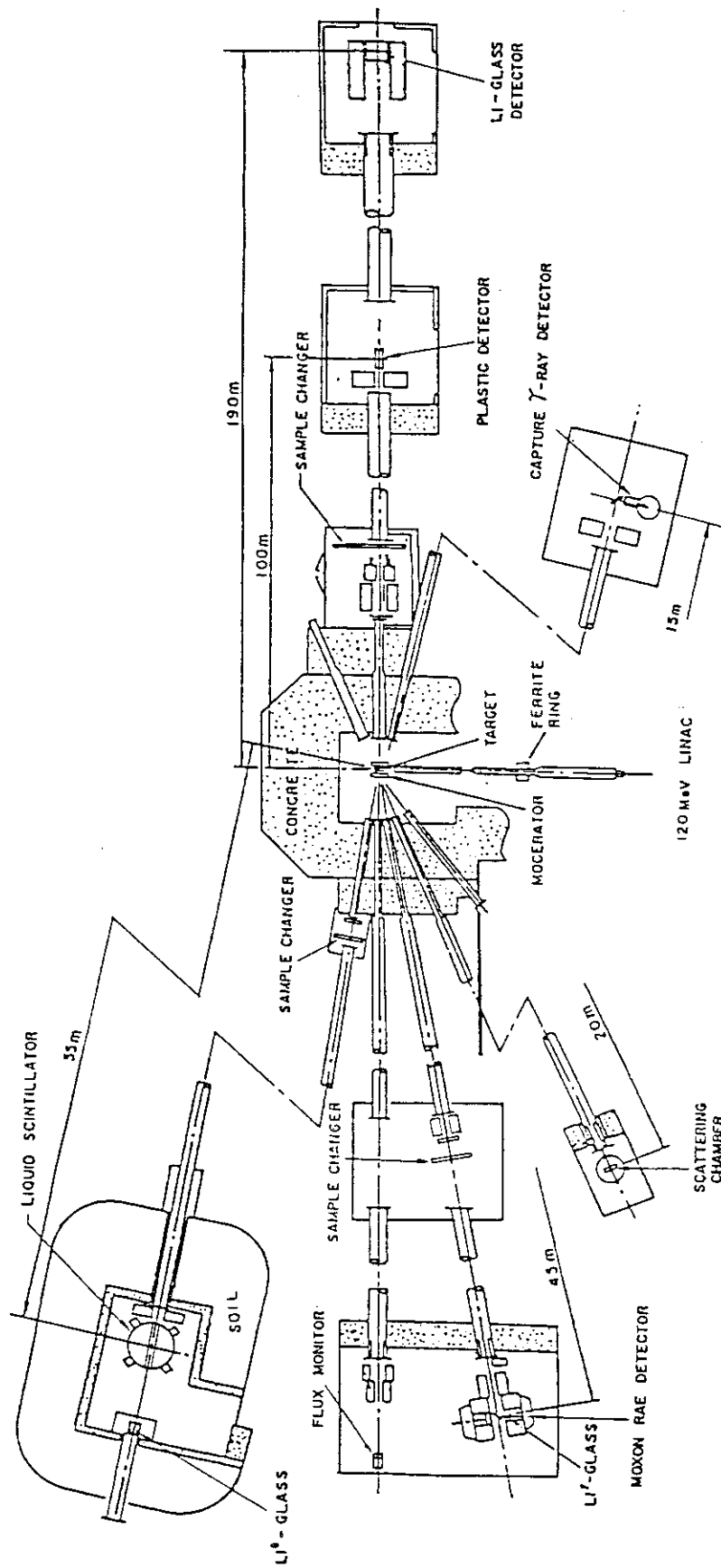


Fig. 1 Block diagram of the JAERI Linac TOF Spectrometer

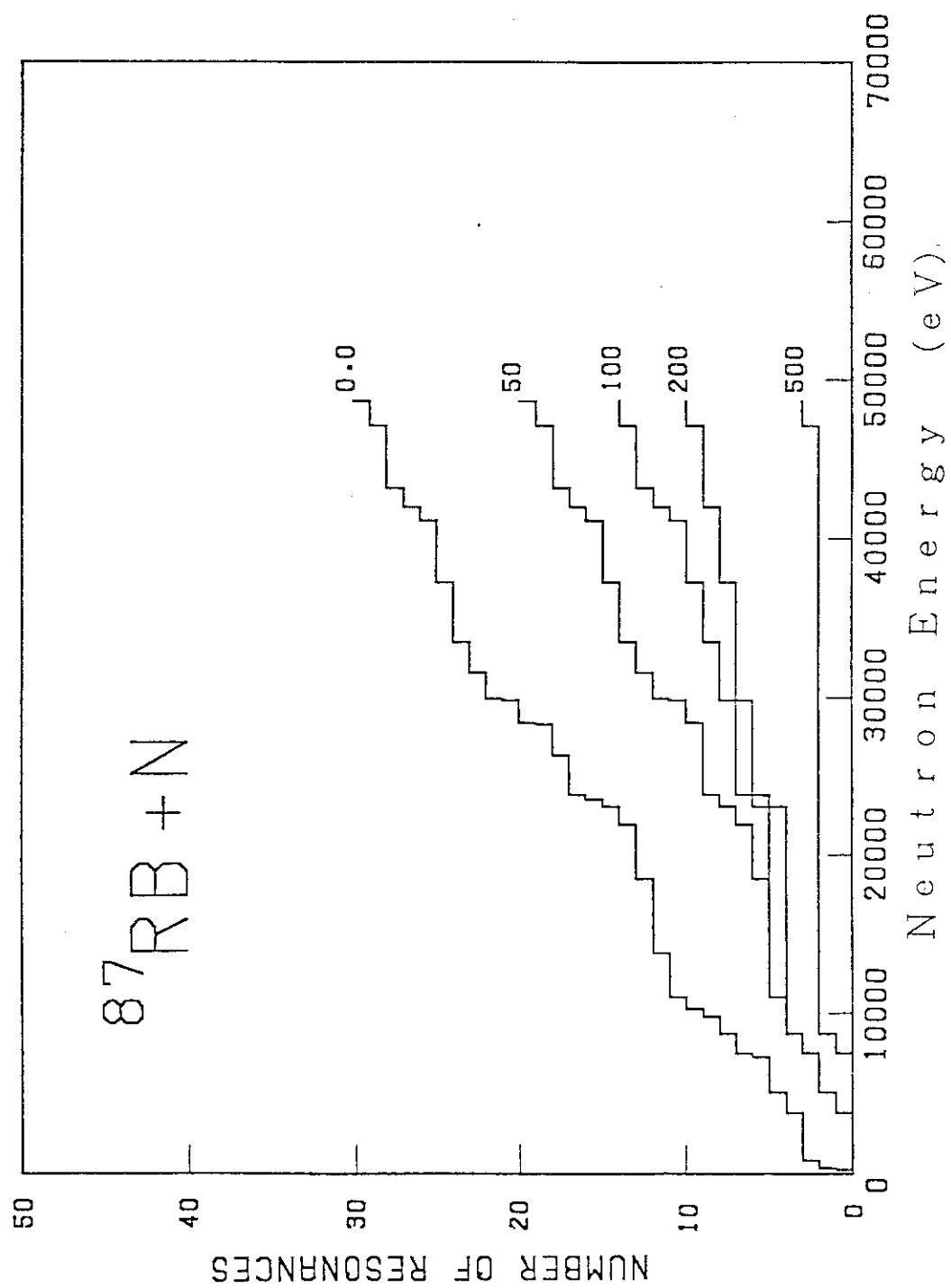


Fig. 2 Cumulative number of resonance levels vs. neutron energy for Rb-87, with several cut-off values in $g\Gamma_0$ shown in the figure.

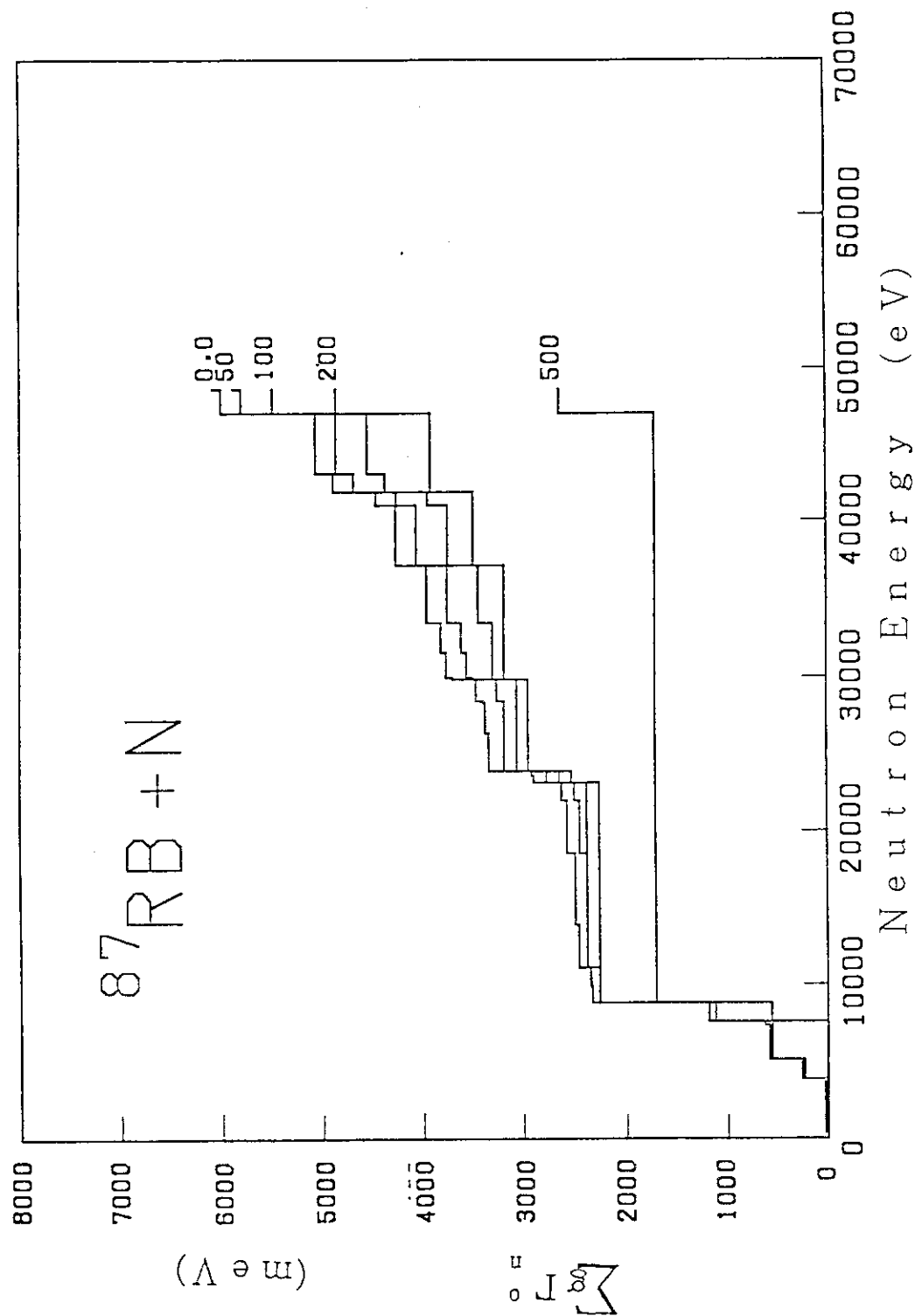


Fig. 3 Cumulative values of $g\Gamma_n^0$ of Rb-87 vs. neutron energy, with several cut-off values in $g\Gamma_n^0$. Four large s-wave levels exist in 3.8-8.8 keV region, and 37 % of $g\Gamma_n^0$ strength below 50 keV is concentrated in this region.

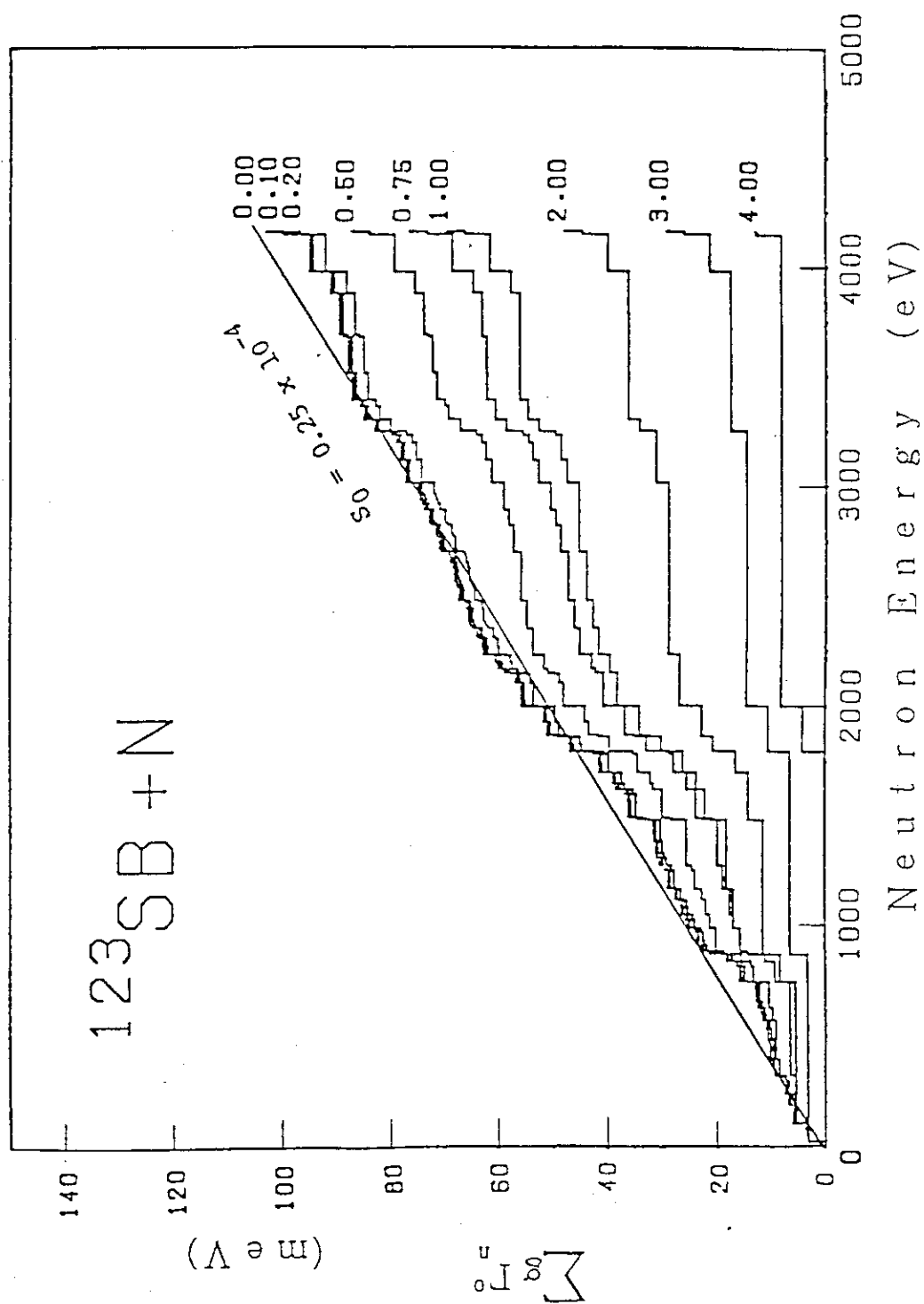


Fig. 4 Cumulative values of $g\Gamma_n^0$ of Sb-123 vs. neutron energy, with several cut-off values in $g\Gamma_n^0$.

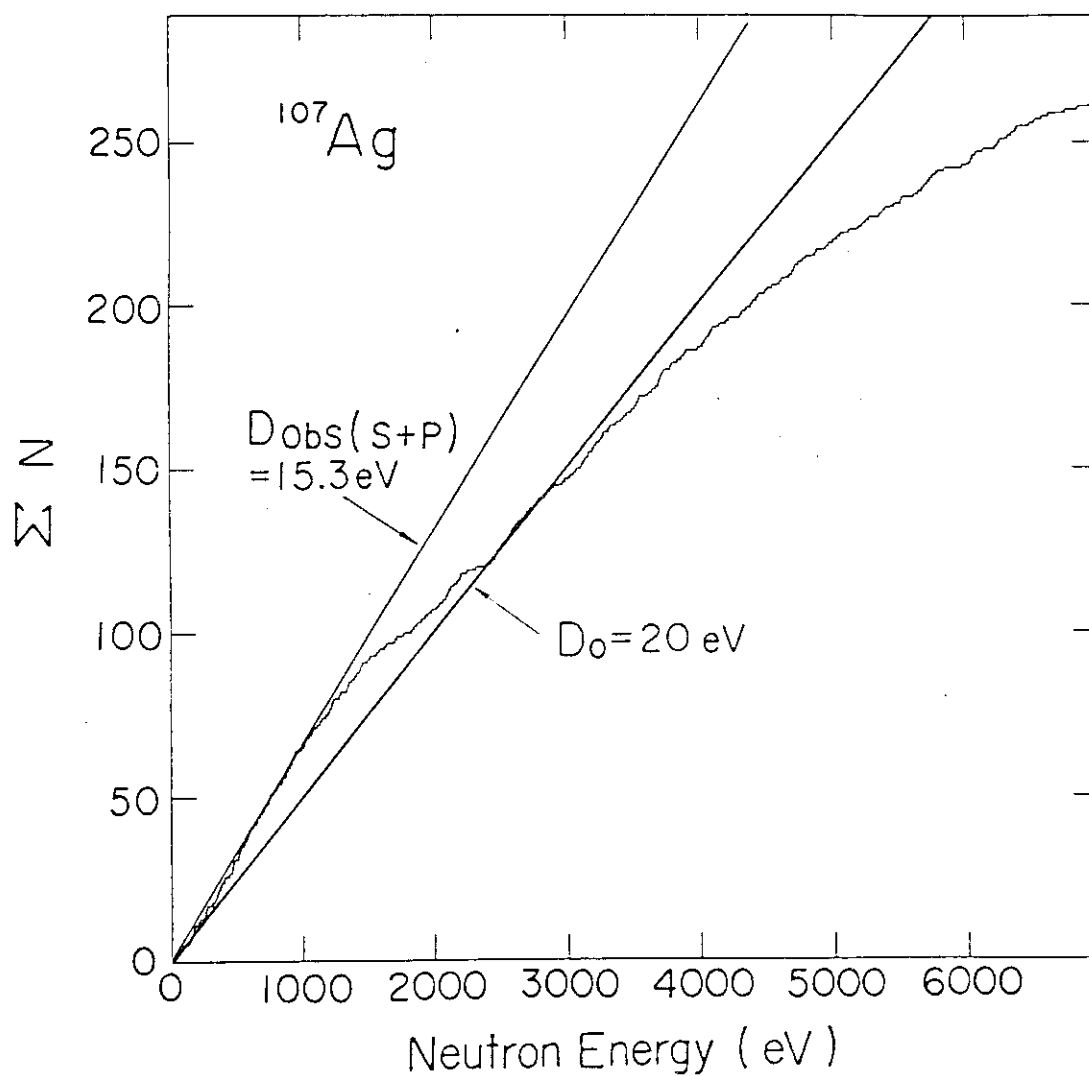


Fig. 5 Cumulative number of observed levels vs. neutron energy for Ag-107. The Dobs value represents only the slope of visually fitted line which includes s- and p-wave contribution but is not corrected for weak missing resonances. The solid slope D_0 gives our final value of the s-wave level spacing after missing levels were corrected for.

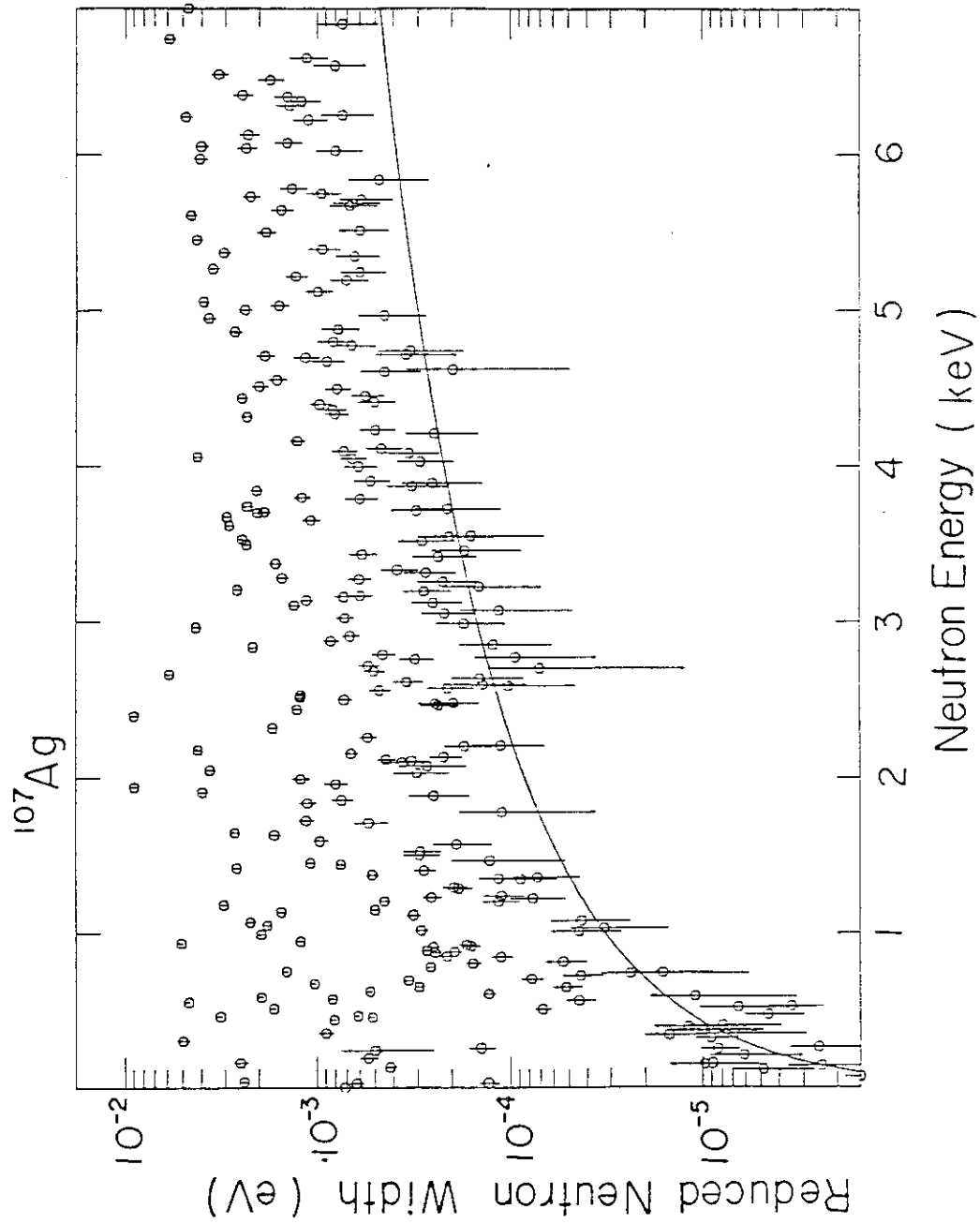


Fig. 6 Reduced neutron widths vs. neutron energy for Ag-107. The curve indicates the detectability of small resonances.

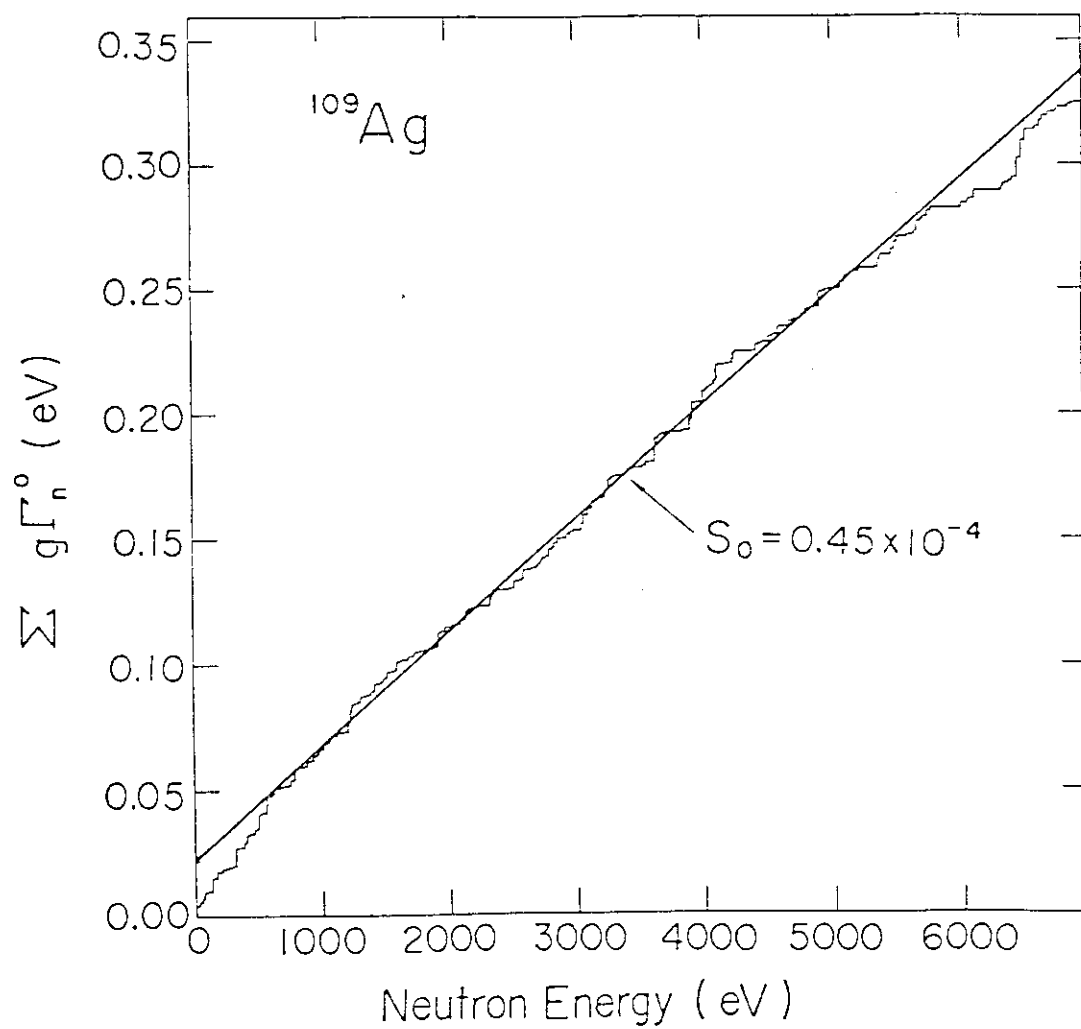


Fig. 7 $\Sigma g\Gamma_n^0$ vs. neutron energy for Ag-109. The slope gives our s-wave strength function.

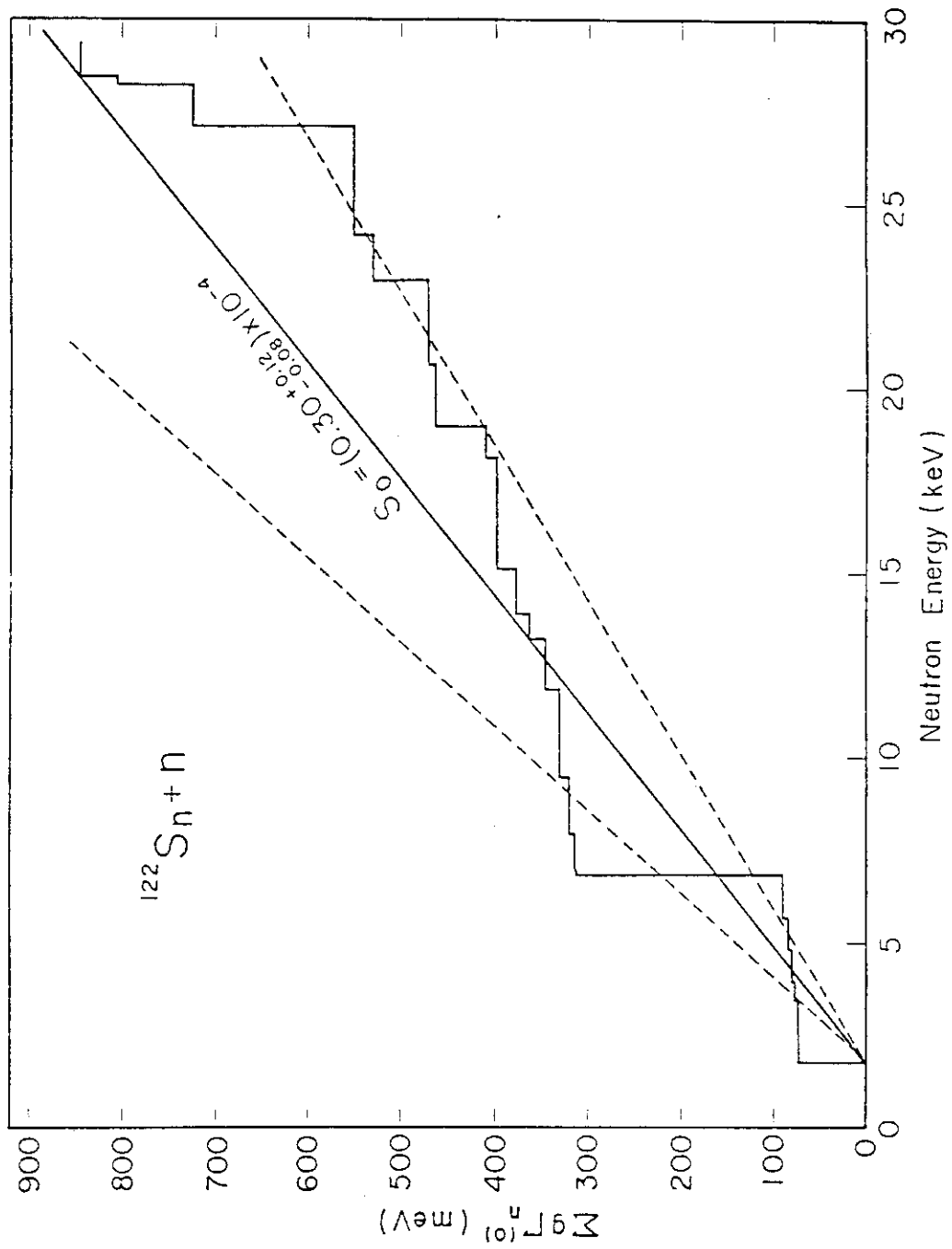


Fig. 8 $\sum g\Gamma_n^0$ vs. neutron energy for Sn-122. The slope gives our s-wave strength function.

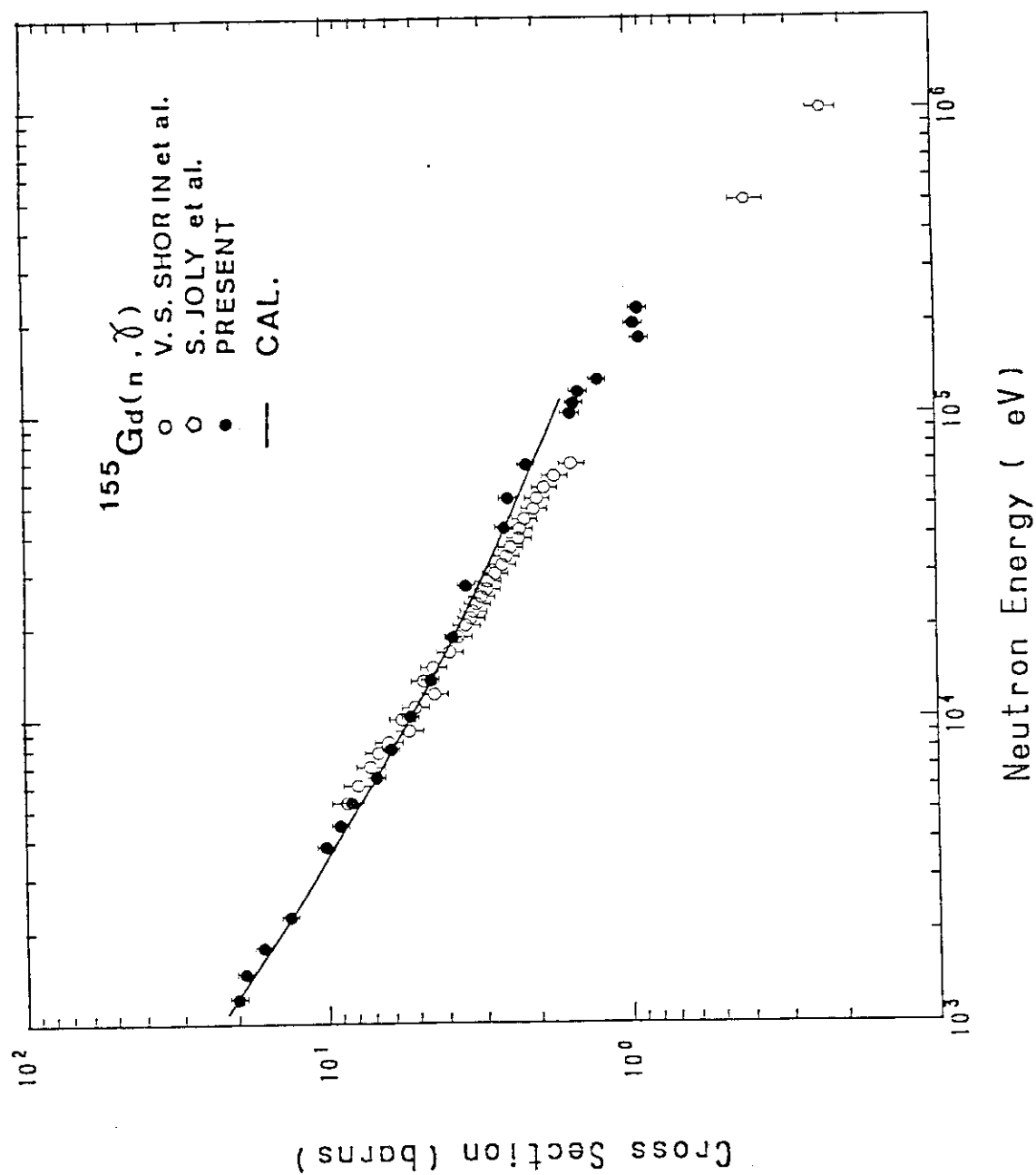


Fig. 9 Neutron capture cross section of Gd-155. The solid line gives the best fit curve calculated with strength function model.

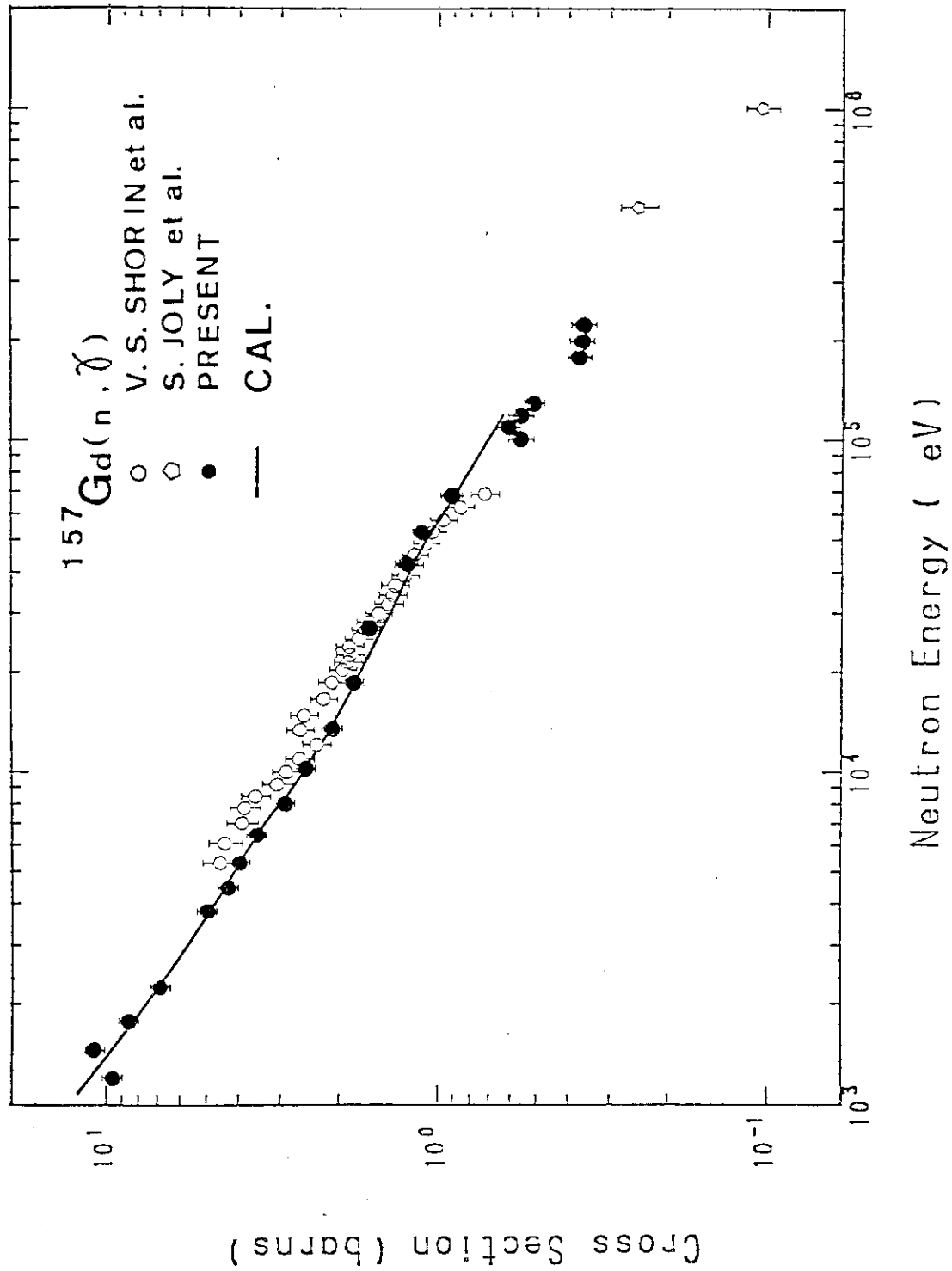


Fig. 10 Neutron capture cross section of Gd-157. The solid line gives the best fit curve calculated with strength function model.

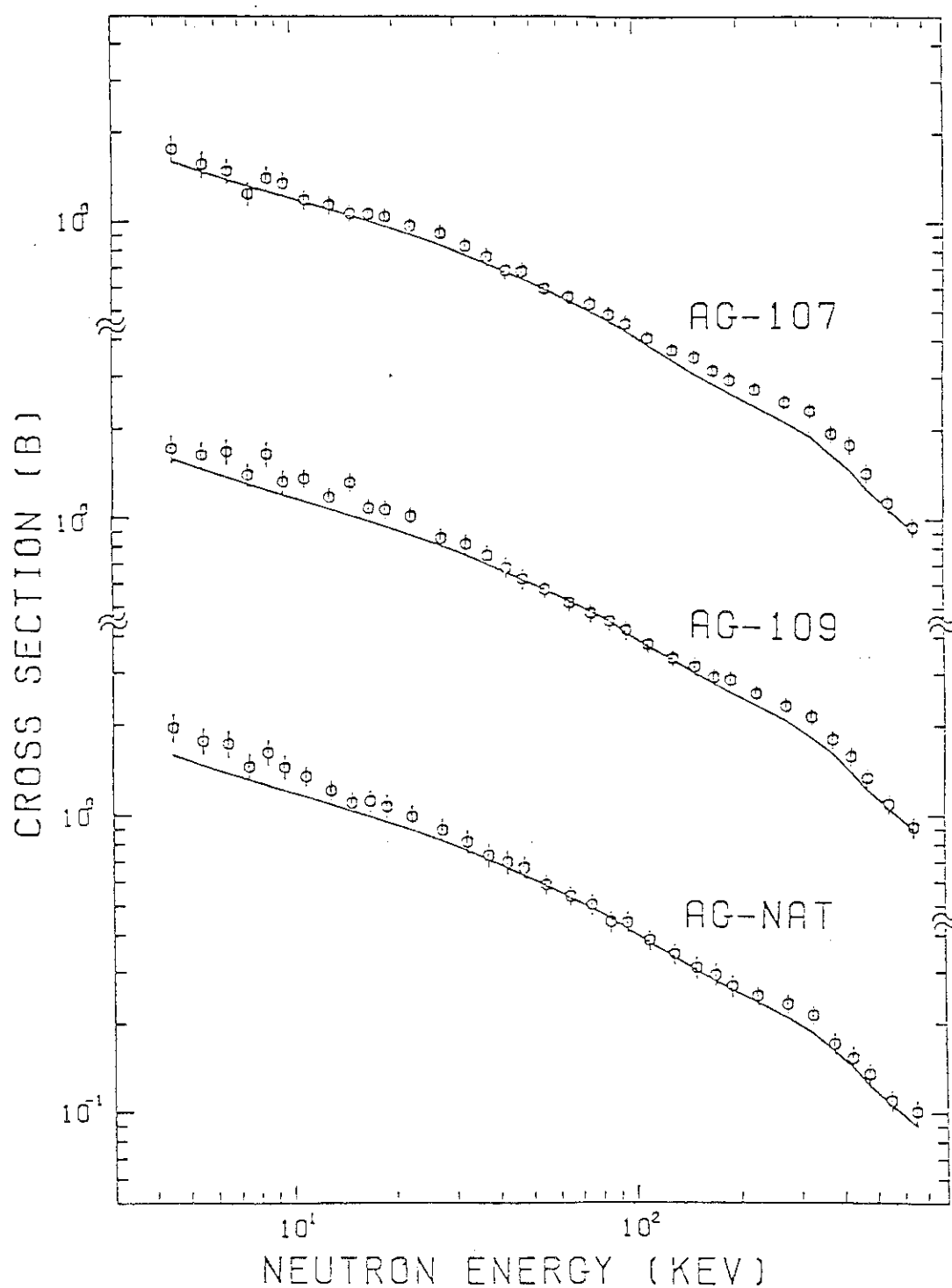


Fig. 11 Average neutron cross sections of Ag-107, Ag-109 and Ag-nat. The solid lines gives the calculated values using average resonance parameters with strength function model. The fit was made simultaneously for Ag-107, Ag-109 and Ag-nat capture cross section data taking into account correlations between measured data.

II-6 PYGMY RESONANCE APPEARED IN keV-NEUTRON CAPTURE GAMMA-RAY SPECTRA OF NUCLEI $N = 82 - 126$

Masayuki Igashira, Kazuyuki Udagawa, Tomohiro Natsume,
Hidehiro Fukui, Michio Shimizu, Haruki Komano,
Hideo Kitazawa and Nobuhiro Yamamuro*

Research Laboratory for Nuclear Reactors,
Tokyo Institute of Technology,
O-okayama, Meguro-ku, Tokyo, 152, Japan

We have measured capture gamma-ray spectra of Pr, Tb, Ho, Ta and Au with keV neutrons and observed the pygmy resonance in all these spectra. Remarkable features of the pygmy resonance were found to be that with neutron number the resonance energy increases linearly and the electric dipole strength exhausted in the resonance increases exponentially.

I. INTRODUCTION

Many workers have observed an anomalous bump around 5.5 MeV in gamma-ray spectra from (n, γ) and $(d, p\gamma)$ reactions on several nuclei $110 < A < 140$ and $180 < A < 210$ at the neutron energies of $-1.5 - 4.0$ MeV[1 - 4]. The bump is generally referred to as "pygmy resonance", and the following features have been clarified for the resonance: (1) The resonance energy is independent of the incident neutron energy. This fact implies that the resonance would not results from the irregularity of the nuclear level density, but from the resonance structure of gamma-ray strength function. (2) The net area of the bump relative to the total area in the gamma-ray spectrum increases with mass number in each mass region.

Harvey and Khanna[5] have explained the pygmy resonance as a concentration of the low energy electric dipole strength, using the schematic model of Goswami and Pal[6].

On the other hand, Joly et al.[7] found a bump around 3.5 MeV in the neutron capture gamma-ray spectra of Tm at the neutron energies of $0.5 - 2.5$ MeV. They have shown that the bump can be expressed by the Brink-Axel gamma-ray strength function[8] with a small resonance of the width 1.0 MeV at 3.5 MeV.

Here, great interest in the pygmy resonances observed so far is to know whether or not these resonances have a common physical origin. From this point of view, we have measured keV-neutron capture gamma-ray spectra in the mass region $140 < A < 200$.

II. EXPERIMENTAL PROCEDURES AND DATA PROCESSING

The experimental arrangement is shown schematically in Fig. 1. Neutrons were generated by the ${}^7\text{Li}(p, n){}^7\text{Be}$ reaction using the pulsed proton beam from the 3.2-MV Pelletron accelerator in Tokyo Institute of Technology. The average proton beam current was typically $4\ \mu\text{A}$ for the repetition rate of 2MHz and the pulse width of about 1 ns. Incident neutrons to a sample were monitored by a

* Present address: Nippon Atomic Industry Group Co., Ltd.,
Ukishima-cho, Kawasaki-ku, Kawasaki, 210, Japan

^6Li -glass scintillation detector located at 4.8 m from the neutron source. Measurements of capture gamma-ray spectra were performed by a time-of-flight technique at several neutron energies between 10 and 800 keV for Tb, Ho and Au, and at 540 and 420 keV for Pr and Ta, respectively. The energy spread of neutrons was 8 - 70 keV. The samples were ~ 50 mm in diameter and ~ 0.03 atoms/b in thickness, and Tb sample was a 100 x 100 mm plate. Each sample was located at 150 mm from the neutron source. Gamma-rays from the sample were detected by a 76 mm ϕ x 156 mm NaI(Tl) detector centered in an annular NaI(Tl) crystal, 254 mm in outer diameter and 280 mm in the length. Both detectors, which were placed in a heavy shield of borated paraffin, lead and cadmium, operated as an anti-Compton gamma-ray spectrometer. The detector system was mounted on a goniometer rotating around an axis at the position of the sample. The distance between the sample and the spectrometer was about 80 cm. Gamma-rays were observed at an angle of 125° with respect to the proton beam direction.

A typical time-of-flight spectrum for Tb sample is shown in Fig. 2. The peak b shows capture gamma-rays by direct neutrons to the sample from the neutron source and the peak c is due to the neutrons scattered by the neutron source assembly. The peak a shows the gamma-rays produced by the $^7\text{Li}(p,\gamma)^8\text{Be}$ and $^7\text{Li}(p,p'\gamma)^7\text{Li}$ reactions. The part A can be regarded nearly as the time-independent background, mainly consisting of the natural background and the beta- and gamma-rays due to the $^{127}\text{I}(n_{th},\gamma)$ reaction in the central NaI(Tl) detector. Four digital windows were set up in the time-of-flight spectrum. One of the windows(B+C) was used to measure the capture gamma-rays from the sample and the other three windows set up in the part A to determine the background(C). The net capture gamma-ray pulse height spectrum was obtained by subtracting the background from the foreground(B+C).

The response of the gamma-ray detector must be known in order to obtain the capture gamma-ray spectrum from the observed pulse height spectrum. The response functions were measured at the gamma-ray energies of 0.5 - 11.0 MeV, using several calibrated sources, the ^{24}Na and Am-Be sources, and the mono-energetic gamma-rays from the $^9\text{Be}(p,\gamma)^{10}\text{B}$, $^{19}\text{F}(p,\alpha\gamma)^{16}\text{O}$ and $^{27}\text{Al}(p,\gamma)^{28}\text{Si}$ reactions. Using the measured response functions, a response matrix was constructed by an interpolation procedure.

The net capture gamma-ray pulse height spectrum was unfolded by the computer code FERDOR[9], using the response matrix. The unfolded capture gamma-ray spectrum $\mathcal{V}(E_\gamma)$ was normalized as

$$\int_0^{B_n+E_n} \mathcal{V}(E_\gamma) E_\gamma dE_\gamma = B_n + E_n, \quad (1)$$

where B_n , E_n , and E_γ are the neutron binding energy, the incident neutron energy, and the gamma-ray energy, respectively. Correction for the gamma-ray attenuation in the sample was made by a Monte-Carlo calculation.

III. RESULTS AND DISCUSSION

Typical capture gamma-ray spectra of Pr, Tb, Ho, Ta and Au are shown in Fig. 3. In the capture gamma-ray spectra of Pr, Tb, Ho and Au, distinct bumps are observed around 1.5, 2.5, 3.0 and 5.5 MeV, respectively. A slight change of the gradient of the gamma-ray spectrum of Ta, which could be attributed to a bump by the present analysis, is observed around 4.5 MeV. The bumps for Tb, Ho and Au were observed for all neutron energies between 10 and 800 keV. The capture gamma-ray spectra of Tb at the neutron energies of 10, 410 and 800 keV are shown in Fig. 4. The energy of the bump is independent of the incident neutron energy, namely its behavior is resonance-like. Therefore, the charac-

teristics of the bump can be reflected phenomenologically in the gamma-ray strength function as a pygmy resonance.

The gamma-ray strength function for residual nuclei were derived from capture gamma-ray spectra, using a spectrum fitting method [10]. The composite formula proposed by Gilbert and Cameron [11] was used for a nuclear level density distribution in the spectrum fitting calculation. The nuclear level density parameters were determined from a cumulative plot of the number of excited levels and from the average level spacing for s-wave neutron resonances at the neutron binding energy. A trial function $f(E_\gamma)$ for the gamma-ray strength function was given by

$$f(E_\gamma) \approx k \left\{ \frac{E_\gamma \sigma_p \Gamma_p^2}{(E_\gamma^2 - E_p^2)^2 + (E_\gamma \Gamma_p)^2} + \sum_{i=1}^2 \frac{E_\gamma \sigma_i \Gamma_i}{(E_\gamma^2 - E_i^2)^2 + (E_\gamma \Gamma_i)^2} \right\}, \quad (2)$$

where E_i , Γ_i and σ_i are the energy, width and peak cross section of the giant electric dipole resonance respectively, taken from ref. [12]. By the first term in the equation (2), we represent the pygmy resonance which was observed as a bump in gamma-ray spectra, assuming that the resonance results from electric dipole transitions. The quantities E_p , Γ_p and σ_p were derived from the spectrum fitting calculation. The normalization constant k was determined from the average total radiative width at the neutron binding energy.

The energies and widths of the pygmy resonance derived from spectrum fitting calculations are shown with neutron number N in Fig. 5. The length of bar shows the resonance width. In the figure, the values for ^{170}Tm , Hg and Tl are taken from other works [1, 4, 7]. The figure shows that the resonance energy increases linearly with neutron number $82 < N < 126$.

In addition, we investigated the electric dipole strength exhausted in the pygmy resonance. The electric dipole sum rule is represented by the equation

$$\int_0^\infty \sigma_\gamma^{(E1)}(E_\gamma) dE_\gamma = 2\pi^2 \frac{\hbar^2}{m_n c} \frac{NZ}{A} (1 + 0.8y), \quad (3)$$

where $\sigma_\gamma^{(E1)}(E_\gamma)$ is the electric dipole photoabsorption cross section, m_n the neutron mass, c the light velocity, y the exchange force factor, A the mass number, N the neutron number and Z the proton number. The right hand side of the equation (3) gives $60NZ/A$ (mb·MeV) for $y = 0$.

Using the equation (2), the photoabsorption cross section $\sigma_\gamma^{(E1)}(E_\gamma)$ is written

$$\sigma_\gamma^{(E1)}(E_\gamma) = E_\gamma f(E_\gamma) / k. \quad (4)$$

Then, the resonance integral for the pygmy resonance gives $(\pi/2)\sigma_p\Gamma_p$ (mb·MeV). The ratio of the electric dipole strength of the pygmy resonance to the sum rule value is

$$(\pi/2)\sigma_p\Gamma_p / (60NZ/A). \quad (5)$$

These ratios for ^{142}Pr , ^{160}Tb , ^{166}Ho , ^{182}Ta and ^{178}Au are shown in Fig. 6. The figure shows that the ratio, a few % at most, increases exponentially with neutron number.

REFERENCES

- [1] Bergqvist, I. and Starfelt, N., Nucl. Phys., 39, 353-374 (1962).

- [2] Bartholomew, G. A., Bergqvist, I., Earle, E. D. and Ferguson, A. J., Can. J. Phys., 48, 687-709 (1970).
- [3] Earle, E. D., Lone, M. A., Bartholomew, G. A., McDonald, W. J., Bray, K. H., Moss, G. A. and Neilson, G. C., Can. J. Phys., 52, 989-998 (1974).
- [4] Barrett, R. F., Bray, K. H., Allen, B. J. and Kenny, M. J., Nucl. Phys., A278, 204-216 (1977).
- [5] Harvey, M. and Khanna, F. C., Nucl. Phys., A221, 77-92 (1974).
- [6] Goswami, A. and Pal, M. K., Nucl. Phys., 35, 544-556 (1962).
- [7] Joly, S., Drake, D. M. and Nilsson L., Phys. Rev., C, 20, 2072-2083 (1979).
- [8] Axel, P., Phys. Rev., 126, 671-683 (1962).
- [9] Kendrick, H. and Sperling, S. M., GA-9882 (1970).
- [10] Bartholomew, G. A., Earle, E. D., Ferguson, A. J., Knowles, J. W. and Lone, M. A., Adv. Nucl. Phys., 7, 229-325 (1973).
- [11] Gilbert, A. and Cameron, A. G. W., Can. J. Phys., 43, 1446-1496 (1965).
- [12] Berman, B. L., Atom. Data Nucl. Data Tables, 15, 319-390 (1975).

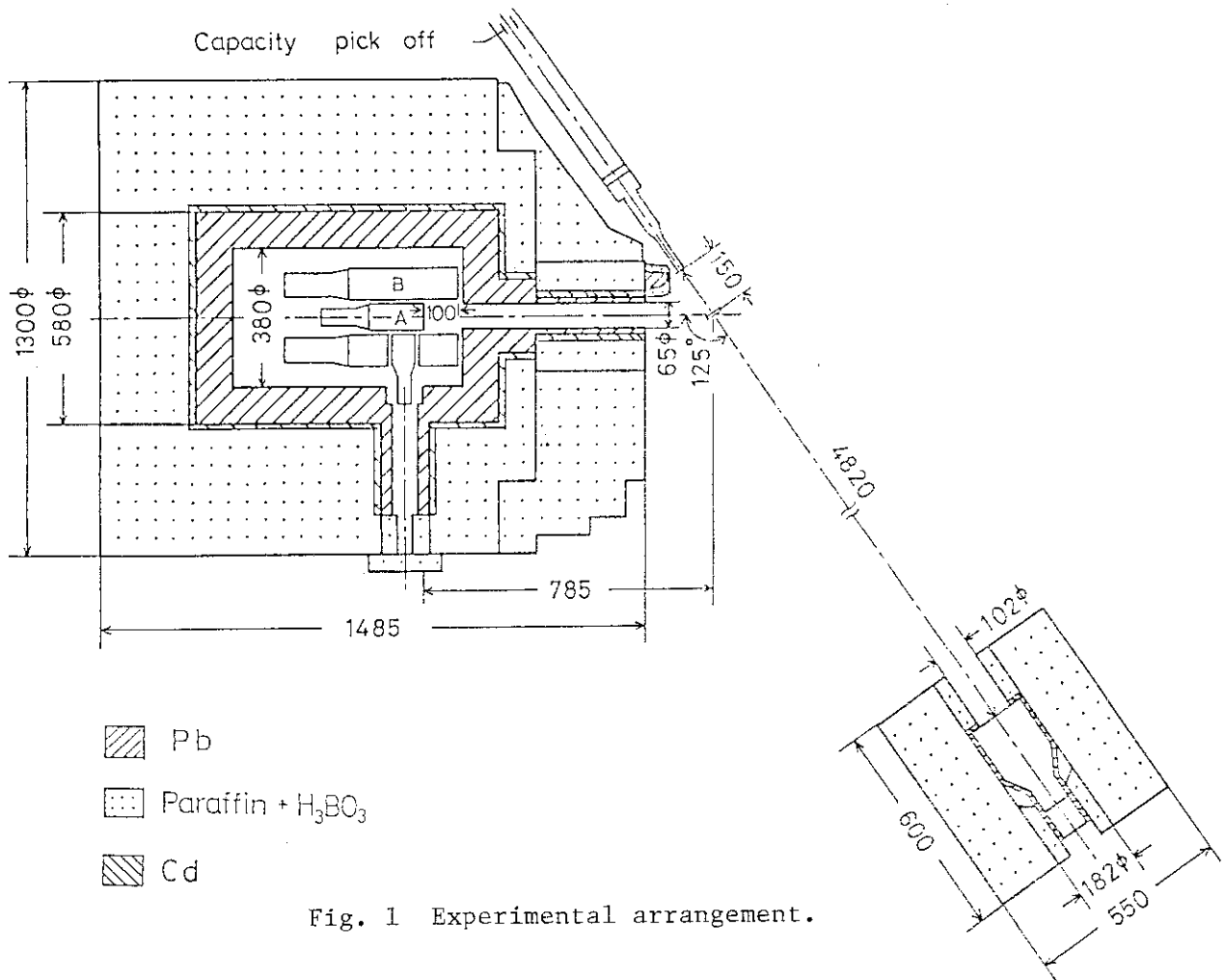


Fig. 1 Experimental arrangement.

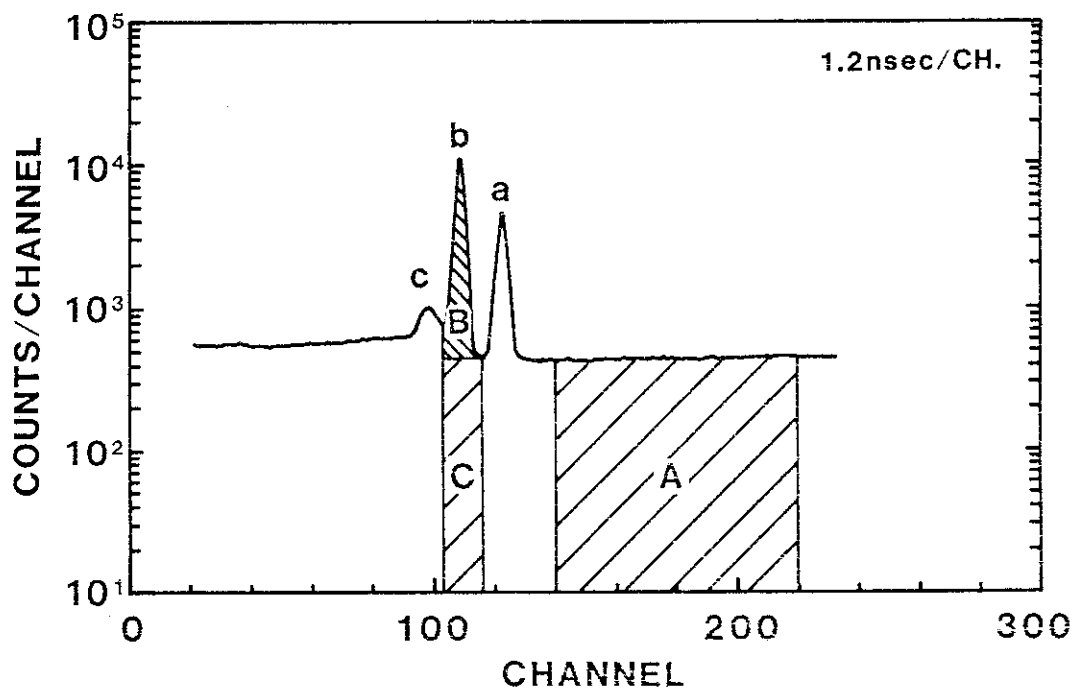


Fig. 2 Time-of-flight spectrum for Tb sample.

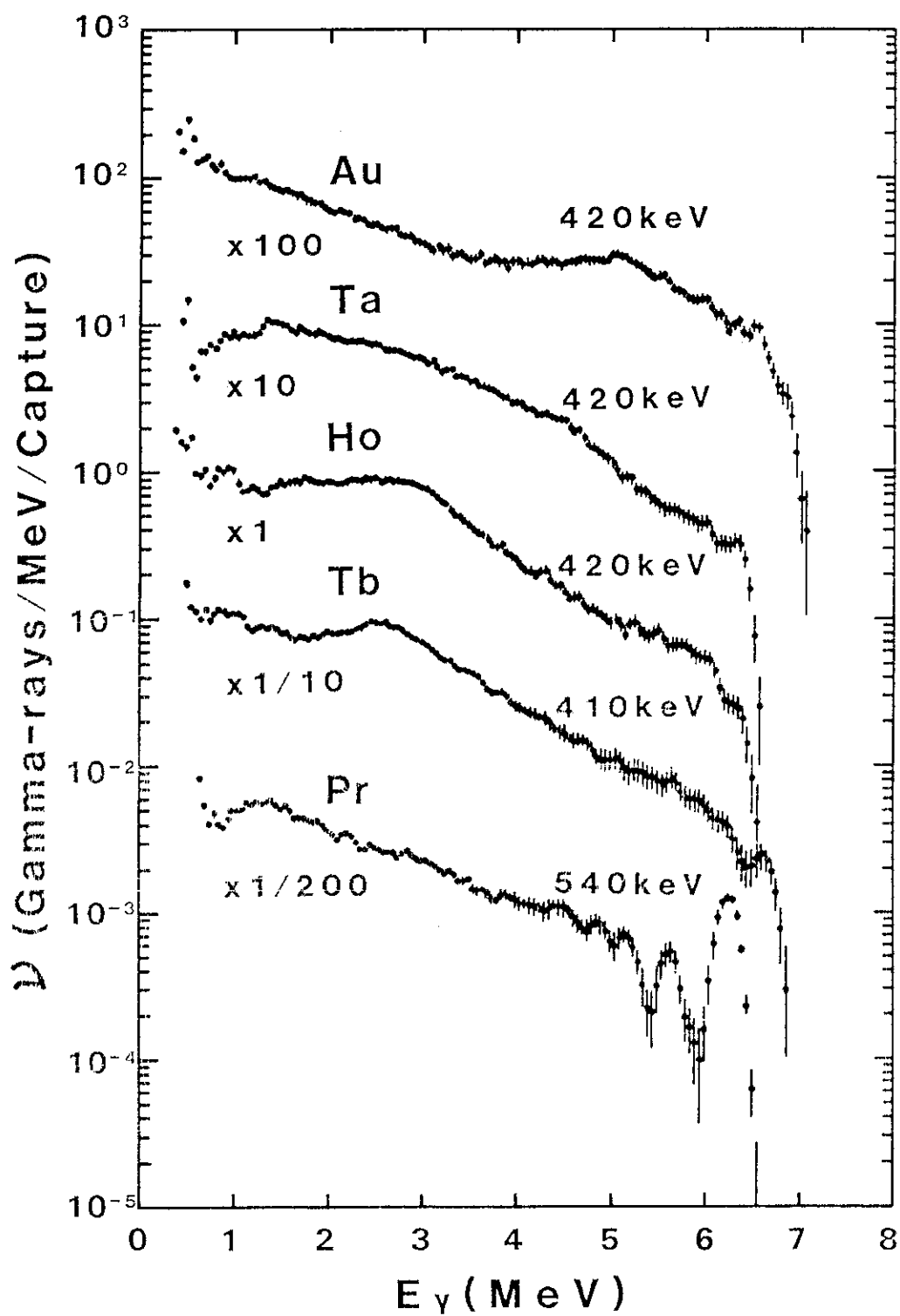


Fig. 3 Capture gamma-ray spectra of Pr, Tb, Ho, Ta and Au.
Incident neutron energies are shown in the figure.

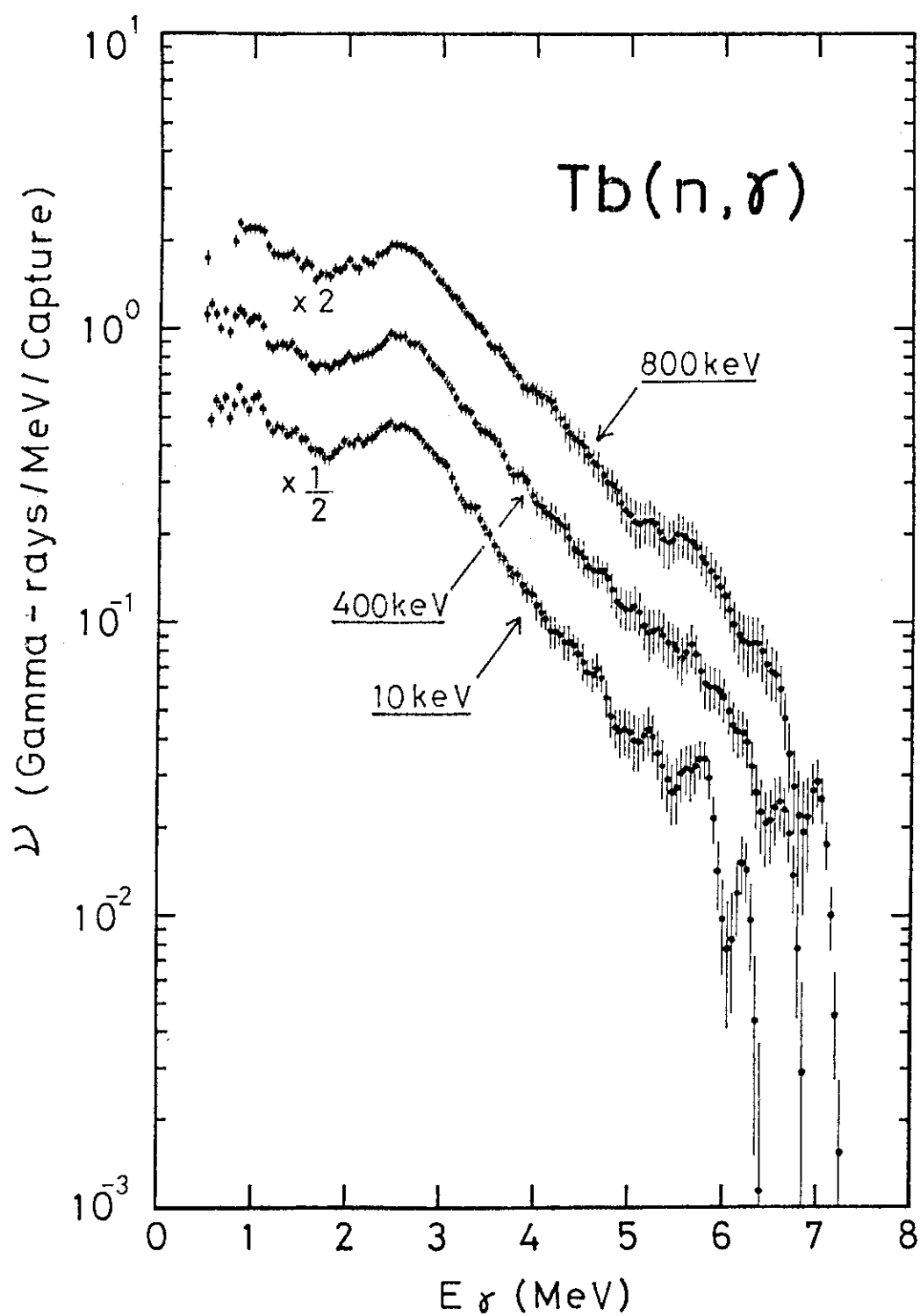


Fig. 4 Capture gamma-ray spectra of Tb at the neutron energies of 10, 410 and 800 keV.

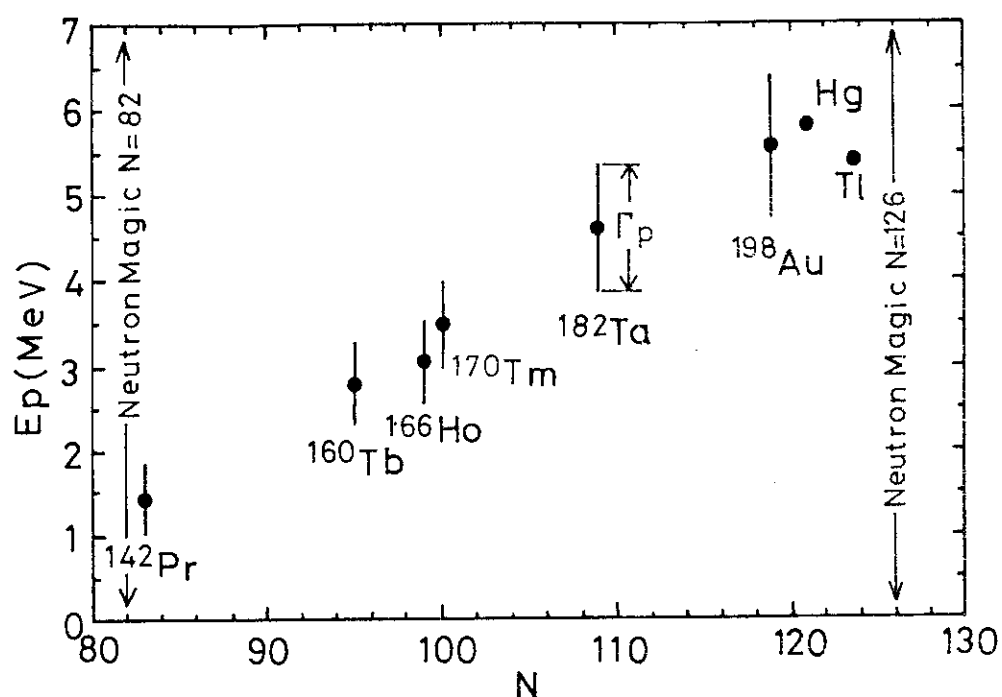


Fig. 5 Energies and widths of the pygmy resonance derived from capture gamma-ray spectra by spectrum fitting calculations.

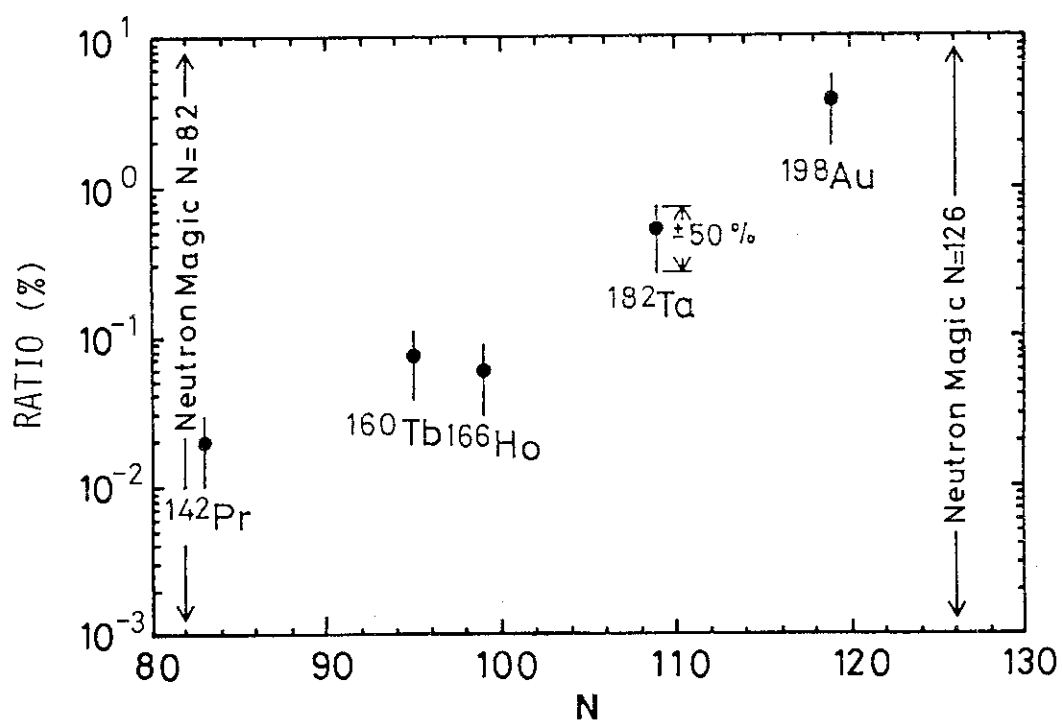


Fig. 6 Ratios of the electric dipole strength of the pygmy resonance to the classical sum rule value.